

ON THE THEORY OF COASTAL UPWELLING

by

ANTS LEETMAA

S.B. University of Chicago

(1965)

SUBMITTED IN PARTIAL FULFILLMENT
OF THE REQUIREMENTS FOR THE
DEGREE OF DOCTOR OF PHILOSOPHY

at the

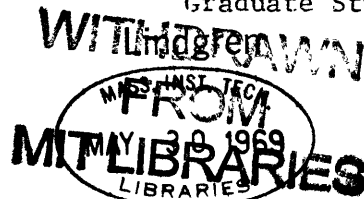
MASSACHUSETTS INSTITUTE OF TECHNOLOGY

March, 1969

Signature of Author
Department of Meteorology, March 25, 1969

Certified by
Thesis Supervisor

Accepted by
Chairman, Departmental Committee on
Graduate Students



CONTENTS

Abstract	1
PART I	
1.0 Introduction	2
2.0 Formulation of the Equations	4
3.0 Stommel-Veronis Model	7
3.1 Example I	11
3.2 Example II	19
3.3 Example III	25
3.4 Discussion	32
3.41 Limit $(\sigma\delta\epsilon)\ll\alpha(1)$	36
3.42 Limit $(\sigma\delta\epsilon)\gg\alpha(1)$	38
3.43 Convergence to the Homogeneous Limit	40
4.0 Comparison with Previous Work	45
5.0 Some Aspects of Thermal Forcing	48
PART II	
6.0 General Features of Coastal Upwelling	50
6.1 Arabian Upwelling	54
6.2 Poleward Countercurrents	57
6.3 Lateral Mixing in the Upwelling Zone	60
6.4 The Boundary Condition at a Coast	62
6.5 Consideration of β -Effects	63
7.0 An Upwelling Model	64
7.1 Formulation of Equations	65
7.2 Square-Wave Stress Model	68
7.3 Boundary Layer Approach for the Semi-Infinite Ocean	80
7.31 Ekman Layers	82
7.32 Couette-Lineykin Layer	83
7.33 Uniform Stress Model	85
7.4 Discussion of Results	91
8.0 Oceanic Applications	92
Appendices	
A. Arabian Upwelling	95
B. The Buoyancy Layer	106

Tables

I	13
II	35

Bibliography	108
--------------	-----

Figures

1. Upwelling off Chile	3
2. Example I: V-velocity	15
3. Example I: U-velocity	16
4. Example I: W-velocity	17
5. Example I: Temperature	18
6. Example II: V-velocity	21
7. Example II: U-velocity	22
8. Example II: W-velocity	23
9. Example II: Temperature	24
10. Example III: V-velocity	27
11. Example III: U-velocity	28
12. Example III: W-velocity	29
13. Example III: Temperature	30
14. Net Transport to Right of Stress	31
15. Example I: V-velocity $\lambda=100$	42
16. Example I: Temperature $\lambda=50$	43
17. Elements of Rotating Stratified Fluids	47
18. Applied Surface Stress	71
19. Square-wave Stress: V-velocity	74
20. Square-wave Stress: U-velocity	75
21. Square-wave Stress: W-velocity	76
22. Square-wave Stress: Temperature	77
23. Square-wave Stress: Streamfunction	78
24. Location of Sections A, B, C	96
25. Section A: Temperature	97
26. Section A: Salinity	98
27. Section A: Oxygen	99
28. Section B: Temperature	100
29. Section B: Salinity	101
30. Section B: Oxygen	102
31. Section C: Temperature	103
32. Section C: Salinity	104
33. Section C: Oxygen	105

ON THE THEORY OF COASTAL UPWELLING

by

Ants Leetmaa

Submitted to the Department of Meteorology on 25 March 1969
in partial fulfillment of the requirement for the degree of
Doctor of Philosophy

ABSTRACT

Some aspects of the linear dynamics of rotating, stratified fluids are studied in detail. A system is considered in which the effects of lateral friction can be neglected. The flow is driven mechanically. The solutions are found to depend strongly on the values of the parameters, $(\sigma\delta) = \sqrt{K \frac{\sigma\Delta T}{\rho}} L$ and $E = \frac{\sigma\Delta T}{\rho}$. For weak stratifications, the solutions converge to the homogeneous limit. The transitions in the dynamics of this system from the homogeneous limit to strong stratification are displayed in detail. Some effects of thermal forcing are considered.

Some of the physical mechanisms which are examined in this study are thought to be of importance in coastal upwelling. The general observational features of coastal upwelling are examined. On the basis of some of these, a continuously stratified linear model of an upwelling zone on a f -plane is presented. The limitations of the model are discussed.

Thesis supervisor: Henry M. Stommel
Title: Professor of Oceanography

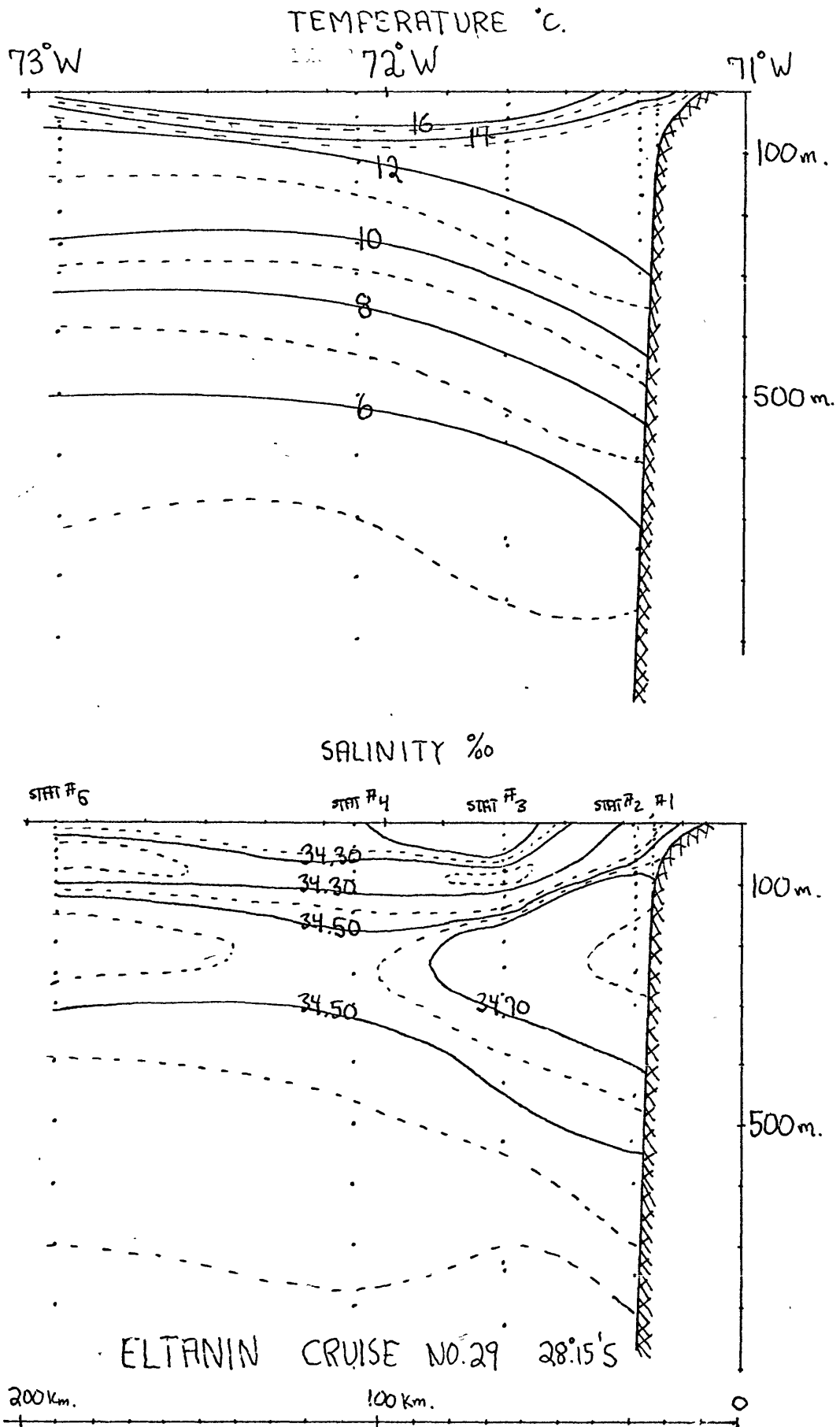
1.0 Introduction

Charts of mean sea surface temperature show that regions of anomalously cold water appear next to the continents on the eastern sides of most ocean basins. These are produced by upwelling. A typical case of upwelling off the coast of Chile is illustrated in figure 1.

When a wind blows parallel to a coast, the Coriolis force causes a transport of water in the surface layer normal to the coast. An off-shore transport requires by continuity that cold, sub-surface water is drawn to the surface at the coast. This is called upwelling. The opposite case, of surface water moving toward the coast, is called downwelling. In either case, the dynamics of the zone in which the water rises or descends is not well understood.

The characteristic width of this zone is of the order of tens of kilometers. An order of magnitude estimate in the Navier-Stokes equations indicates that lateral friction and inertial forces become important only on a scale of the order of kilometers. Because of this, the previous theoretical models in which lateral friction or non-linear effects are important will not be discussed.

Recent work by Barcilon and Pedlosky (1967a,b) and Veronis (1967a,b) indicates that stratification can greatly modify the dynamics of rotating fluids. For certain ranges in stratification,



Ekman layers no longer control the dynamics, and the effects of viscosity penetrate into the interior of the fluid. There are geophysical situations in which such effects might be important. Sverdrup (1937) postulated that in the upwelling zone part of the surface stress was directly transmitted to the interior, i.e. the interior thermal wind balanced part of the surface stress. He, however, did not present a detailed theoretical model of the upwelling zone. An attempt to incorporate Sverdrup's ideas into a dynamical model of upwelling was made by Yoshida (1967). His model consisted essentially of a two layer system, and the effects of continuous stratification are not apparent.

A simple, continuously stratified model of an upwelling zone is presented in this work. To study the effects of stratification in this zone, a simpler rotating, stratified fluid system is studied. A physical understanding of the interaction between rotation and stratification in this system is obtained. The physical insight obtained from this study helps us to understand the more complex dynamics of the upwelling zone. This theoretical upwelling model exhibits some of the features which are observed in coastal upwelling. The limitations of the model are discussed.

2.0 Formulation of equations

Consider the steady motion of an incompressible, Boussinesq fluid in a coordinate frame rotating with constant angular velocity

f/a about the vertical. The equations of motion are:

$$\vec{u}' \cdot \nabla \vec{u}' + f \hat{k} \times \vec{u}' = - \frac{1}{\rho_0} \nabla p' - g \hat{k} + \nu \nabla^2 \vec{u}'$$

$$\nabla \cdot \vec{u}' = 0$$

$$\vec{u}' \cdot \nabla T' = \kappa \nabla^2 T'$$

$$\rho' = \rho_0 (1 - \alpha (T' - T_0))$$

where u' , p' , ρ' , T' , ν , κ are respectively the velocity, pressure, density, temperature, constant kinematic viscosity, and constant thermometric conductivity. The unit vector in the vertical is \hat{k} . The equation of state is assumed to be linear where α is a constant thermal expansion coefficient, and ρ_0 and T_0 are reference values of density and temperature. The centrifugal accelerations are assumed to be small compared to gravity and have been neglected.

The simplest model in which thermal effects are important is considered. The heat equation is linearized by imposing an external temperature gradient. The fluid is contained between two horizontal surfaces separated by a distance D . The upper surface is maintained at a temperature $T_0 + \Delta T$; the lower surface is maintained at T_0 where $\Delta T > 0$. In the absence of any motion the equilibrium temperature is given by:

$$T_e = (T_0 + \Delta T) + \Delta T z/D \quad 0 \leq z \leq D$$

The problem is assumed to be independent of y , i.e. $\frac{\partial}{\partial y} = 0$. The

equations are non-dimensionalized as follows:

$$\begin{aligned}(u', v') &= U(u, v) \quad ; \quad w' = \frac{D}{L} U w \quad ; \quad x' = Lx \\ z' &= Dz \quad ; \quad T' = T_e + \frac{UfL}{g\alpha D} T \\ \rho' &= \rho_0 - \rho_0 g Dz + \rho_0 g \alpha \Delta T Dz (1 + z/2) + \rho_0 fULP\end{aligned}$$

where u, v, w, T, ρ are non-dimensional variables. Note that T and ρ represent deviations of the temperature and the pressure from their equilibrium values. The length scale "L" represents the characteristic horizontal scale imposed on the system by the boundary conditions at $z=0$ whose scale of variation is "L". The non-dimensional equations are:

$$\begin{aligned}R_0(uu_x + ww_z) - v &= -p_x + E\nabla^2 u \\ R_0(uv_x + wv_z) + u &= E\nabla^2 v \\ \delta^2 R_0(uw_x + ww_z) &= -p_z + T + \delta^2 E\nabla^2 w \\ u_x + w_z &= 0 \\ \sigma R_0(uT_x + wT_z) + (\sigma\delta)w &= E\nabla^2 T\end{aligned}$$

where

$$\begin{aligned}\sigma &\equiv \text{Prandtl No.} = \nu/k \\ E &\equiv \text{EKMAN NO.} = \frac{\nu}{fD^2} \\ R_0 &\equiv \text{ROSSBY NO.} = \frac{U}{fL} \\ \delta &\equiv \text{ASPECT RATIO} = D/L \\ S &= \frac{g\alpha\Delta T_e}{f^2 L}\end{aligned}$$

and

$$\nabla^2 = \delta^2 \frac{\partial^2}{\partial x^2} + \frac{\partial^2}{\partial z^2}$$

In the sequel, $(\sigma\delta)$ will be called the stratification.

A right-handed coordinate system is used where z is positive upward. The velocities u, v, w are respectively in the x, y, z directions. The notation $()_x$ is shorthand for $\frac{\partial}{\partial x} ()$. Since the motion will be driven by surface stresses, the velocity amplitude, U , is chosen to be $\frac{\tau_0 D}{\rho_0 \nu}$ where τ_0 is the amplitude of the stress. We assume that $\sigma = o(1)$ and $\epsilon \ll o(1)$. To linearize the system the further restriction is made that $R_0 \ll \epsilon \ll o(1)$. Neglecting terms of $O(R_0)$ the equations become:

$$\begin{aligned} -v &= -p_x + E \nabla^2 u \\ u &= E \nabla^2 v \\ 0 &= -p_z + 1 + \delta^2 E v^2 w \\ 0 &= u_x + w_z \\ (\sigma \delta) w &= E \nabla^2 T \end{aligned}$$

When $\delta = o(1)$, this set of equations is the same as those considered by Barcilon and Pedlosky. However, further simplification occurs if we assume that $\delta \ll o(1)$.

3.0 The Stommel-Veronis Model

Consider a model in which the horizontal scale is large compared to the vertical one, i.e. $\delta \ll o(1)$. Neglecting terms of $o(\delta^2 \epsilon)$ the equations become:

$$\begin{aligned} -v &= -p_x + E u_{zz} \\ u &= E v_{zz} \end{aligned}$$

$$0 = -p_z + T$$

$$0 = u_x + (v)_z$$

$$(\sigma\delta)\omega = E T_{zz}$$

This was the set of equations examined by Stommel and Veronis (1957). A single equation for the pressure can be formed:

$$\begin{array}{ccc} \textcircled{1} & \textcircled{2} & \textcircled{3} \\ E^2 p_{zz} + p_{zz} + (\sigma\delta\delta) p_{xxzz} = 0 \end{array}$$

There exist certain natural scales for z which arise out of the possible balances between the three terms.

The Ekman Solution:

A balance between terms $\textcircled{1}$ and $\textcircled{2}$ occurs only if $(\sigma\delta\delta E) < O(1)$.

The vertical scale, ξ , then is:

$$\xi = E^{-1/2} z$$

The Frictional Solution:

A balance between terms $\textcircled{1}$ and $\textcircled{3}$ occurs if $(\sigma\delta\delta E) > O(1)$. Then the vertical scale, ξ , is:

$$\xi = \left(\frac{E^2}{\sigma\delta\delta}\right)^{-1/6} z$$

The Lineykin Solution:

A balance between terms $\textcircled{2}$ and $\textcircled{3}$ occurs if $(\sigma\delta\delta E) < O(1)$.

Then the vertical scale, ξ , is:

$$z = (\sigma \delta)^{1/2} \xi$$

The Couette Solution:

The solution, which is valid whenever the model is valid, for which all three terms in the pressure equation are identically zero is:

$$P(x, \xi) = A(x) \xi + B(x)$$

This solution plays a dominant role in the dynamics of the following examples.

Physically the existence of these various z-scales indicates that, for any given value of the parameters, there are regions in the flow in which the primary balances in the momentum equations are not those which were assumed in the initial scaling.

The solution in any parameter range will be a composite of these. Simple examples will be considered to exhibit some of the effects of stratification in rotating fluids. Because complete solutions can be obtained which are valid for all ranges of stratification, boundary layer analyses will only be done after these solutions have been exhibited to gain further physical insight. The only restrictive assumption which is made is that the Ekman depth is a small fraction of the total depth. This is equivalent to the assumption made earlier that $E \ll 1$. In the examples we let $E^{1/2} = 1/40$ i.e. $\frac{\text{EKMAN DEPTH}}{\text{TOTAL DEPTH}} = \frac{1}{40}$.

For computational convenience in the following examples, the unit of depth is defined as the Ekman depth, i.e. $z = \epsilon^{1/2} \xi$.

The pressure equation becomes:

$$P_{8\xi} + P_{4\xi} + \lambda^{-2} P_{xx\xi\xi} = 0 \quad (1)$$

where

$$\lambda^{-1} = (\sigma \delta \epsilon)^{1/2}$$

and

$$\begin{aligned} \lambda &= (\text{LINEYKIN DEPTH}) / (\text{EKMAN DEPTH}) \\ &= [(\text{FRICTIONAL DEPTH}) / (\text{EKMAN DEPTH})]^3 \end{aligned}$$

As in Stommel and Veronis (1957), periodic boundary conditions will be used to eliminate the need for horizontal boundaries. It should be noted that in the following examples, the temperature referred to is always the perturbation temperature. The total temperature field consists of this plus the mean gradient.

Temperature boundary conditions are expected to play a large role in determining the nature of the solution. In the following examples the temperature boundary condition will be specified either on the perturbation heat flux or on the perturbation temperature. This allows a more thorough understanding of the dependence of the solution on the thermal boundary conditions to be obtained.

In a laboratory situation to which the Stommel and Veronis model might apply, the total temperature is specified at $z = 0$; -1. Thus a situation in which the perturbation temperature is specified at $z=0$ could be experimentally realized. However, in this situation, a system in which the flux of perturbation temperature is specified is probably not meaningful physically. For an oceanic situation, the appropriate boundary condition at $z=0$ is one where some combination of temperature and heat flux is specified. The exact form of this is unknown.

3.1 Example I:

Consider the following problem. Specify the boundary conditions:

$$\text{@ } \xi = 0; \quad \frac{\partial v}{\partial \xi} = \cos x \quad ; \quad \frac{\partial u}{\partial \xi} = 0 \quad ; \quad w = T = 0$$

$$\text{@ } \xi = -10; \quad u = v = w = T = 0$$

The solution to equation (1) which will satisfy the boundary conditions is:

$$P(x, \xi) = P(\xi) \sin x$$

where

$$P(\xi) = \sum_{i=1}^6 \pi_i \exp \sigma_i \xi + \pi_7 \xi + \pi_8$$

The σ_i 's satisfy the condition that:

$$\sigma_i^6 + \sigma_i^2 - \lambda^{-2} = 0$$

The following relations are true:

$$\sigma_4 = -\sigma_1$$

$$\sigma_2 = \sigma_3^*$$

$$\sigma_5 = -\sigma_2 = \sigma_6^*$$

The ()* denotes complex conjugate. The σ_i 's were determined numerically and a short list of them for various values of (λ) is given in Table I. Note that σ_1 is real.

$$\sigma_2 = \sigma_{2r} + i \sigma_{2i}$$

Application of the boundary conditions determines the Π_i 's :

$$\Pi_1 = 1/(\lambda^2 \sigma_1^3 (\sigma_1^2 - \sigma_3^2) (\sigma_2^2 - \sigma_1^2)) + \Pi_4 \exp(-40\sigma_1)$$

$$\Pi_2 = 1/(\lambda^2 \sigma_2^3 (\sigma_2^2 - \sigma_1^2) (\sigma_3^2 - \sigma_2^2))$$

$$\Pi_3 = \Pi_2^*$$

$$\begin{aligned} \Pi_4 = & [(\sigma_1^3 (\sigma_2^3 - \sigma_3^3) \sigma_1^4 (\sigma_3^2 - \sigma_2^2) - \sigma_1 \sigma_3^2 (\sigma_2 - \sigma_3) \sigma_2^2) \exp(-40\sigma_1) \cdot \\ & (1/(\lambda^2 \sigma_1^3 (\sigma_1^2 - \sigma_3^2) (\sigma_2^2 - \sigma_1^2)) - \Pi_2 \sigma_2^2 \sigma_3^2 (\sigma_2 - \sigma_3))] / [\sigma_1 (\sigma_1^3 - \sigma_2^3) \cdot \\ & (\sigma_3^2 - \sigma_2^2) - (\sigma_1^2 - \sigma_2^2) (\sigma_3^3 - \sigma_2^3) - (\sigma_1^3 (\sigma_2^3 - \sigma_3^3) - \sigma_1^4 (\sigma_3^2 - \sigma_2^2) - \\ & \sigma_1 \sigma_2^2 \sigma_3^2 (\sigma_2 - \sigma_3) \exp(-80\sigma_1)] \end{aligned}$$

$$\begin{aligned} \Pi_5 = & [2\sigma_1^4 (\sigma_3^2 - \sigma_1^2) \Pi_1 \exp(-40\sigma_1) - \Pi_2 (\sigma_3^3 \sigma_1^2 - \sigma_3^2 \sigma_1^3)] / \\ & [\sigma_2 ((\sigma_2^3 - \sigma_3^3) (\sigma_1^2 - \sigma_3^2) - (\sigma_2^2 - \sigma_3^2) (\sigma_1^3 - \sigma_3^3))] \end{aligned}$$

$$\Pi_6 = \Pi_5^*$$

TABLE I

λ	σ_i	σ_{ar}	σ_{ai}
1/30	3.1016	1.5591	2.6909
1/10	2.1377	1.0938	1.8658
1/3	1.3857	.7762	1.2500
1	.8260	.6593	.8808
3	.3313	.6896	.7283
10	.1000	.7053	.7089
30	.0333	.7069	.7073
100	.0100	.7071	.7071

$$\pi_7 = - \left[\frac{1}{\lambda^2 \sigma_1^2 (\sigma_1^2 - \sigma_3^2)} (\sigma_2^2 - \sigma_1^2) + \text{REAL} (2\sigma_2 \pi_2) \right]$$

$$\pi_8 = 40\pi_7 - \left[\lambda^2 \sigma_1^2 \pi_4 + 2 \text{REAL} (\lambda^2 \sigma_2^2 \pi_5) \right] - \lambda^2 \sigma_1^2 \pi_1 \exp(-40\sigma_1)$$

Utilizing the momentum equations, the fields are represented in terms of the pressure as follows:

$$V = \left[P(\xi) - \lambda^2 P(\xi)_{6\xi} \right] \cos x$$

$$u = \lambda^2 P(\xi)_{4\xi} \cos x$$

$$\omega = \lambda^2 P(\xi)_{3\xi} \sin x$$

$$T = P(\xi)_{\xi} \sin x$$

These are plotted in figures 2-5 for various values of λ . The value of λ is indicated on each curve. The symbol, H, designates the homogeneous case. This was computed for an example in which the stratification was absent.

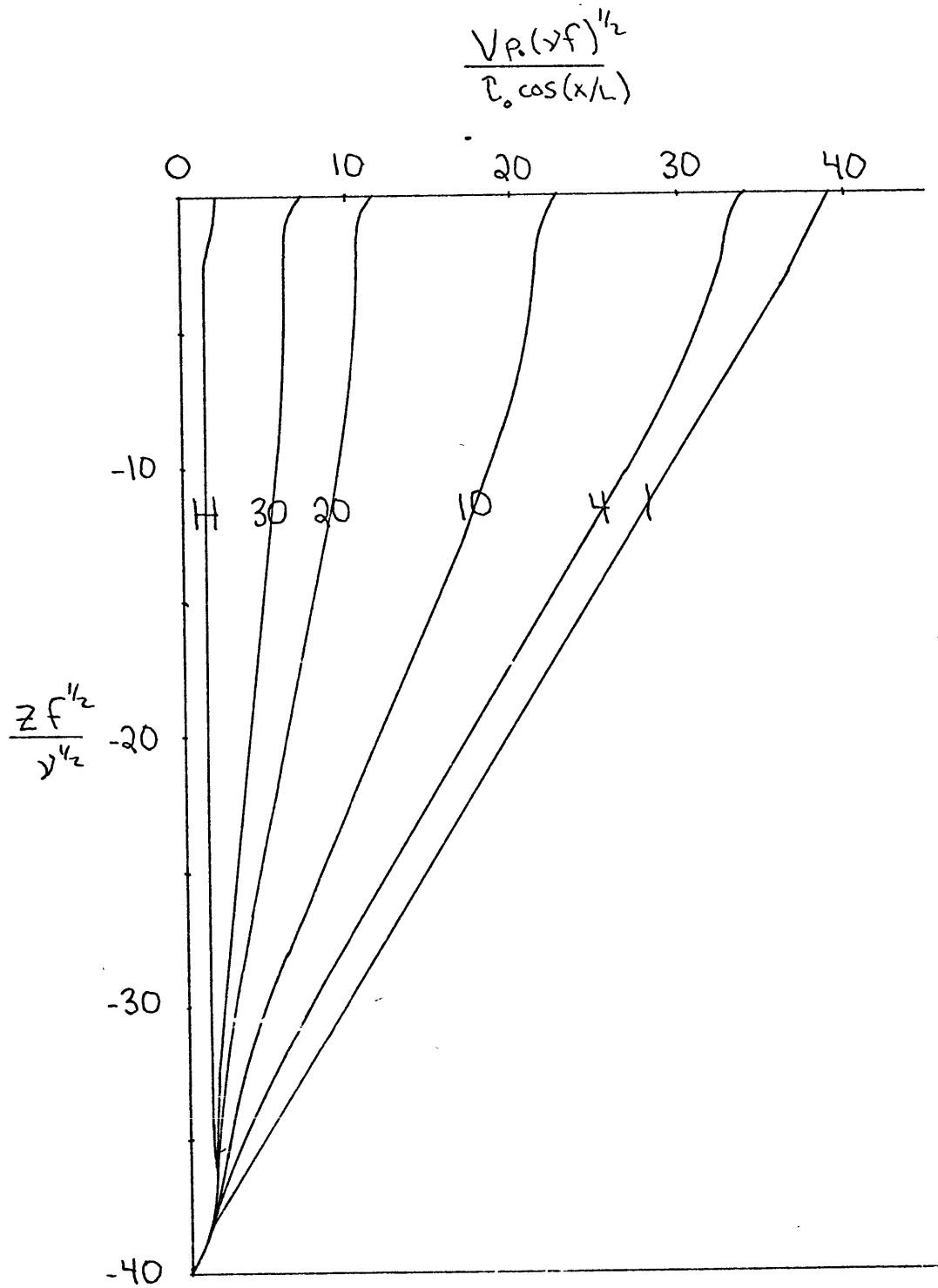


FIGURE 2

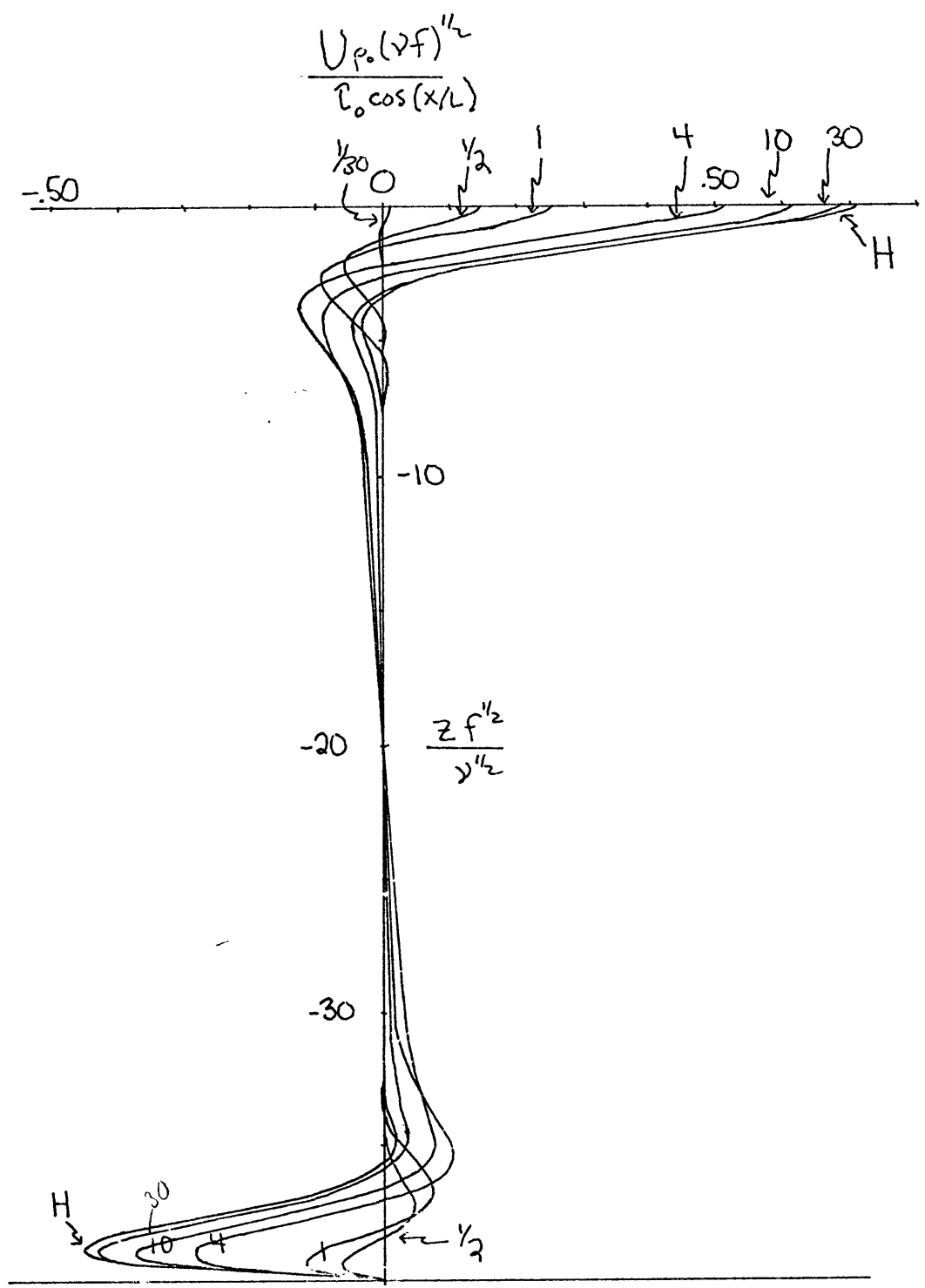


FIGURE 3

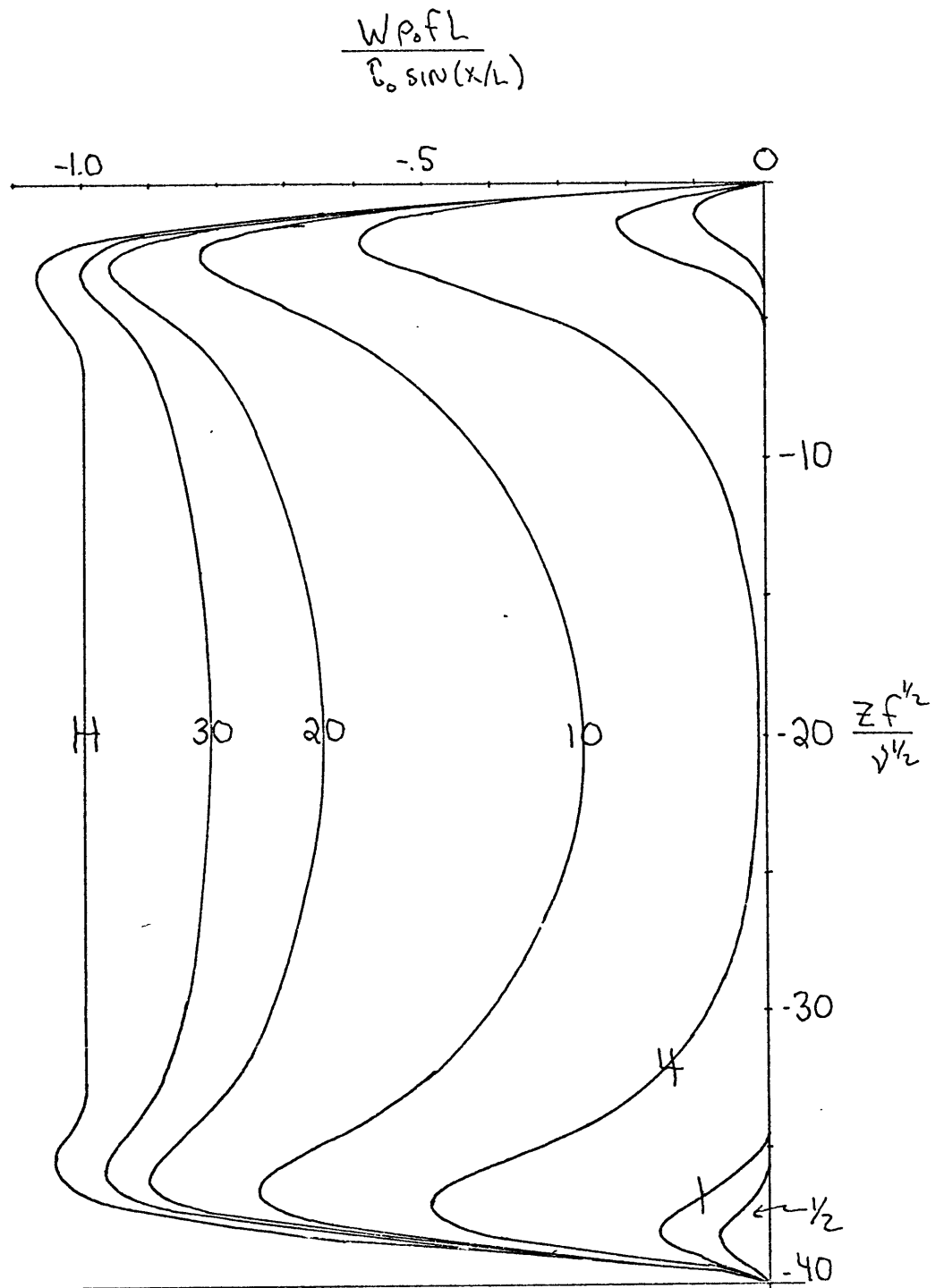


FIGURE 4

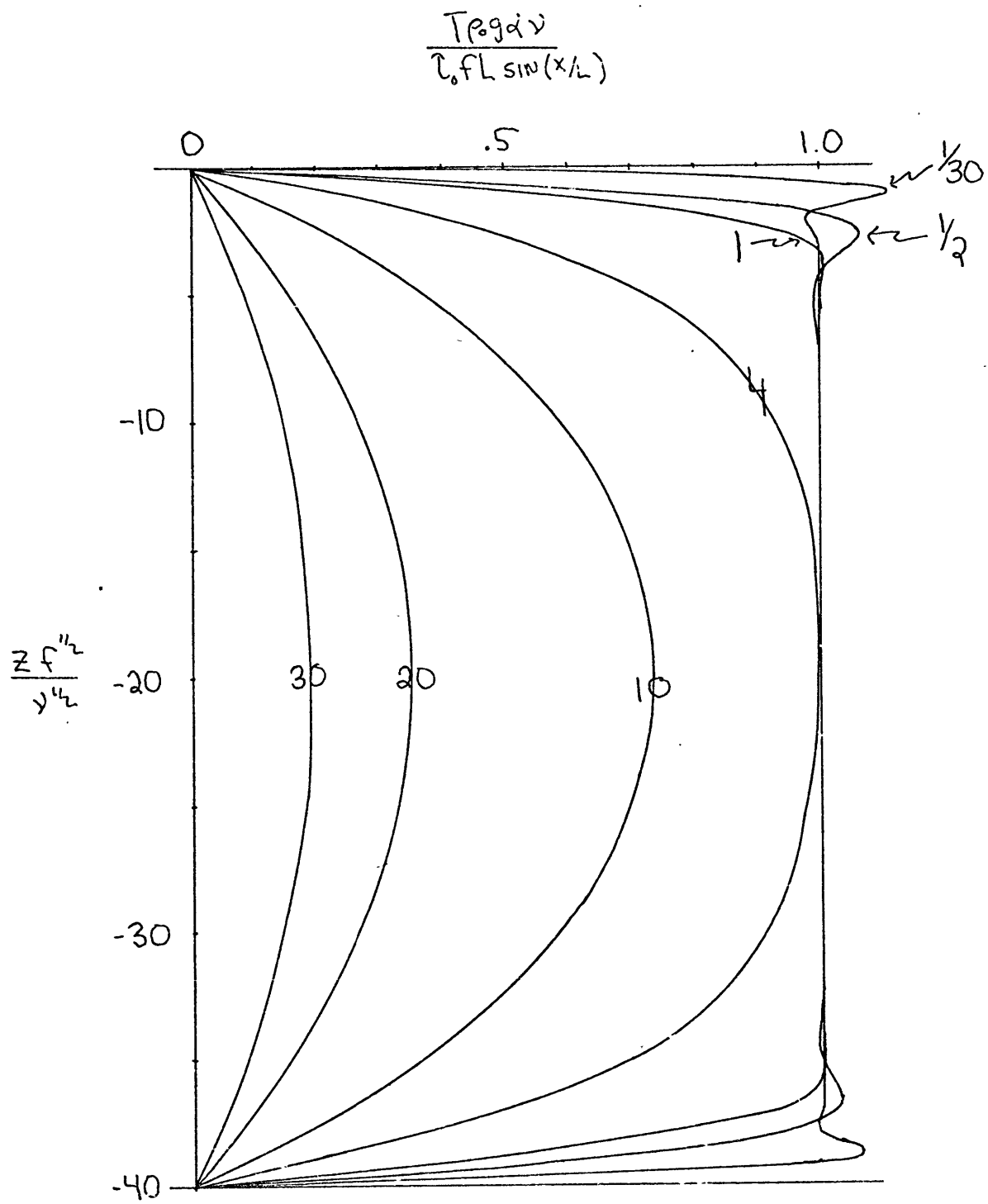


FIGURE 5

3.2 Example II:

Specify that $\partial \xi = 0; \bar{\Gamma}_\xi = 0$. The rest of the boundary conditions remain the same as in Example I. The Π_i 's now are:

$$\Pi_1 = \frac{[(\sigma_2 \sigma_3 (\sigma_2 + \sigma_3) + \sigma_1 (\sigma_3^2 + \sigma_2^2 + \sigma_2 \sigma_3) - \sigma_1^3) \Pi_4 \exp(-40\sigma_1)]}{[(\sigma_3 - \sigma_1)(\sigma_1(\sigma_1 + \sigma_3) - \sigma_2(\sigma_2 + \sigma_3))]}$$

$$\Pi_2 = \frac{[\sigma_1^2 (\sigma_1 \sigma_3 (\sigma_1 + \sigma_3) + \sigma_1 (\sigma_3^2 + \sigma_1^2 + \sigma_1 \sigma_3) - \sigma_1^3) \Pi_4 \exp(-40\sigma_1)]}{[\sigma_2^2 (\sigma_3 - \sigma_2)(\sigma_2(\sigma_2 + \sigma_3) - \sigma_1(\sigma_1 + \sigma_3))]}$$

$$\Pi_3 = \Pi_2^*$$

$$\Pi_4 = \frac{[(\sigma_1 - \sigma_3)(\sigma_1(\sigma_1 + \sigma_3)) - \sigma_2(\sigma_2 + \sigma_3)] \sigma_3^2 \sigma_2^2 \Pi_7}{[\sigma_1(\sigma_1 - \sigma_3)^2 (\sigma_1^2 (\sigma_2 + \sigma_3) - \sigma_2^2 (\sigma_1 + \sigma_3)) (\sigma_1(\sigma_1 + \sigma_3) - \sigma_2(\sigma_2 + \sigma_3)) - \sigma_1(\sigma_1^2 (\sigma_3^2 + \sigma_2^2 + \sigma_3 \sigma_2) - \sigma_3^2 \sigma_2^2 + \sigma_1^3 (\sigma_2 + \sigma_3)) (\sigma_1(\sigma_3^2 + \sigma_2^2 + \sigma_2 \sigma_3) + \sigma_2 \sigma_3 (\sigma_2 + \sigma_3) - \sigma_1^3) \exp(-80\sigma_1)]}$$

$$\Pi_5 = \frac{[\sigma_1^3 (\sigma_3^2 + \sigma_1^2 + \sigma_1 \sigma_3) + (\sigma_1 + \sigma_3) \sigma_1^4 - \sigma_3^2 \sigma_1^3] \exp(-40\sigma_1) \Pi_1 - \sigma_3^2 \sigma_1^2 \Pi_7}{[\sigma_2^2 (\sigma_1^2 + \sigma_3 \sigma_1 + \sigma_3^2) - \sigma_2 \sigma_1^2 \sigma_3^2 - \sigma_2^4 (\sigma_1 + \sigma_3)]}$$

$$\Pi_6 = \Pi_5^*$$

$$\pi_7 = 1$$

$$\pi_9 = 40 - \lambda^2 [\sigma_1^2 \pi_1 \exp(-40\sigma_1) + \sigma_1^2 \pi_4 + 2 \text{REAL}(\sigma_2^2 \pi_5)]$$

The fields are expressed in terms of the pressure as in Example

I. These are plotted in figures 6-9.

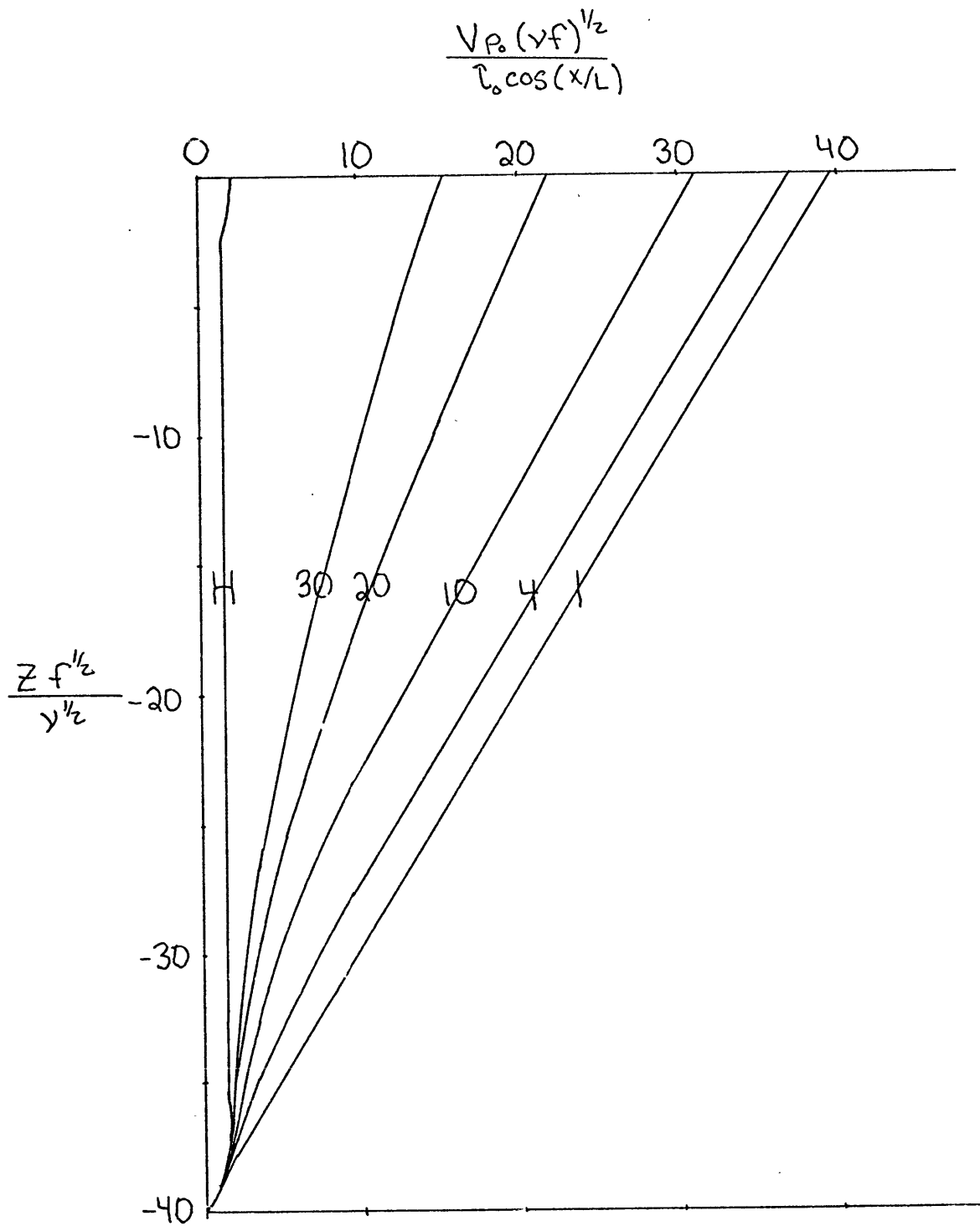


FIGURE 6

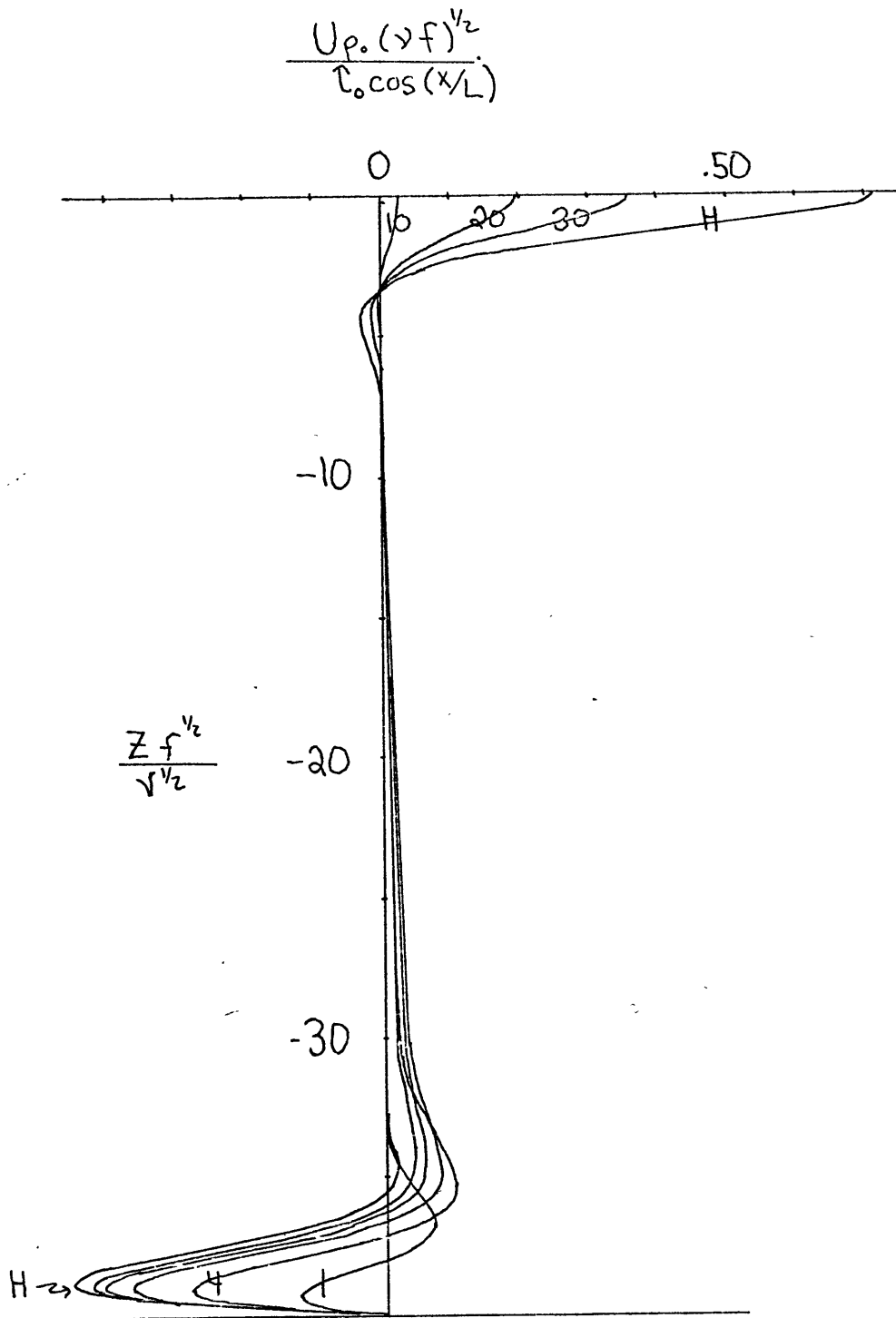


FIGURE 7

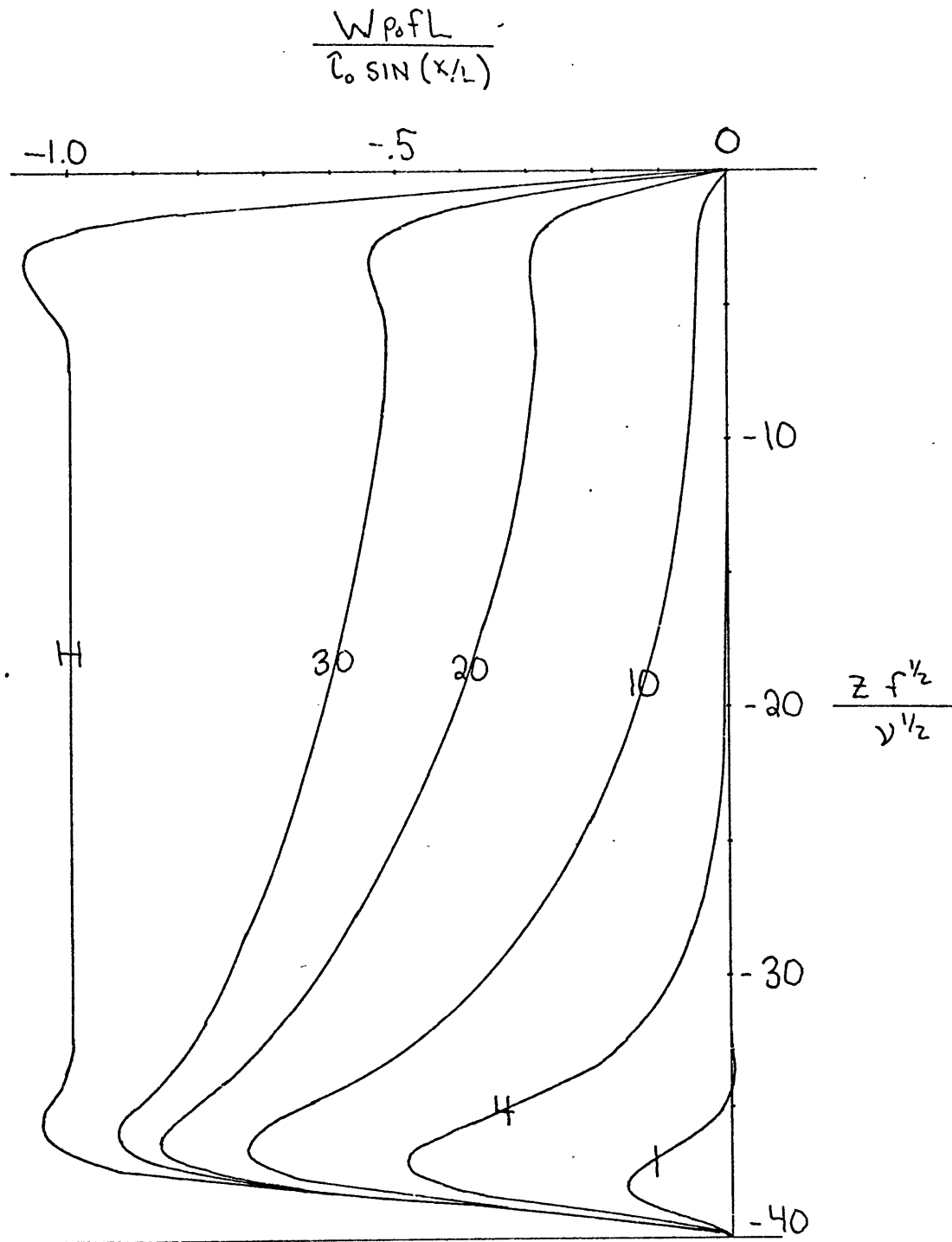


FIGURE 8

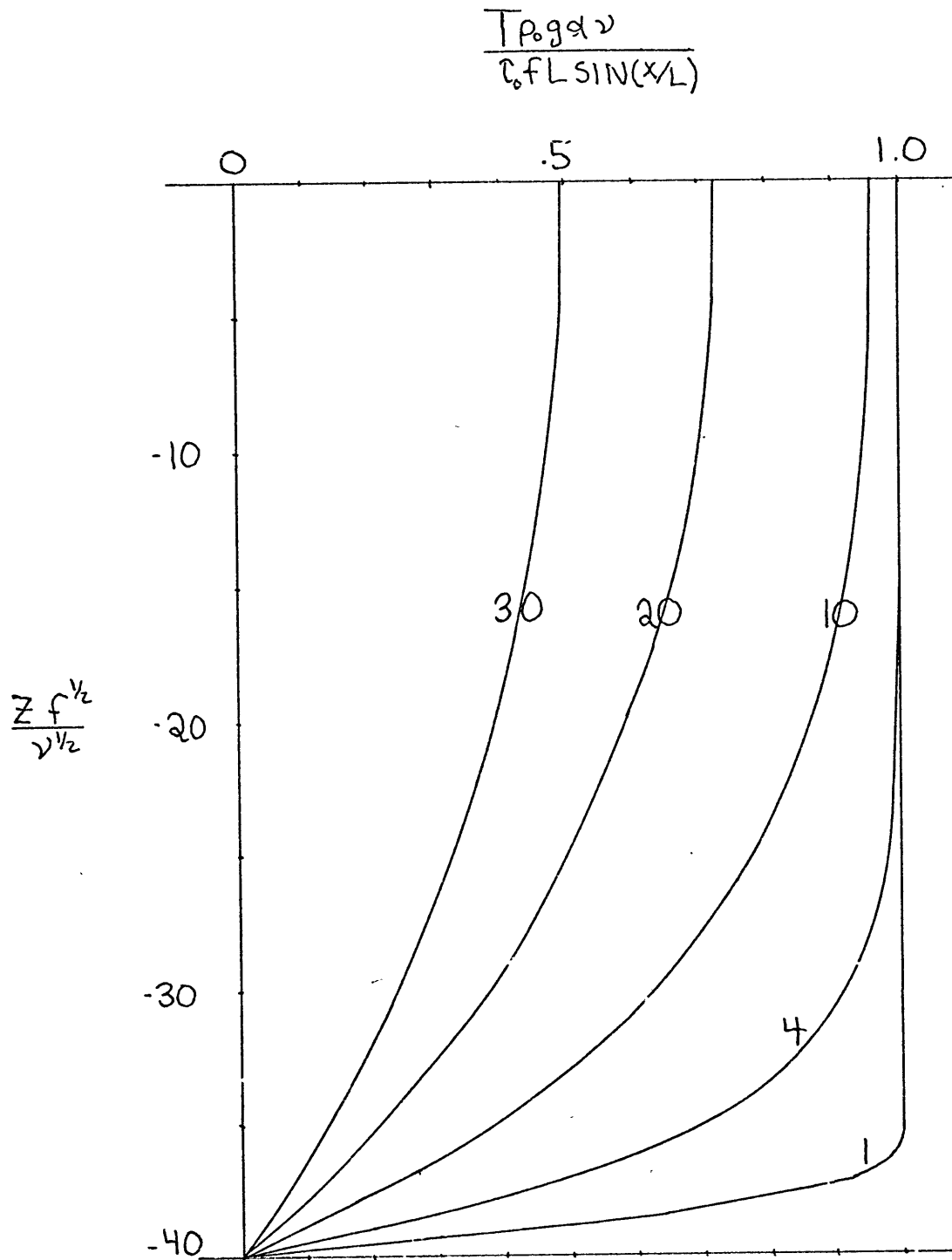


FIGURE 9

3.3 Example III:

Apply a stress in the x-direction. Couette flow cannot exist because of the lack of y-dependence. Consider the following problem:

$$\begin{aligned} @ \xi = 0 ; \quad \frac{\partial u}{\partial \xi} = \cos x \quad ; \quad \frac{\partial v}{\partial \xi} = \omega = T = 0 \\ @ \xi = -40 ; \quad u = v = \omega = T = 0 \end{aligned}$$

The Π_i 's are:

$$\Pi_1 = (\sigma_3^2 + \sigma_2^2) / (\lambda^2 \sigma_1^3 (\sigma_1^2 - \sigma_3^2) (\sigma_2^2 - \sigma_1^2)) + \Pi_4 \exp(-40 \sigma_1)$$

$$\Pi_2 = (\sigma_3^2 + \sigma_1^2) / (\lambda^2 \sigma_2^3 (\sigma_2^2 - \sigma_1^2) (\sigma_3^2 - \sigma_2^2))$$

$$\Pi_3 = \Pi_2^*$$

$$\begin{aligned} \Pi_4 = [(\sigma_1^3 (\sigma_2^3 - \sigma_3^3) - \sigma_1^4 (\sigma_3^2 - \sigma_2^2) - \sigma_1 \sigma_2^2 (\sigma_2 - \sigma_3) \sigma_2^2 \cdot \\ \exp(-40 \sigma_1) ((\sigma_3^2 + \sigma_2^2) / \lambda^2 \sigma_1^3 (\sigma_1^2 - \sigma_3^2) (\sigma_2^2 - \sigma_1^2)) - \\ \Pi_1 \sigma_2^2 \sigma_3^2 (\sigma_2 - \sigma_3)] / [\sigma_1 ((\sigma_1^3 - \sigma_2^3) (\sigma_3^2 - \sigma_2^2) - (\sigma_1^2 - \sigma_2^2) \\ (\sigma_3^3 - \sigma_2^3)) - (\sigma_1^3 (\sigma_2^3 - \sigma_3^3) - \sigma_1^4 (\sigma_3^2 - \sigma_2^2) - \sigma_1 \sigma_2^2 \sigma_3^2 \\ (\sigma_2 - \sigma_3)) \exp(-80 \sigma_1)] \end{aligned}$$

$$\Pi_5 = [2\sigma_1^4(\sigma_2^2 - \sigma_1^2)\Pi_1 \exp(-40\sigma_1) - \Pi_7(\sigma_3^3\sigma_1^2 - \sigma_3^2\sigma_1^3)] / [\sigma_2((\sigma_2^3 - \sigma_3^3)(\sigma_1^2 - \sigma_3^2) - (\sigma_2^2 - \sigma_3^2)(\sigma_1^3 - \sigma_3^3))]$$

$$\Pi_6 = \Pi_5^*$$

$$\Pi_7 = -[(\sigma_3^2 + \sigma_2^2) / (\lambda^2\sigma_1^2(\sigma_1^2 - \sigma_3^2)(\sigma_2^2 - \sigma_1^2) + \text{REAL}(2\sigma_2\Pi_2))]$$

$$\Pi_8 = 40\Pi_7 - [\lambda^2\sigma_1^2\Pi_4 + 2\text{REAL}(\lambda^2\sigma_2^2\Pi_5)] - \lambda^2\sigma_1^2\Pi_1 \exp(-40\sigma_1)$$

The fields are given in terms of the pressure by the same expressions as in Example I. These are plotted in figures 10-13. Because no Couette flow exists, the applied stress has to be balanced by the boundary layers. For $(\sigma^{\delta\epsilon}) \ll \alpha_1$ the stress is absorbed by the Ekman layers. However, for $(\sigma^{\delta\epsilon}) \gg \alpha_1$ the balancing agency is the vertically integrated pressure gradient of the rotational-frictional layer. The net transport to the right in the boundary layers is exhibited as a function of λ in figure 14. This drops to zero as the pressure gradient balance becomes important.

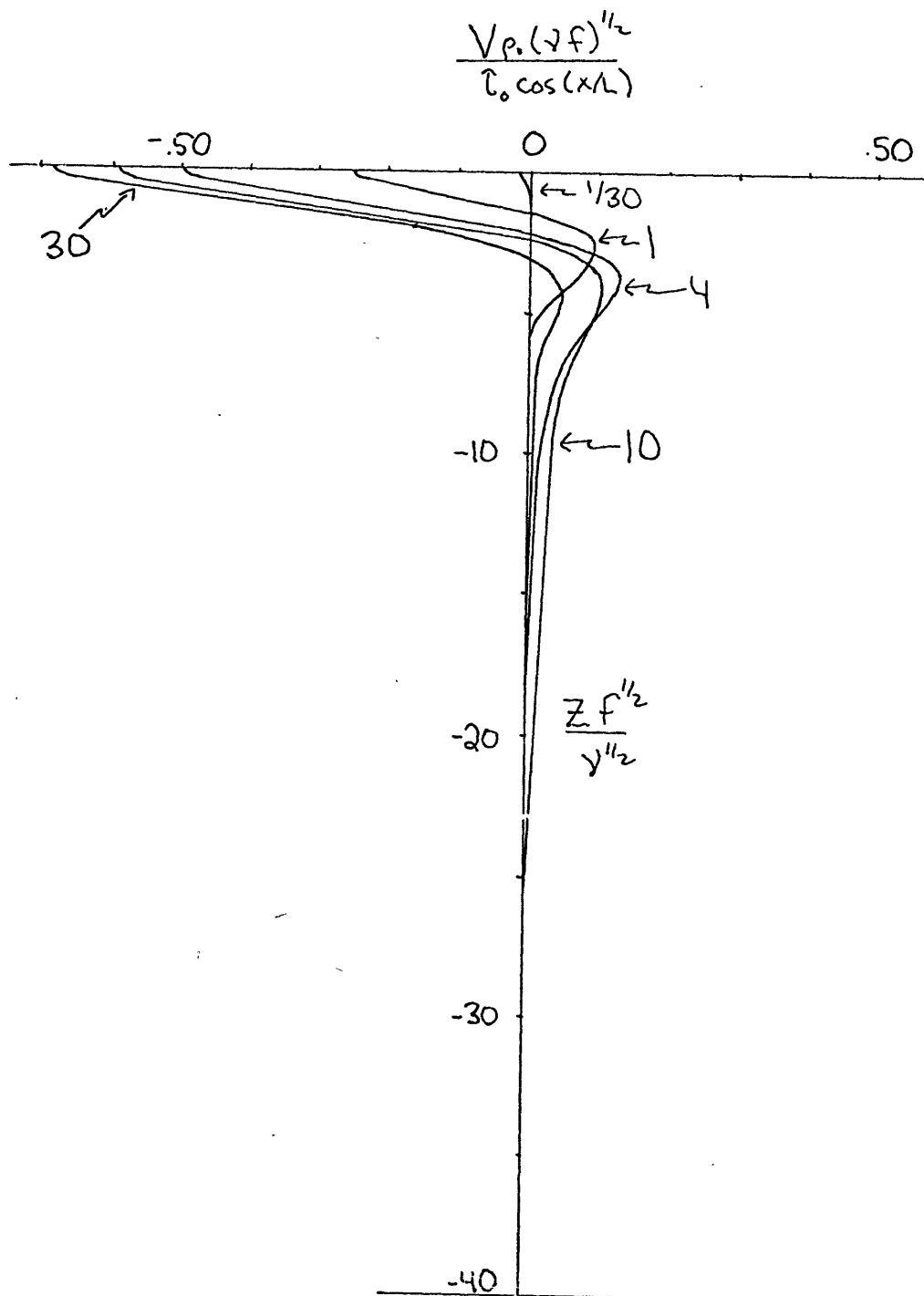


FIGURE 10

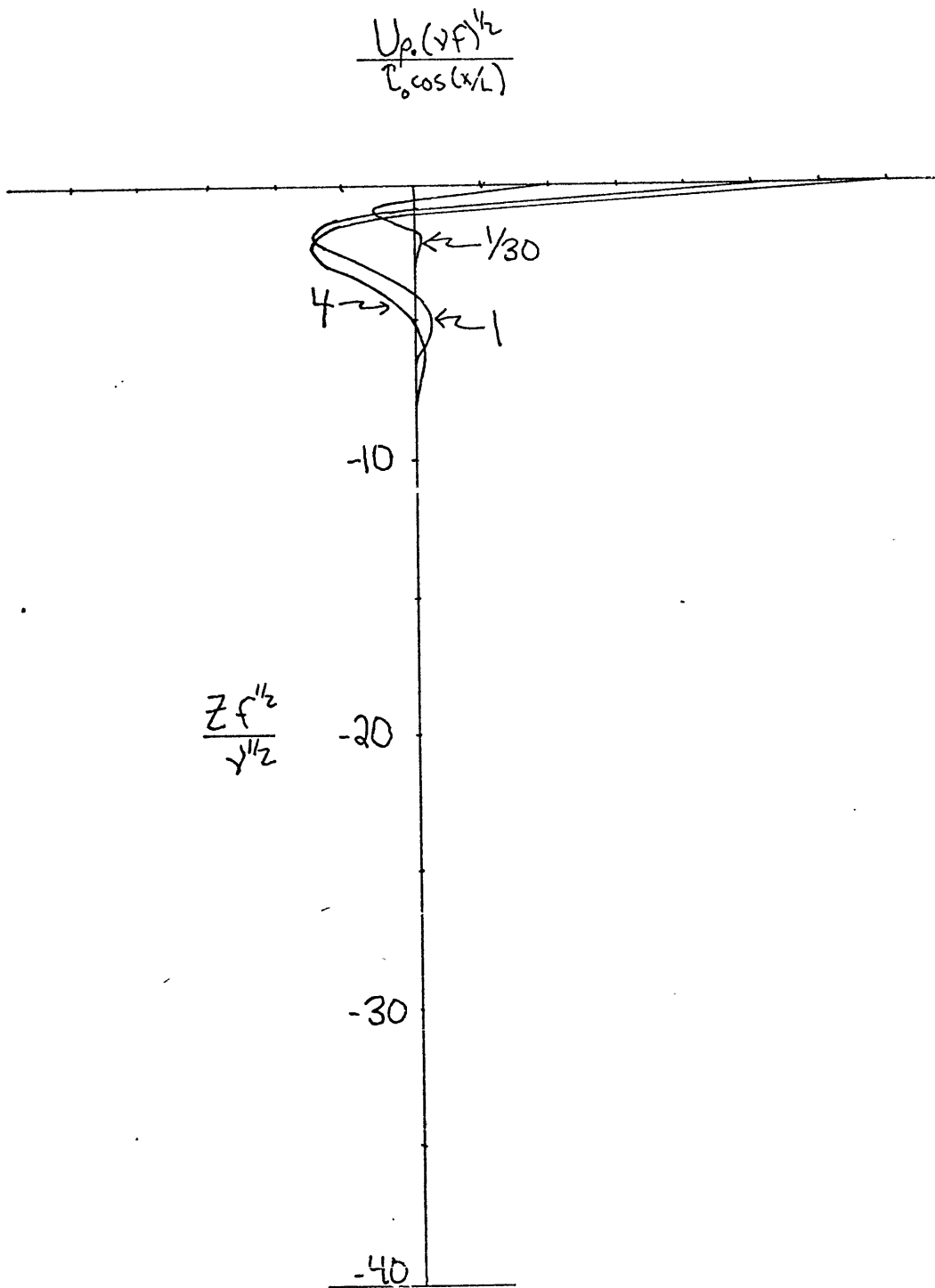


FIGURE 11

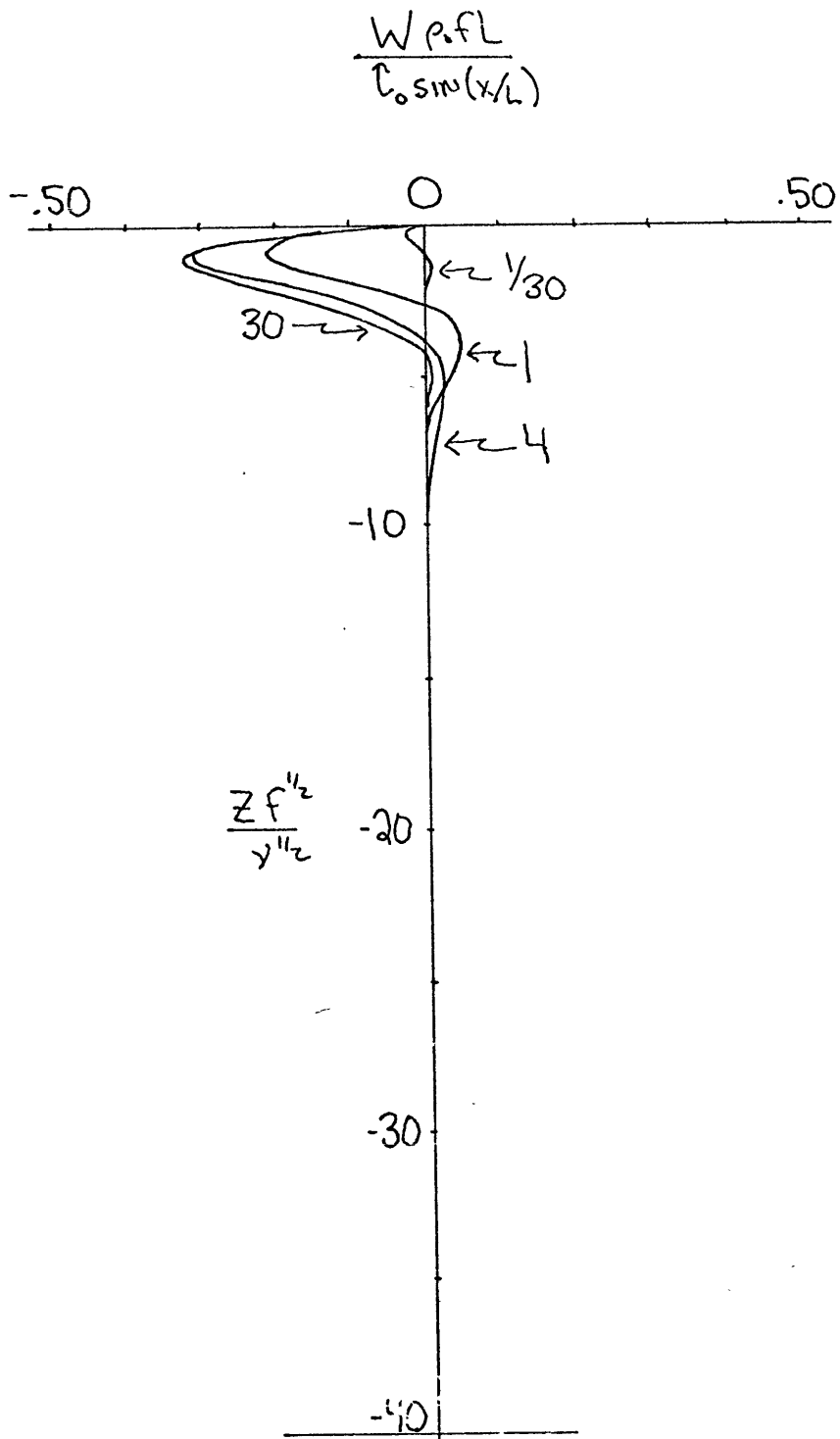


FIGURE 12

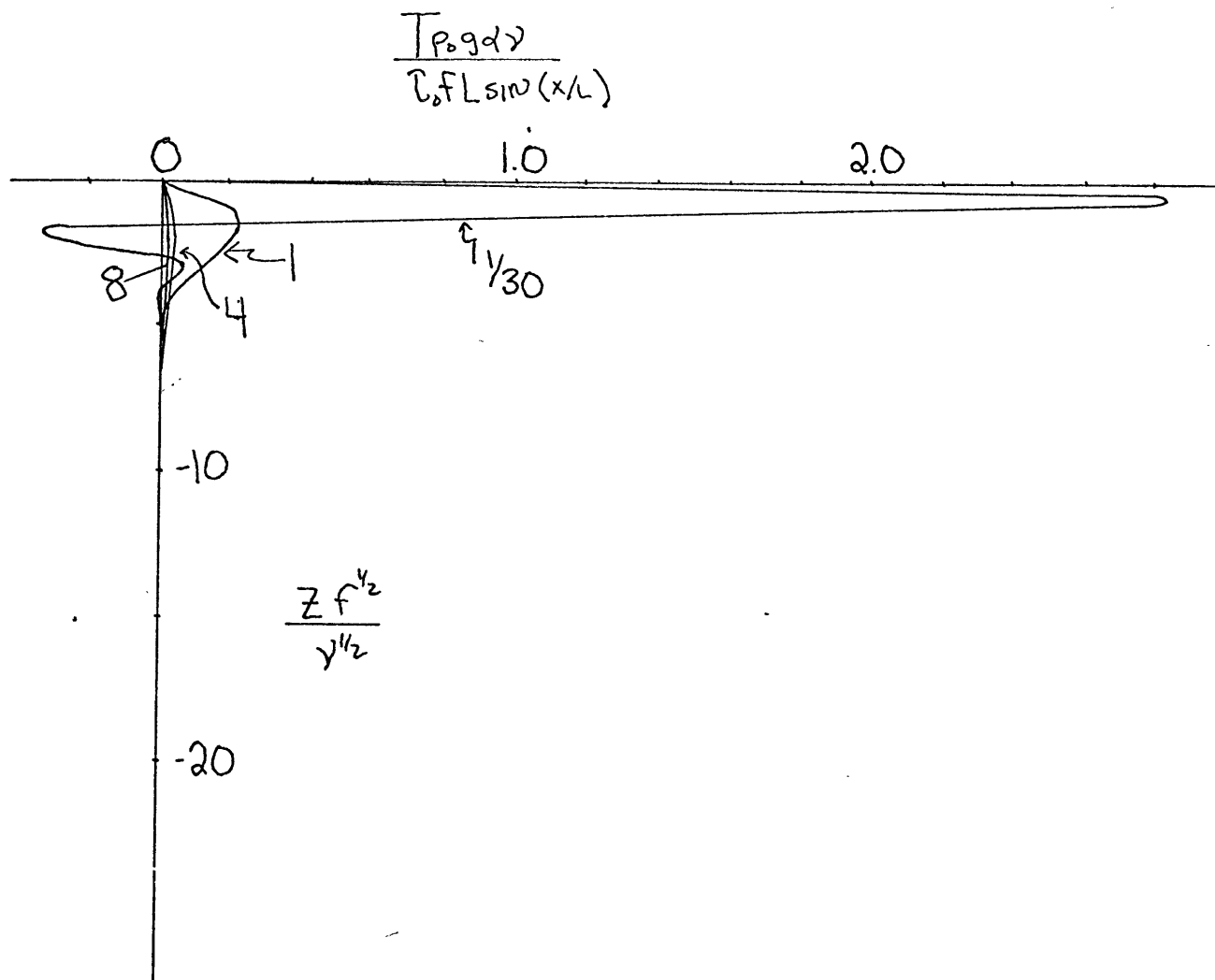


FIGURE 13

NET TRANSPORT TO RIGHT OF STRESS

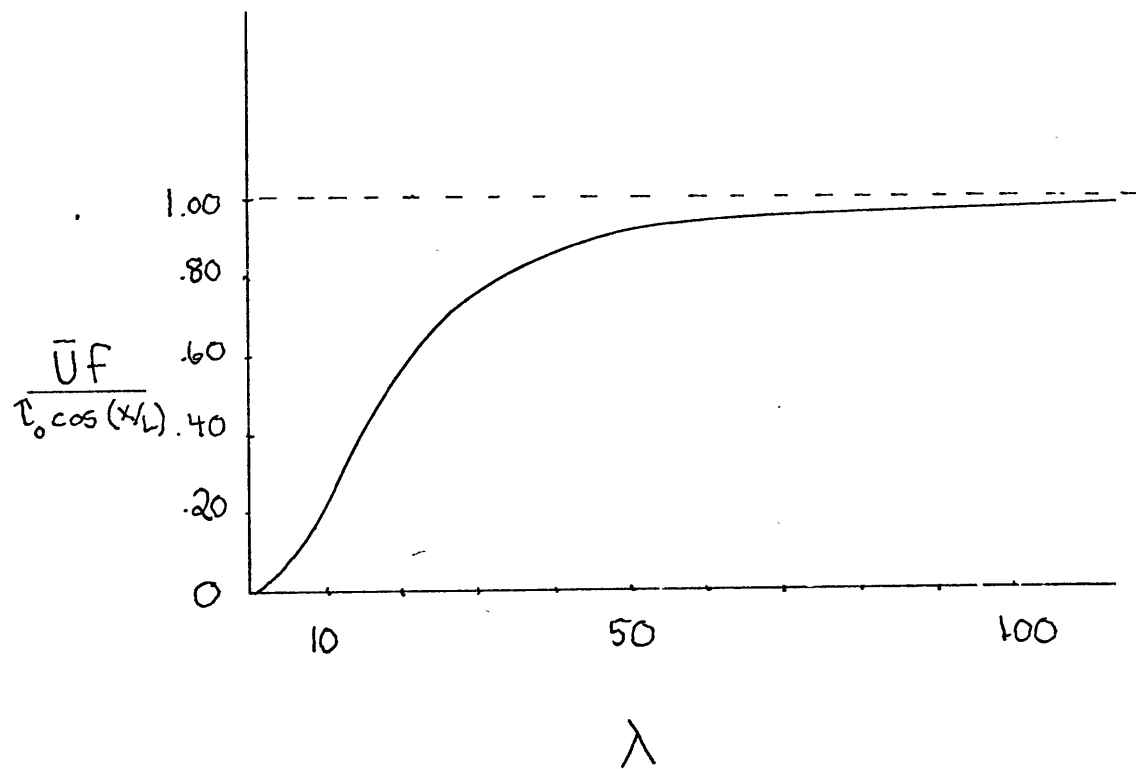


FIGURE 14

3.40 Discussion of Results:

It is clear from these examples that temperature boundary conditions are of primary importance in determining the nature of the solution. A startling example of this is the solution of Example II when the temperature is allowed to be constant in ξ by specifying that $\bar{T}_\xi = 0$ also at $\xi = -40$. The complete solution which is valid for all ranges of stratification, for which the model is valid, is a Couette flow. This is:

$$\bar{U} = \bar{W} = 0$$

$$\bar{V} = (\xi + 40) \cos \kappa$$

$$\bar{T} = \sin \kappa$$

The equations it satisfies are:

$$-\bar{V} = -\bar{P}_\kappa$$

$$0 = \bar{V}_{\xi\xi}$$

$$0 = -\bar{P}_\xi + \bar{T}$$

$$0 = \bar{T}_{\xi\xi}$$

The flow is geostrophic and hydrostatic. The thermal wind

$$\bar{V}_\xi = \bar{T}_\kappa$$

transmits the applied stress from the upper surface directly to the bottom. This solution does not converge to the homogeneous limit. This non-convergence is probably related to the physically unrealistic boundary conditions.

An examination of equation (2) shows that the solution to the pressure equation consists of a Couette flow, in which Π_1, Π_2 can be functions of the stratification, and six exponential terms. As was shown, three of these grow and three decay away from $\xi=0$. For convenience the decaying ones are called the upper solution, and the growing ones, which contribute mainly at $\xi=-\infty$, are called the lower solution.

For $(\sigma\delta\epsilon) \ll \alpha(1)$, as will be shown in section 3.41, the real exponentials correspond to the Lineykin solution, and the complex exponentials are the Ekman solution. Consider a situation in which both the Lineykin and Ekman solutions exist but the separation between the upper and lower surface is large enough so that the upper and lower Lineykin solutions decay to zero before they reach each other. In Example I this occurs for $\lambda \sim b$. Consider the top solution. Integration of the v-momentum equation shows that for each of these exponentials, if 'a' is greater than the decay

$$\int_{-a}^0 u d\xi = \int_{-a}^0 V_{\xi\xi} d\xi = V_{\xi}(0) - V_{\xi}(-a) = V_{\xi}(0)$$

depth, the surface stress is balanced by a body force. In the homogeneous case, all of the surface stress is balanced by a body force in the Ekman layer. Stratification, however, introduces a real exponential which can also balance a stress through a body force. Consequently stratification has introduced two additional solutions among which the surface stress can be distributed--the Lineykin and Couette solutions. In the other limit of $(\sigma\delta\epsilon) \gg \alpha(1)$

(section 3.42) the real and complex exponentials no longer correspond to the Lineykin and Ekman solutions, but the idea of the stress being balanced by the real exponential, the complex exponentials, and the Couette flow still holds.

Table II indicates how the surface stress in Example I is distributed amongst the real exponential, the complex exponentials, and the Couette solution at $\xi=0$ for various values of λ . In the limit of $\lambda \ll o(1)$ all the stress is absorbed by the Couette flow. In the other limit of $\lambda \gg o(1)$, it is not clear which of the solutions does balance the stress. This will be resolved in the next section.

TABLE II

The Distribution of Stress @ $z = 0$

λ	Real Exponential	Complex Exponentials	Couette
0.033	-0.004	0.004	1.00
0.050	-0.006	0.006	1.00
0.100	-0.016	0.016	1.00
0.250	-0.055	0.055	1.00
0.333	-0.083	0.083	1.00
0.500	-0.149	0.149	1.00
1.000	-0.417	0.417	1.00
2.000	-0.856	0.856	1.00
3.000	-0.965	0.965	1.00
4.000	-0.989	0.989	1.00
6.000	-0.998	0.998	1.00
10.000	-1.000	1.000	1.00

3.41 The Limit $(\sigma\delta\epsilon) \ll o(1)$:

As can be seen from Table I, and easily shown, the complex exponentials in this limit correspond to the Ekman solution. For an $O(1)$ applied stress, in the Ekman layer we have $u, v = o(\epsilon^{1/2})$, $w = o(\epsilon)$, $T = o(\sigma\delta\epsilon)$. For the Loneykin solution we get the following equations:

$$\begin{aligned} -\hat{V} &= -\hat{p}_x \\ \hat{u} &= \hat{V}_{\eta\eta} \\ 0 &= -\hat{p}_\eta + \hat{T} \\ 0 &= \hat{u}_x + \hat{w}_\eta \\ \hat{w} &= \hat{T}_{\eta\eta} \end{aligned}$$

where

$$z = (\sigma\delta)^{-1/2} \eta$$

and

$$\begin{aligned} \hat{V}; \hat{p} &= o((\sigma\delta)^{-1/2}) \\ \hat{T} &= o(1) \\ \hat{u} &= o(\epsilon(\sigma\delta)^{1/2}) \\ \hat{w} &= o(\epsilon) \end{aligned}$$

For the Couette flow:

$$\begin{aligned} \bar{V}; \bar{p}; \bar{T}; z &= o(1) \\ \bar{u} = \bar{w} &= 0 \end{aligned}$$

Because the order of magnitude of the temperature in the Lineykin and Couette solutions is much greater than it is in the Ekman solution, these solutions have to satisfy the temperature boundary conditions by themselves. If the boundary condition is, as in Example I, that $T=0$ then $\bar{T} = -\hat{T}$. Through the thermal wind relationship this implies that $\hat{V}_\eta + \hat{V}_z = 0$. Consequently all the stress in this limit is taken up by the Ekman layer.

If we specify, as in Example II, that at $\xi=0$, $T_z=0$, then because $\bar{T}_z=0$ we also have $\hat{T}_\eta=0$. This implies that the top Lineykin solution is absent. (Note: $\hat{T}_\eta=0$ $(\sigma\delta\delta)''''$ We are interested in the cases in which the lower Lineykin solution does not reach the upper surface. In this range of stratification,

$\lambda \sim 10$ or $(\sigma\delta\delta)'''' = \frac{1}{\epsilon^{1/2}\lambda}$, consequently $(\sigma\delta\delta)'''' \sim 4 \sim 0(1)$. Thus we must still require that the upper Lineykin solution vanishes.)

Because $\omega_{EKMAN} + \hat{\omega} = 0$ at $\xi=0$, this also requires that the upper Ekman layer be absent. This Ekman layer will be absent until the stratification is weak enough so that the lower Lineykin solution reaches the upper surface. The heat flux contribution of this solution is small and is of the order of $(\sigma\delta\delta)''''$. This is cancelled by the upper Lineykin solution.

3.42 The Limit $(\sigma\delta\epsilon) \gg \omega$ -- Rotational-Frictional Layer:

The scale depth for this layer, as was pointed out earlier, is

$$z = \left(\frac{E^2}{\sigma\delta\delta}\right)^{1/4} \xi$$

The dynamics of this layer are those of the frictional layer studied by Stommel and Veronis (1957). In the analogy between homogeneous rotating fluids and stratified fluids (Veronis (1967 a,b)), this layer is the thermal equivalent to the Stewartson $E^{1/3}$ -layer. The dynamics of this layer are non-rotating. However, there is a rotational effect. The v -field is a subsidiary calculation once u is known. This coupling is made possible because the system is rotating. The momentum equations for this boundary layer are:

$$0 = -\tilde{p}_x + \tilde{u}_{\xi\xi}$$

$$\tilde{u} = \tilde{v}_{\xi\xi}$$

$$0 = -\tilde{p}_z + \tilde{T}$$

$$0 = \tilde{u}_x + \tilde{w}_{\xi}$$

$$\tilde{w} = \tilde{T}_{\xi\xi}$$

where

$$\tilde{p} = o\left(\left(\frac{E^2}{\sigma\delta\delta}\right)^{1/4}\right)$$

$$\tilde{u} = o\left((\sigma\delta\delta)^{-1/2}\right)$$

$$\tilde{w} = o\left(\left(\frac{E}{(\sigma\delta\delta)^2}\right)^{1/2}\right)$$

$$\tilde{v} = o\left((\sigma\delta\delta)^{-5/4} E^{-1/3}\right)$$

$$\tilde{T} = o(1)$$

The temperature in this layer is assumed to be the same order as the interior temperature, which in this case is $O(1)$. This allows the temperature boundary conditions at the top and bottom surfaces to be satisfied. Setting the temperature scale fixes the rest of the scales. The boundary layer contribution to the surface stress is $O\left(\frac{1}{(\sigma_s \delta E)^{1/2}}\right)$, i.e. $\hat{V}_z \ll O(1)$. However, if as in Example II, the temperature boundary condition can be satisfied by the Couette flow itself, the rotational-frictional layer is absent.

Because there is a thermal $E^{1/3}$ -layer, the question arises; why isn't there a thermal $E^{1/4}$ -layer in this problem? The equations for this layer are the same as those for the thermal $E^{1/3}$ -layer except for the first momentum equation which becomes:

$$\tilde{p}_x = 0$$

This implies that \tilde{T} is independent of χ . However, for these simple solutions, all the variables are functions of x . Consequently this layer does not occur.

3.43 Convergence to the Homogeneous Limit:

Consider the situation in which the separation between the upper and lower surfaces is large enough so that the upper and lower Lineykin solutions essentially decay to zero before they reach each other. As was shown in section 3.40, the fraction of the applied stress taken up by each exponential solution is a direct indication of the net transport to the right of the stress associated with that exponential. Consequently for these solutions which decay rapidly enough, there is no net transport to the right of the surface stress. The integrated transport in the Ekman layer is balanced by an equal, but opposite, integrated transport in the Lineykin layer.

Suppose the stratification is sufficiently weak that the upper Lineykin solution begins to contribute at the lower surface and vice versa. The value of the stress at $\xi = 0$ is then the sum of the upper and lower contributions. This sum is always -1 , but it is no longer simply related to the net transport in the upper Lineykin layer. The upper and lower Lineykin solutions have opposite but equal transports. Consequently as their decay depth gets larger and larger, their transports begin to cancel. For extremely weak stratifications, neither solution decays appreciably in the distance between the upper and lower surface. As a result, the net Lineykin transport in this region is zero; Transports occur only in the lower and upper Ekman layers. This is the homogeneous limit for the u -velocity.

Similar convergences occur for the other fields. In each case the Lineykin solution is instrumental in bringing about this convergence to the homogeneous limit. In figure 15 is illustrated how the Ekman, Lineykin, and Couette solutions combine to give the v -velocity for $\lambda = 100$. It appears that the Lineykin exponentials are well represented for weak stratifications by the first two terms, i.e. $1+z$, in their Taylor expansions. Figure 16 is a similar illustration for the temperature field when $\lambda = 50$.

The interior vertical velocity is essentially given by the Lineykin solution. Recall from section 3.1 that

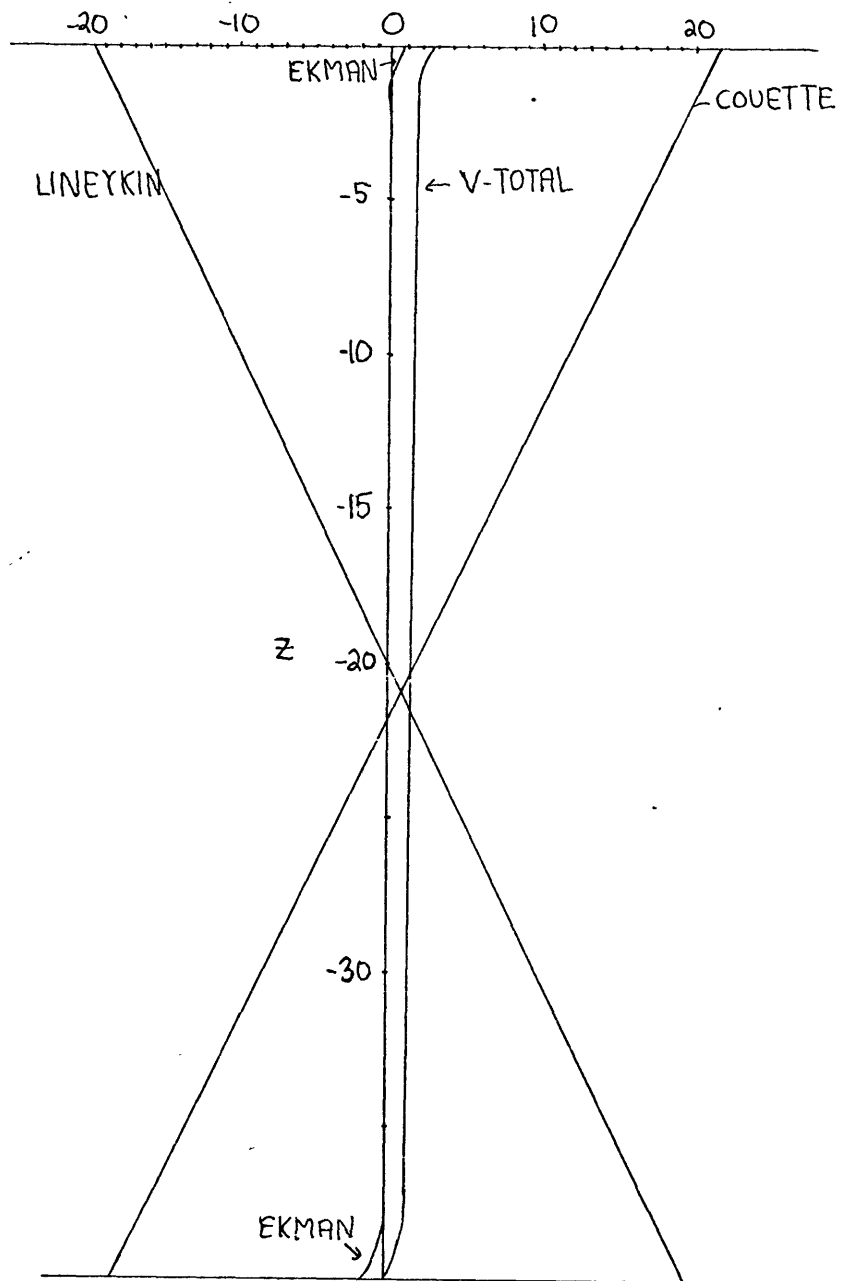
$$\frac{1}{\lambda^2} \omega = T_{\xi\xi}$$

Since the Lineykin solutions are exponentials, $\frac{\partial^2}{\partial \xi^2} \sim \sigma_1^2$. However, σ_1^2 for large λ is proportional to $1/\lambda$. Consequently for large λ

$$\omega_{\text{LINEYKIN}} \approx T_{\text{LINEYKIN}} \approx 1$$

This is the value for the interior vertical velocity in the homogeneous case.

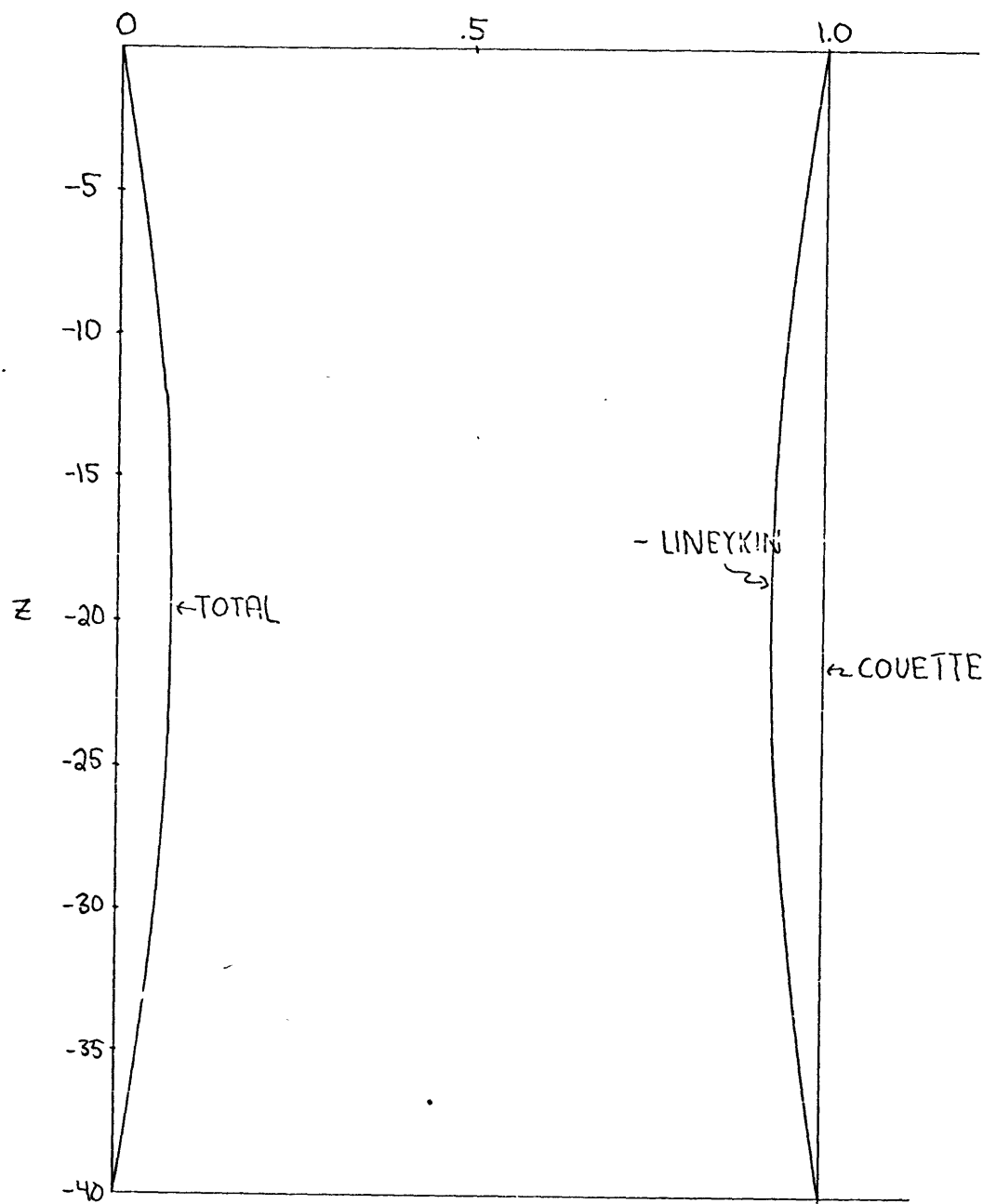
Convergence to the homogeneous limit depends crucially on the fact that the interior cannot satisfy all the boundary conditions by itself and that viscous boundary layers are required to correct the interior fields to the boundary values. This is illustrated in Example II. For strong stratifications, i.e. $\lambda \sim 10$, the interior Couette solution satisfies the boundary conditions at $\xi=0$ by itself. Viscous boundary layers are absent. The convergence



V-VELOCITY

$$\lambda = 100$$

FIGURE 15



TEMPERATURE

$$\lambda = 50$$

FIGURE 16

to the homogeneous limit at $\zeta=0$ does not begin to occur until the stratification is sufficiently weak so that the lower Lineykin solution reaches the upper surface.

Probably the most graphic illustration that convergence to the homogeneous limit requires the presence of viscous boundary layers is the simple problem mentioned in the beginning of section 3.40. In that case the interior solution, a Couette flow, satisfied all the boundary conditions at $\xi=0, -40$; convergence to the homogeneous limit did not occur.

4.0 Comparison with Previous Work:

In the studies of Barcilon and Pedlosky (1967a,b), a stratification (σ/δ) of order $E^{1/2}$ represented an important transition in the dynamics of the fluid. This occurs because the order of the vertical velocity at the base of an Ekman layer driven by velocity boundary conditions is $E^{1/2}$. For stratifications less than this value Ekman layers played a dominant role in the dynamics. For stratifications greater than this, the stratification inhibits the interior vertical velocity to be less than $O(E^{1/2})$. Consequently in this range of stratification the Ekman layers are thought to be non-divergent and viscous-diffusive processes control the dynamics of the fluid.

However if, as in the examples studied here, we specify a stress boundary condition, then the w at the base of the Ekman layer is $O(E)$. Consequently $E^{1/2}$ no longer appears as a crucial stratification. Now divergent Ekman layers can exist, and are influential in the dynamics, up to an $O(1)$ stratification. In fact, as can be seen from Example I, they exist until $(\sigma/\delta) \sim \epsilon^{-1}$ or $\lambda = 1$. At this point the Ekman and Couette layers combine to give the rotational-frictional layer. The details of this merger were previously unknown.

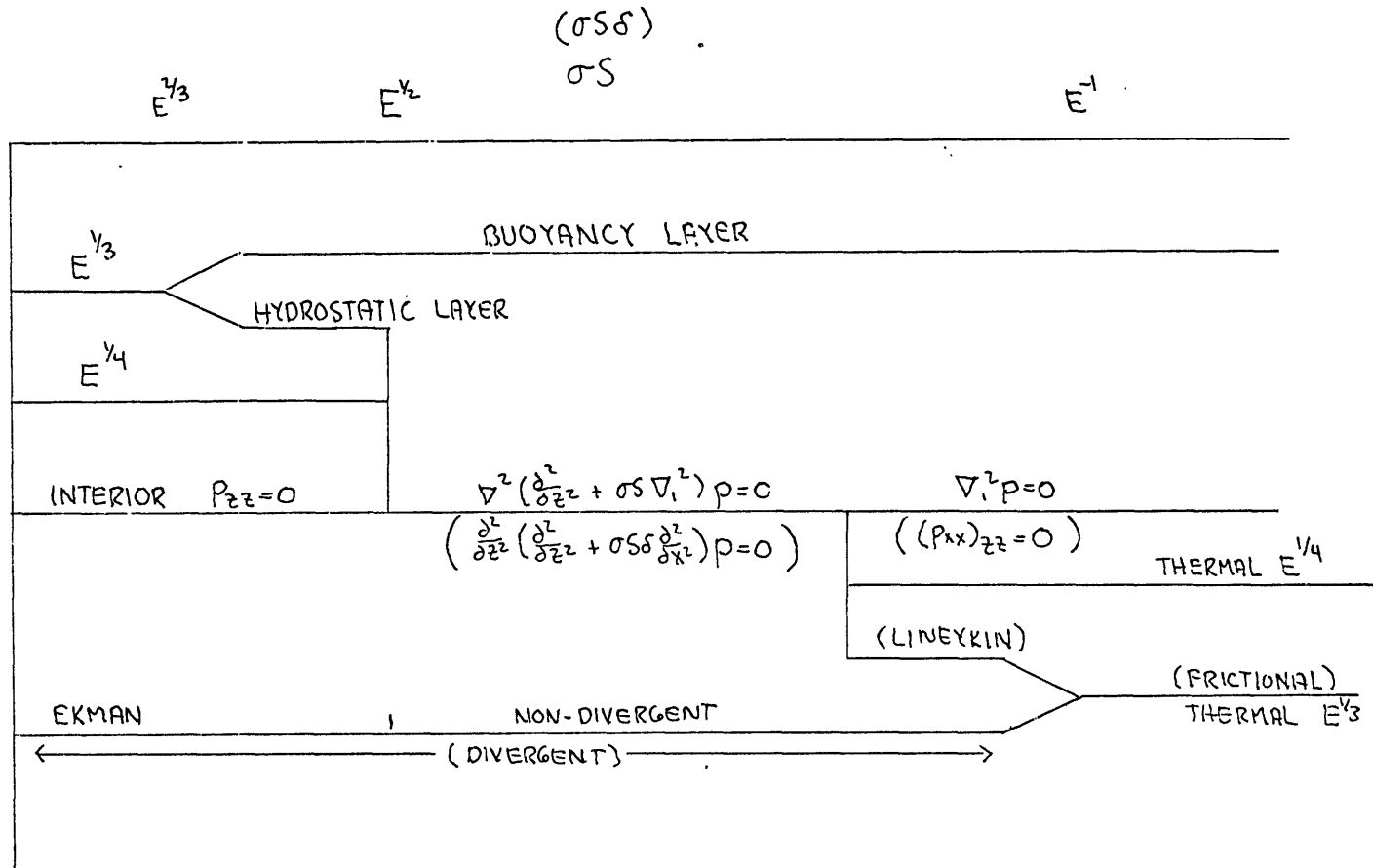
This $O(E)$ flux out of the Ekman layer is absorbed by the Lineykin solution. This solution only exists as a boundary layer for a small range in stratifications less than $(\sigma/\delta) \sim \epsilon^{-3/2}$ or $\lambda \sim 4$. For weaker stratifications the boundary layer merges with the

interior and, as was discussed in the previous section, is instrumental in bringing about the convergence to the homogeneous limit.

The Lineykin layer is physically analogous to the hydrostatic layer (Barcilon and Pedlosky (1967b)). The formal difference occurs only in that for the hydrostatic layer the diffusion of momentum and heat occurs in the horizontal direction while for the Lineykin layer it occurs in the vertical direction. In the examples which were considered, the small aspect ratio and periodic boundary conditions made it possible to neglect the effects of the hydrostatic layer and concentrate primarily on the effects of the Lineykin solution.

A schematic description of the various elements of the dynamics of rotating, stratified fluids as a function of stratification is shown in figure 17. This representation was obtained from Barcilon (1969) (Barcilon and Pedlosky (1967b)). The results of the present investigation are indicated by being enclosed in parentheses.

FIGURE 17



ELEMENTS OF ROTATING, STRATIFIED FLUIDS

5.0 Some Aspects of Thermal Forcing:

All the previous examples which were considered were forced mechanically by applying a stress at $z = 0$. However, some interesting effects occur if the fluid is also thermally forced. Consider the Stommel and Veronis model and apply the following boundary conditions:

$$\text{@ } \xi = 0 : \frac{\partial v}{\partial \xi} = a \cos x$$

$$T = b \sin x$$

$$\frac{\partial u}{\partial \xi} = w = 0$$

$$\text{@ } \xi = -40; \quad u = v = w = T = 0$$

The solution, as in the previous examples, is of the form:

$$P(x, \xi) = \left[\sum_{i=1}^6 \Pi_i \exp(\sigma_i \xi) + \Pi_7 \xi + \Pi_8 \right] \sin x$$

It is easy to show that $\Pi_7 \equiv a$. For $(\sigma \delta \delta \epsilon) < 0$ the solution again consists of Ekman layers, a Loneykin solution, and a Couette flow. As before the Loneykin and Couette solutions have to satisfy the temperature boundary conditions by themselves, i.e.

$$\text{@ } \xi = 0 \quad \hat{T} + \bar{T} = b$$

Here the "—" signifies the Couette solution and the "∧" the Loneykin solution. Since $\bar{T} = \Pi_7 = a$, we have that $\hat{T} = b - a$. Through the thermal wind relationship

$$\hat{V}_\xi = \hat{T} = b - a$$

The stress condition at $\xi = 0$ is

$$\hat{V}_\zeta + \bar{V}_\zeta + V_{E.L.}\zeta = a$$

or

$$V_{E.L.}\zeta = a - b$$

where $()_{E.L.}$ stands for an Ekman layer variable. From this last expression it is clear that thermal forcing can have great effects. The net transport in the Ekman layer is now proportional to $a - b$. For example, if $b = 2a$, then the net transport in the Ekman layer is in fact to the left of the 'apparent' applied stress "a". This results, of course, because of the thermal wind shear associated with the thermal forcing. In the limit $(\sigma\delta\epsilon) \gg \rho\alpha$ the only effect of the thermal forcing would be to modify the solution near $\zeta = 0$. The interior solution would still be the Couette flow

$$\begin{aligned}\bar{V} &= a(\zeta + 40) \cos x \\ \bar{T} &= a \sin x\end{aligned}$$

These solutions of course won't converge to the homogeneous limit unless some provision is made to let the applied temperature perturbation go to zero as the stratification decreases.

PART II

6.0 General Features of Coastal Upwelling:

Frequently along coastlines regions of anomalously cold water appear. These are thought to be caused by upwelling. On the eastern sides of ocean basins upwelling is a common occurrence along the coastlines of Peru and Chile, California, and the west coast of Africa. Wooster and Reid (1963) present a survey of the general oceanic conditions in these regions. Their paper is also an excellent source for references to the literature on upwelling. On the western sides of oceans, the prominent regions of upwelling are the east coasts of Somaliland and Arabia during the southwest monsoon. The details of upwelling vary from place to place and depend strongly on local conditions. In this section only the salient features of the upwelling zones will be discussed. On the basis of some of these a theory of upwelling will be constructed.

The observational studies indicate that there are some general features which are common to all upwelling zones. Upwelling seems to be confined to the surface layers. Sverdrup and Fleming (1941) found the depth of upwelling off California to be about 200 meters. Off Peru and Chile the depth from which upwelled water is brought to the surface rarely exceeds 200 meters (Gunther (1936)). Off the Somali coast this depth appears to be less than 300 meters (Warren, et al. (1966)); off Arabia it appears to be 100-200 meters. The scarcity of systematic observations and the presence of

continental shelves makes it difficult to relate this depth to general oceanic and atmospheric conditions.

The upwelled water has a temperature 2-5°C colder than that of the surface water further offshore. Generally this colder water is fresher than the offshore surface water. The salinity difference is of the order of a couple of tenths of a part per thousand. The density difference between the upwelled water and the offshore surface water varies considerably and is of the order of 1 part in σ_t . The upwelled water has high concentrations of nutrients such as phosphates and silicates but is undersaturated in oxygen. All these features of course vary from place to place and depend strongly on the local conditions. It is difficult, on the basis of the limited information which is available, to determine any systematic variations.

Upwelling is usually confined to a zone within 70 km. of the coast. Within this zone the velocities increase toward the coast. The ship drift observations of Gunther (1936) indicate that the surface drift in the zone is of the order of a knot. Sverdrup and Fleming (1941), using dynamic computations, get a similar value for the surface velocity relative to 100 meters. Comparable surface shears are found off Arabia. By assuming that all the upwelled water moves offshore in the mixed layer in which the magnitude of the offshore velocity can be estimated by assuming Ekman layer dynamics, Sverdrup and Fleming (1941) obtain estimates for the vertical and offshore velocities in the upwelling zone. The offshore velocity is of the order of 10 cm/sec. This requires a vertical

velocity in the upwelling zone of 10^{-2} - 10^{-3} cm/sec. All of these values of course depend on the magnitude of the wind. In the upwelling situation Sverdrup and Fleming studied, this was about 16 knots.

The regions of strong upwelling are of limited extent along the coast. Their extent along the coast is of the order of hundreds of kilometers, and they are separated from one another by regions with higher surface temperatures. There seems to be little correlation between the location of the zones and bottom topography (Gunther (1936)). However, the regions of strong upwelling occur frequently at capes. This, no doubt, is related to the winds which generally are strongest in these regions. There is a strong correlation between the strength of the component of a wind parallel to a coast and upwelling (Wooster and Reid (1963)). Variable winds consequently make the upwelling process strongly time dependent. No systematic observations have been made to study the response time for upwelling. However, an estimate of this can be made by computing the time required for water to ascend from a characteristic depth of upwelling, i.e. 100 meters, to the surface. For w of the order of 10^{-2} - 10^{-3} cm/sec, this takes 10-100 days. This consistent with observations (Sverdrup and Fleming (1941); Smith, et al (1966)) which indicate that the general features of the upwelling zone are set up in a period of a week or so.

The upwelling zones on the western side of the ocean basins appear to be quite similar to those on the eastern side. However, on the western side there is an additional complicating factor.

Off Somaliland, during the southwest monsoon, it isn't clear whether the upwelling is due to the local winds, i.e. to the off-shore transport in the mixed layer, or to the Somali Current. The Somali Current as it crosses the equator and flows northward increases in transport and begins to feel the effects of the earth's rotation. Consequently the density surfaces rise toward the coast. This process will be called geostrophic upwelling. When the current reaches a steady state, no more water is upwelled and the surface oxygen values, close to the coast, should reach saturation. However, near the Somali coast, several months after the onset of the southwest monsoon, the surface oxygen values are only 60% of saturation (Warren, et al, (1966)). This either indicates that the current is not yet in steady state or that water is being forced away from the coast in the surface layers. Close to the Somali coast extremely cold water, which is about 8°C colder than the off-shore surface water, is brought to the surface. This extreme upwelling probably occurs because the two types of upwelling are acting concurrently.

At about 9°N the Somali Current leaves the coast so that further north, off the Arabian coast, the strong geostrophic upwelling associated with the Somali current is absent. In Appendix A are shown temperature, salinity, and oxygen profiles along three sections off the Arabian coast during the southwest monsoon. From these profiles some general features of the flow close to the coast are immediately apparent.

6.1 Arabian Upwelling:

There appears to be little continuity in the surface currents along the coast. In section C, a hot, saline surface current, 29.9°C 36.15‰, flows next to the coast. Its high temperature and salinity indicate that the origin of this water is probably the Gulf of Aden. Note that this water does not appear in section B. Although cold water is not directly at the surface at the shoremost station (5006) of this section, water of 20°C and 2 ml/l oxygen is found 20 meters below the surface. The surface temperature at this station is 26.8°C. This indicates that upwelling has probably recently stopped. The upwelled water appears to be drawn from a depth of 100-150 meters. Dynamic calculations indicate that at station 5008, the geostrophic velocity at the surface relative to 50 meters is 80 cm/sec.

At section B active upwelling is in progress. At station 5033 water of 19.8°C and a salinity of about 35.65‰ is at the surface. The oxygens are 50% of saturation. Near the edge of the upwelling zone at stations 5036, 5037 the geostrophic velocity shear in the top 100 meters is 40 cm/sec/100 meters. The extremely warm and saline water found next to the coast in section C probably lies at the right edge of this profile.

The conditions at section A indicate that upwelling is in progress. Water of 18.9°C and 35.68‰ is found at the surface at station 5047. The oxygen values are 50% of saturation. From the water mass characteristics and geostrophic calculations there again

appears to be a current running parallel to the coast in the surface layers. The geostrophic velocity shear at stations 5049 and 5050 near the edge of the upwelling zone is about 50 cm/sec/100 meters. It is difficult to tell where the water in this current originates. The surface temperature, salinity and oxygen values about 160 kilometers from the coast in profile B are similar to those found close to the coast in this section so this might indicate some continuity of flow between these two sections.

Water in these three sections appears to upwell from a depth of 100-150 meters. In all three sections there exists a narrow coastal current whose width is about 20 kilometers within which there are large geostrophic shears. This coastal current appears not to be continuous. Consequently it might be related to the local upwelling. This is to be expected because the upwelling tilts the density surfaces up towards the coast, and this results in a geostrophic current which runs parallel to the coast.

The salinity profiles are all very confused, which makes it difficult to trace water movement at intermediate depths. This is similar to what Hamon (1967) found in this region. This confused picture probably is directly related to the several sources of different salinity such as the Persian Gulf and the Gulf of Aden which are found in this region. From profiles A and C it appears that there might be a movement of water at 200-300 meters along the coast because of the oxygen values over .5 ml/l. However, at profile B, next to the coast, no values greater than .3 ml/l are found at 200 meters. Furthermore the salinity at this depth next to the coast

for this section is higher than it is either in section A or C. Consequently there probably is no continuity in this flow next to the coast at 200 meters. This is in contrast with what is observed in the upwelling zones along the eastern sides of ocean basins.

6.2 Poleward Counter-Currents:

On the eastern sides of the ocean basins are found deep poleward countercurrents whose axes lie at about 300 meters. These are described in the article by Wooster and Reid (1963). The counter-currents are found in both hemispheres and transport water from equatorial regions toward the poles. Their high temperature, salinity, and low oxygen values--water mass properties characteristic of equatorial water--enable the counter-currents to be traced into mid-latitudes. These features can be seen in figure 1, in which a profile off Chile is exhibited. The counter-current has a width of 30-50 kilometers, and its velocity along the coast is 10-20 cm/sec (Wooster and Gilmartin (1961)). This current is thought to supply part of the water which is upwelled. Because of this, it is commonly called a compensation current. However, there are indications that this might not be the case. Observations off California (Reid, et al. (1958)) show that this current is in fact strongest during the winter, i.e. when the upwelling is essentially absent. During the spring and early summer, when upwelling is strongest, the current is weakest. This is exactly opposite of what simple dynamical models, which attribute the origin of the current to β -effects, would predict (Latun (1962), Yoshida (1967)). Furthermore, when the current is strongest, it reaches to the surface; however, during periods of upwelling it is destroyed above 200 meters. Consequently the possibility exists that this current, instead of

being a compensation current, is a result of a different physical process.

An examination of the dynamic topography of the 200 db surface with respect to the 1000 db surface (Wooster and Reid (1963)) shows that a narrow pressure gradient of the right sense to drive this countercurrent exists along the coast. This pressure gradient is confined to within 100 kilometers of the coast. The existence of a pressure gradient, of the same width as the upwelling zone, in the same region as the upwelling zone, indicates that it is probably in some way related to the upwelling.

Because the main oceanic thermocline is shallower in equatorial regions than in mid-latitudes, upwelling in low latitudes brings to the surface water whose temperature is not much warmer than the upwelled water in mid-latitudes even though the surface temperature in equatorial regions is much higher than it is in mid-latitudes. However, the salinity of equatorial water is much higher than that of water in mid-latitudes. Consequently the density of upwelled water in low latitudes can be greater than it is in mid-latitudes. This density difference, integrated throughout a water column, would produce a poleward pressure gradient, of limited width, such as is observed.

An examination of Gunther's data shows that the density of upwelled water tends to be greater in low latitudes than in middle latitudes. The difference in σ_t between low and middle latitudes is about .10-.30. Of course, strong upwelling in high latitudes can reverse this density difference.

It also appears that, at least off South America, upwelling in low latitudes is more persistent and stronger than it is in middle latitudes. One factor which might contribute to this is the simple Ekman notion that the offshore transport in the mixed layer is of the order of τ/f , where τ is the magnitude of the wind stress and f is the Coriolis parameter. This relationship indicates that for two upwelling zones of equal width in which the wind stresses are equal, the upwelling is more intense in the one that is at the lower latitude. Over a period of time, this would have the tendency to produce the proper pressure gradient.

However, off the Arabian coast the distribution in density of upwelled water, if anything, is such as to produce an equatorward pressure gradient, i.e. opposite to that observed off Peru and Chile. The upwelling is also probably more uniform in time and space because the Arabian coastline is of limited north-south extent and the monsoon winds are relatively steady. These factors might not be conducive to the formation of a counter-current which probably depends on north-south variations in the upwelling.

6.3 Lateral Mixing in the Upwelling Zone:

Estimates of the horizontal, turbulent diffusivity off the California coast were made by Sverdrup and Fleming (1941). Guided by observations of the mean distribution of water mass properties along σ_t -surfaces, they deduced that the horizontal diffusivity was of the order of 10^6 cm²/sec. Horizontal eddies, 20-40 kilometers in diameter were observed in the flow field. These were thought to be responsible for a lateral exchange of this order. Clearly if these eddies were important in the exchange process in the upwelling zone, whose scale is comparable to that of the eddies, it would be difficult to maintain the integrity of the upwelling zone. Furthermore, upwelling off California is highly time dependent and the eddies themselves, to some extent are products of upwelling. As the upwelling progresses, the pressure gradient normal to the coast increases, and the velocity parallel to the coast grows larger. Instability or irregularity in the flow tends to create these eddies which in turn limit the growth of the velocity.

Consequently the value, 10^6 cm²/sec, is probably a gross over-estimation of the importance of lateral friction within the zone. The "actual" eddy coefficient is probably several orders of magnitude less than this. However, its magnitude is unknown and probably varies from location to location. To make estimates of horizontal Ekman numbers in section 7.1, a value of 10^4 cm²/sec will be settled on. Most likely the value 10^6 cm²/sec is a more appropriate one to

describe the mean conditions away from the upwelling zone. However, because we are interested in studying the dynamics of the zone itself, the smaller value will be used in the order of magnitude estimates. The theory will be constructed so that it does not depend on the value of this coefficient.

It is instructive to make an estimate of the relative importance of horizontal to vertical exchange processes within the upwelling zone. This is done using the value, 10^6 cm²/sec, for the eddy coefficient even though this is probably much too large. This calculation indicates that vertical mixing is at least an order of

$$\nu_H \frac{\partial^2}{\partial x^2} / \nu_V \frac{\partial^2}{\partial z^2} = \frac{10^6 (3 \times 10^4)^2}{10^3 (5 \times 10^6)^2} \sim \frac{1}{25}$$

magnitude more important than lateral mixing. A smaller lateral diffusivity would of course further decrease this ratio. These considerations indicate that the dynamics of the upwelling zone should not be strongly influenced by lateral friction.

However, because of the strong effects lateral friction has in some of the cases of rotating, stratified fluids studied by Barcilon and Pedlosky (1967a,b) and Veronis (1967a,b), its effects will be considered in Appendix B. It is shown there that for the theoretical model which is considered, the effects of lateral friction are unimportant.

6.4 The Boundary Condition at a Coast:

In a model of the upwelling zone in which lateral friction is neglected, it is impossible to satisfy all the boundary conditions on the temperature and velocity fields at a coast. In practice oceanic coasts are ill-defined and are far from being vertical walls. There appear to be heat fluxes (see fig. 1) through these "walls" at least on the scale on which observations have been made. The precise boundary conditions at such a coast are unknown. Consequently the only boundary condition which will be imposed is that there be no normal flow through the coast.

However, in the published studies of rotating, stratified fluids mentioned in the previous section, the condition of normal flow at a wall is intimately connected to the thermal boundary condition there. Satisfaction of the thermal boundary condition can induce a circulation which can modify the interior solution. It is shown in Appendix B, that for the model which will be considered, that the inclusion of lateral friction, which allows the heat flux to be brought to zero, does not modify the solution.

6.5 Consideration of β -Effects:

North-south motion on a β -plane creates a vertical velocity. If β -effects are negligible in an upwelling model, this w must be much less than the one caused by the diffusion of relative vorticity. In the linear theory the vorticity equation is of the form:

$$\beta v = f \omega_z + \text{DIFFUSION OF RELATIVE VORTICITY}$$

Consequently the w created by β -effects is of the order of

$$\omega_\beta = \frac{\beta}{f} \sigma(v) \sigma(z) \sim \frac{2 \times 10^{-13}}{10^{-4}} \times 50 \times 10^4 \sim 10^{-3}$$

This can be of the same order as the vertical velocities actually observed in the upwelling zone. However, for the sake of simplicity, the theoretical model which will be considered will ignore β -effects.

In geostrophic upwelling as a current flows poleward the upwelling becomes more intense because the value of the Coriolis parameter increases, i.e. because of the β -effect.

7.0 An Upwelling Model:

In the previous sections, some observational features of the upwelling zones have been examined. For a theoretical analysis, the simplest coastal model would seem to be a vertical coast at $x=0$ with a uniformly stratified ocean extending to $x=-\infty$. A steady stress in the y -direction (i.e. parallel to the coast) is applied everywhere at the surface. The rotation vector is vertical ($f > 0$) and constant. As before, we assume that the linearized equations are valid. The effects of lateral friction and conduction will also be ignored except that some discussion of their role is made in Appendix B. With these assumptions, the set of dynamical equations is that which was studied in the Stommel and Veronis model of Part I.

A solution to this problem is postponed until section 7.30. As a preliminary to this problem, section 7.20 analyses a somewhat similar problem in which the coast is moved to $x = +\infty$, and the uniform stress is replaced by an alternating square wave distribution. The similarity arises in that in the square wave solution, u vanishes when the stress changes sign, and to this extent, such places may be considered as a "coast". This method of solution is motivated by considering the regions of different sign of the stress as being "images" of each other, and the solution is obtained in the sense of the "method of images".

7.1 Formulation of Equations:

The set of non-dimensional, linear equations with lateral friction included is:

$$\begin{aligned} -V &= -\rho_x + E_H u_{xx} + E_V u_{zz} \\ u &= E_H v_{xx} + E_V v_{zz} \\ 0 &= -\rho_z + T + \delta^2 (E_H w_{xx} + E_V w_{zz}) \\ 0 &= u_x + w_z \\ (\sigma_V \delta \delta) w &= (\sigma_H / \sigma_H) E_H T_{xx} + E_V T_{zz} \end{aligned}$$

where

$$E_H = \frac{\gamma_H}{fL^2} ; E_V = \frac{\gamma_V}{fD^2} ; \sigma_V = \frac{\gamma_V}{K_V} ; \sigma_H = \frac{\gamma_H}{K_H}$$

The constant eddy viscosity coefficients in the horizontal and vertical directions are respectively, γ_H, γ_V ; the constant eddy coefficients of thermometric conductivity in the horizontal and vertical directions are K_H, K_V . The assumptions in deriving this set of equations and the non-dimensionalizations are the same as in Part I. The horizontal and vertical Prandtl numbers are both assumed to be of order unity.

In the estimation of the above parameters, the following numerical values are used: $f \sim 10^{-4} \text{ sec}^{-1}$; $\Delta T_V = 10^\circ \text{C}$; $d = 2.5 \times 10^{-4} \text{ T}^{-1}$
 $L = 1000 \text{ km.}$; $D = 1000 \text{ METERS.}$, $\gamma_V = 10^3 \text{ cm}^2/\text{sec.}$; $\gamma_H \sim 10^4 \text{ cm}^2/\text{sec.}$

A discussion of the value used for γ_H has already been made in section 6.3. The value used for D is an order of magnitude estimate

of the depth of the main thermocline. Because we are thinking of a system which has a mean stratification, we want D to represent the depth over which this stratification occurs. In the ocean this is a thermocline depth. The value of L is not a measure of the total width of an ocean basin. The only restriction on L is that $L \gg L_0$, where L_0 is a natural length scale defined in terms of the other parameters in the problem. Physically L_0 is the width of the upwelling zone, which at this point is still undetermined in terms of the parameters of the problem. In the square wave problem L is proportional to the wavelength of the square wave. For the semi-infinite ocean, where there is no other horizontal length scale than L_0 , the restriction is made that $L \gg L_0$. The width and dynamics of the upwelling zone will be shown to be independent of L . For convenience in estimating E_H , L is chosen to be 1000 kilometers. Using these values one gets that:

$$E_H \sim 10^{-8} \quad ; \quad E_V \sim 10^{-3}$$

$$(\sigma_V \delta \delta) \sim 2.5 \times 10^{-3} \quad ; \quad \lambda \sim 600$$

The nature of the dynamics depends on the relative magnitudes of these. From the above estimates and from those made in section 6.3, it appears that the effects of lateral friction, on the scales we are concerned with, are small. Formally the restriction is made that:

$$E_H \ll (\sigma_V \delta \delta) E_V$$

This implies, in terms of the formalism of Barcilon and Pedlosky (1967b), that the parameter $(\sigma_V \delta \delta)$ as compared to E_H puts the

fluid into the very strongly stratified regime. Here Ekman layers are absent, and the only vertical boundary layer of the type considered by Barcilon and Pedlosky, in which horizontal viscosity is important, is the buoyancy layer. It is shown in Appendix B that this layer has negligible dynamical influence. A comparison of $(\sigma_v \delta)$ with ϵ_v indicates that we are in the essentially homogeneous regime in which Ekman layers exist and play a dominant role is the interior dynamics. As is shown in section 7.30, a vertical boundary layer, in which vertical viscosity is important, is also present.

Consequently a set of equations is considered in which all terms of order $\epsilon_H, \delta^2 \epsilon_H, \delta^2 \epsilon_v$ are neglected. This set is:

$$\begin{aligned} -v &= -p_x + \epsilon_v u_{zz} \\ u &= \epsilon_v v_{zz} \\ 0 &= -p_z + T \\ 0 &= u_x + w_z \\ (\sigma_v \delta) w &= \epsilon_v T_{zz} \end{aligned}$$

These can be combined to give the following equation:

$$\epsilon_v^2 p_{zz} + p_{zz} + (\sigma_v \delta) p_{zzxx} = 0 \quad (2')$$

7.2 The Square-Wave Stress Model:

Consider a model, in which the applied stress is a square-wave. This stress can be represented as a Fourier sine series. Consequently the solution can be represented as a sum of the single sine wave solutions which were studied in Part I. The physics of each of these is well understood. By knowing how these sum to give a solution, a physical understanding of the square-wave problem can be obtained. This solution is not expected to differ significantly from the case in which the stress does not drop to zero. Consequently the insight obtained from this approach enables us to solve the problem using boundary layer techniques. This in turn will indicate the dependence of the solution upon the parameters.

The actual series which will be used is the sine series modified through the introduction of the Lanczos convergence factors (Lanczos (1956)). This new representation reduces the Gibbs phenomena, which occurs near the points of discontinuity in the stress, to about a 2% overshoot. It also insures rapid convergence of the series. In the square wave representation, the small wave-length components contribute primarily in the region close to where the stress drops to zero. Recall that

$$(\sigma_v S \delta) = \left(\frac{1}{k_v} \frac{g \Delta T}{f^2 L} \frac{D}{L} \right)$$

Consequently decreasing the horizontal length scale is equivalent to increasing the mean stratification. This means that near points

of discontinuity in the stress, the stratification is effectively increased. The flow in these regions would consequently be similar to the cases of strongly stratified flow studied in Part I.

Because of the special nature of the applied stress, u , v , T_x are proportional to the sine of x . Consequently in the regions in which the stress drops to zero, i.e. where $\sin x$ is zero, all three of these fields are also zero. If a coast is imagined to exist at this point, the boundary conditions of no normal flow, no tangential flow, and no heat flux are automatically satisfied.

Consider Example II in Part I with the following stress applied at the surface, $z=0$:

$$\rho_0 \nu \frac{\partial v}{\partial z} = \tau_0 \begin{cases} 1 & nL < x < (n+1)L & n \text{ even} \\ -1 & nL < x < (n+1)L & n \text{ odd} \end{cases}$$

The other boundary conditions remain as before:

$$\begin{aligned} @ z=0 & \quad \rho_0 \nu \frac{\partial u}{\partial z} = 0 \\ & \quad \frac{\partial T}{\partial z} = w = 0 \\ @ z=-D & \quad u=v=w=T=0 \end{aligned}$$

The applied stress can be represented as the following Fourier series:

$$\tau = \frac{4}{\pi} \tau_0 \sum_{n=1}^{\infty} \frac{\sin \left[\frac{(2n-1)\pi x}{L} \right]}{(2n-1)}$$

This representation has the Gibbs phenomena near the points of discontinuity in the stress. To reduce this to about a 2% overshoot,

and to insure rapid convergence, the representation is modified through the introduction of the Lanczos convergence factors (Lanczos (1956)). The new representation is:

$$\hat{u} = \frac{4}{\pi} \int_0^m \sum_{n=1}^m \frac{\sin\{[(2n-1)\pi]/2m\}}{[(2n-1)\pi/2m]} \frac{\sin[(2n-1)\pi x/L]}{(2n-1)}$$

The number of terms, m , which is kept in the present example is 80. This large number is used to insure that the solution near the coast is well represented. The maximum number that can be used is determined by the scale on which lateral friction becomes important. This is much larger than 80 for the example which is considered. The applied stress is illustrated in figure 18. The width of a basin can be thought to be one-half of a square-wave. In the non-dimensional units which will be used for x , this is π radians.

We recall that equation (1') is:

$$P_{\delta\zeta} + P_{4\zeta} + (\sigma_v S \delta E_v) P_{xx\zeta\zeta} = 0 \quad (1')$$

The boundary conditions are:

$$\begin{aligned} @ \zeta = 0; \quad \frac{\partial v}{\partial \zeta} &= \sum_{n=1}^m L^{(n)} \frac{\sin[(2n-1)x]}{(2n-1)} \\ \frac{\partial u}{\partial \zeta} &= \frac{\partial \zeta}{\partial \zeta} = w = 0 \end{aligned}$$

$$@ \zeta = -40 \quad u = v = w = T = 0$$

where

$$L^{(n)} = \frac{\sin\{[(2n-1)\pi]/2m\}}{[(2n-1)\pi/2m]}$$

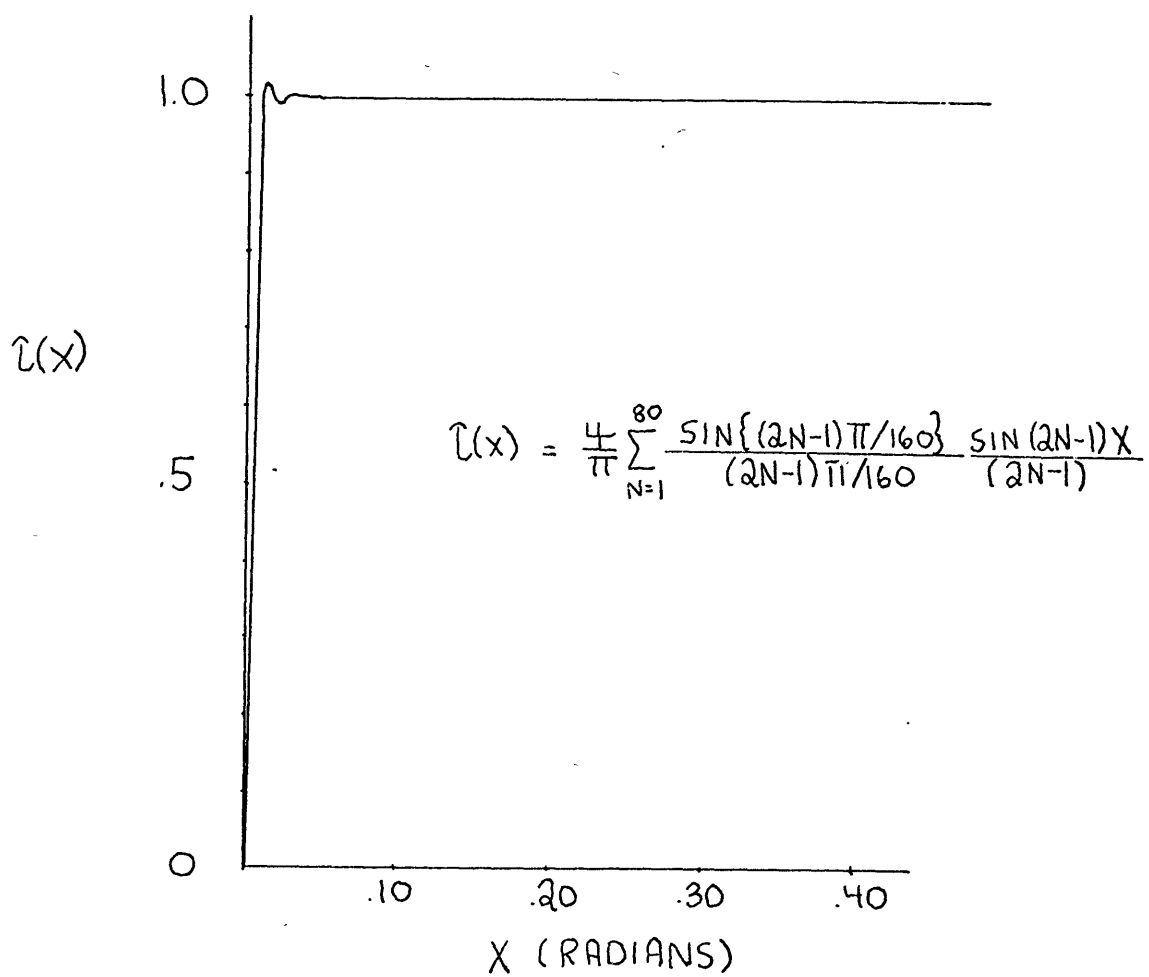


FIGURE 18

In this square-wave problem there actually has been a slight change in the non-dimensionalization. For computational convenience the non-dimensionalizations are:

$$\begin{aligned} (u', v') &= \frac{4C_0}{\rho_0 \pi (\lambda/f)^{1/2}} i_z(u, v) \\ w' &= \frac{4C_0}{\rho_0 f L} w \\ T' &= \frac{4C_0 f L}{\pi^2 \rho_0 g d^2} T \\ P' &= \frac{4C_0 f^{1/2} L}{\pi^2 \nu^{1/2}} P \\ x &= \frac{L}{\pi} x \quad ; \quad z = (\lambda/f)^{1/2} \xi \end{aligned}$$

The solution is of the form:

$$P = \sum_{n=1}^{\infty} P_n(x, \xi)$$

where

$$P_n(x, \xi) = \frac{L^{(n)}}{(2n-1)^2} \cos[(2n-1)x] \hat{P}_n(\xi)$$

The $\hat{P}_n(\xi)$ satisfy the following equation

$$\hat{P}_{n8\xi} + \hat{P}_{n4\xi} - (\sigma_v \delta \epsilon_v) (2n-1)^2 \hat{P}_{n2\xi} = 0$$

and are subject to the boundary conditions:

$$\begin{aligned} @ \xi = 0 \quad & \hat{P}_{n\xi} - \frac{\lambda^2}{(2n-1)^2} \hat{P}_{n\eta\xi} = -1 \\ & \hat{P}_{n5\xi} = 0 \\ & \hat{P}_{n3\xi} = 0 \\ & \hat{P}_{n2\xi} = 0 \end{aligned}$$

$$\begin{aligned} @ \xi = -40 \quad & \hat{P}_n - \frac{\lambda^2}{(2n-1)^2} \hat{P}_{n6\xi} = 0 \\ & \hat{P}_{n4\xi} = \hat{P}_{n3\xi} = \hat{P}_{n\xi} = 0 \end{aligned}$$

The analytic solution for each $\hat{P}_n(z)$ is similar to that found in Example II with the following minor changes. The σ_n 's now satisfy:

$$\sigma_n^6 + \sigma_n^2 - (\sigma_v S \delta E_v) (2n-1)^2 = 0$$

The sign of the applied stress is also changed in the boundary conditions. This occurs because now $p \sim \cos x$.

The other fields are represented in terms of the pressure as follows:

$$\begin{aligned} T(x, z) &= \sum_{n=1}^m L^{(n)} \frac{\cos(2n-1)x}{(2n-1)^2} \hat{P}_{n3z}(z) \\ w(x, z) &= \sum_{n=1}^m L^{(n)} \lambda^2 \frac{\cos(2n-1)x}{(2n-1)^2} \hat{P}_{n3z}(z) \\ u(x, z) &= \sum_{n=1}^m L^{(n)} \lambda^2 \frac{\sin(2n-1)x}{(2n-1)^3} \hat{P}_{n4z}(z) \\ v(x, z) &= \sum_{n=1}^m L^{(n)} \frac{\sin(2n-1)x}{(2n-1)} \left[-\hat{P}_n(z) + \frac{\lambda^2}{(2n-1)^2} \hat{P}_{n6z}(z) \right] . \end{aligned}$$

As was shown, the value of λ is between 10^2 and 10^3 for the values of the parameters which were used. For this example, λ is chosen to be

$$\lambda = (\sigma_v S \delta E_v)^{-1/2} = 400$$

The solutions for each individual sine wave were computed and summed numerically. The complete solutions for the velocity fields and the temperature are shown in figures 19-22. A stream function can be defined as follows:

$$\psi_x = w. \quad ; \quad \psi_z = -u$$

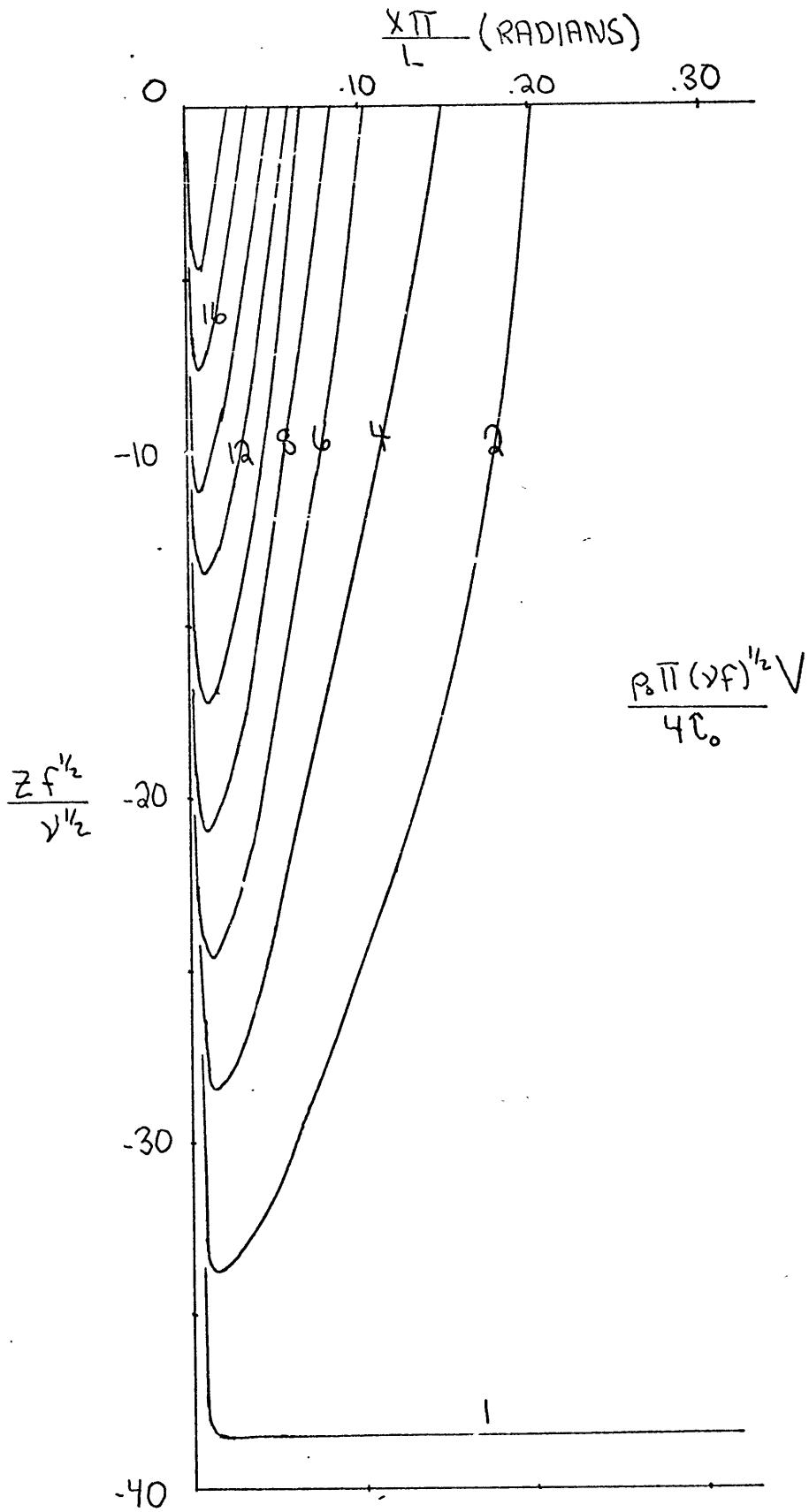


FIGURE 19

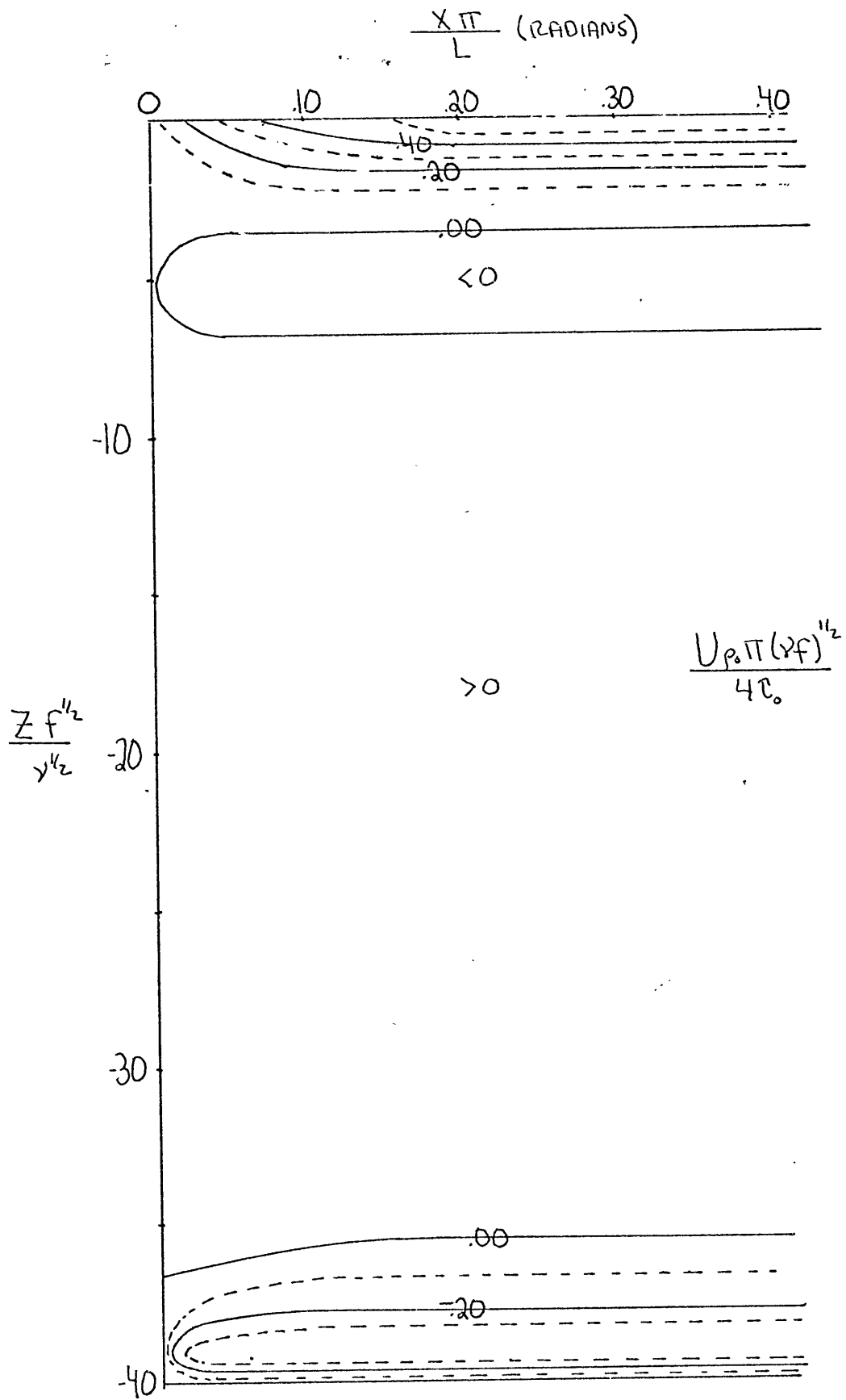


FIGURE 20

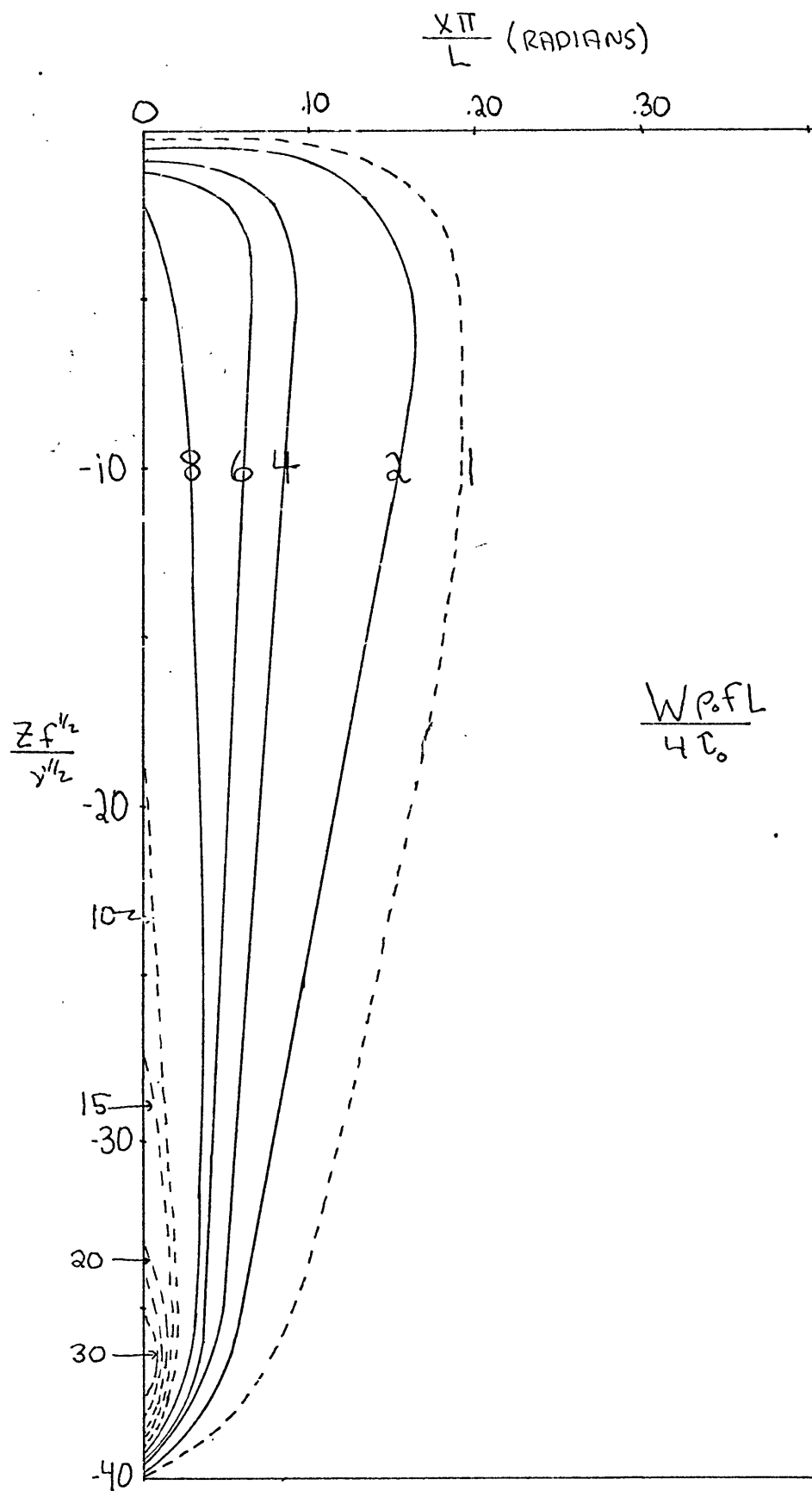


FIGURE 21

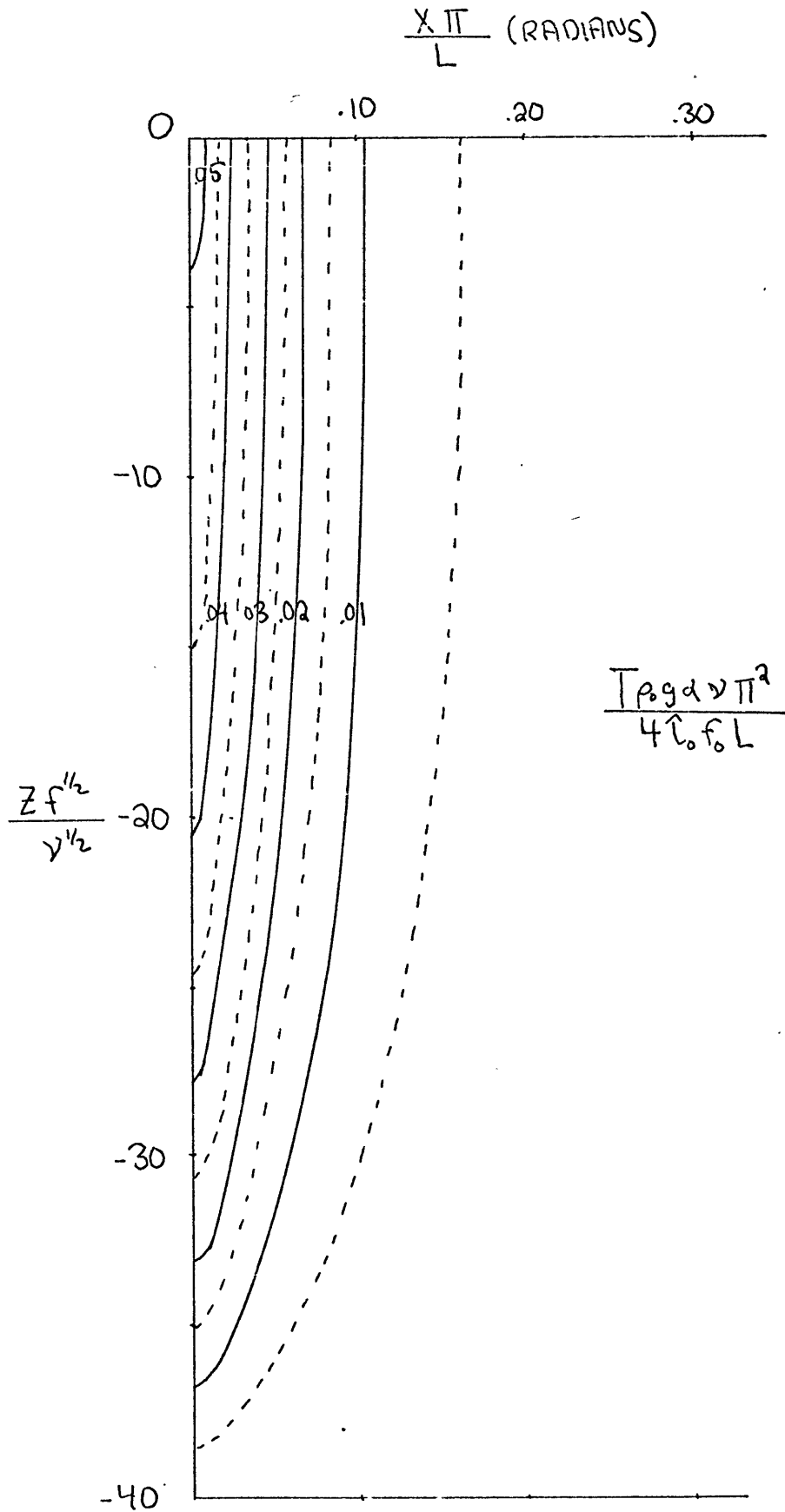


FIGURE 22

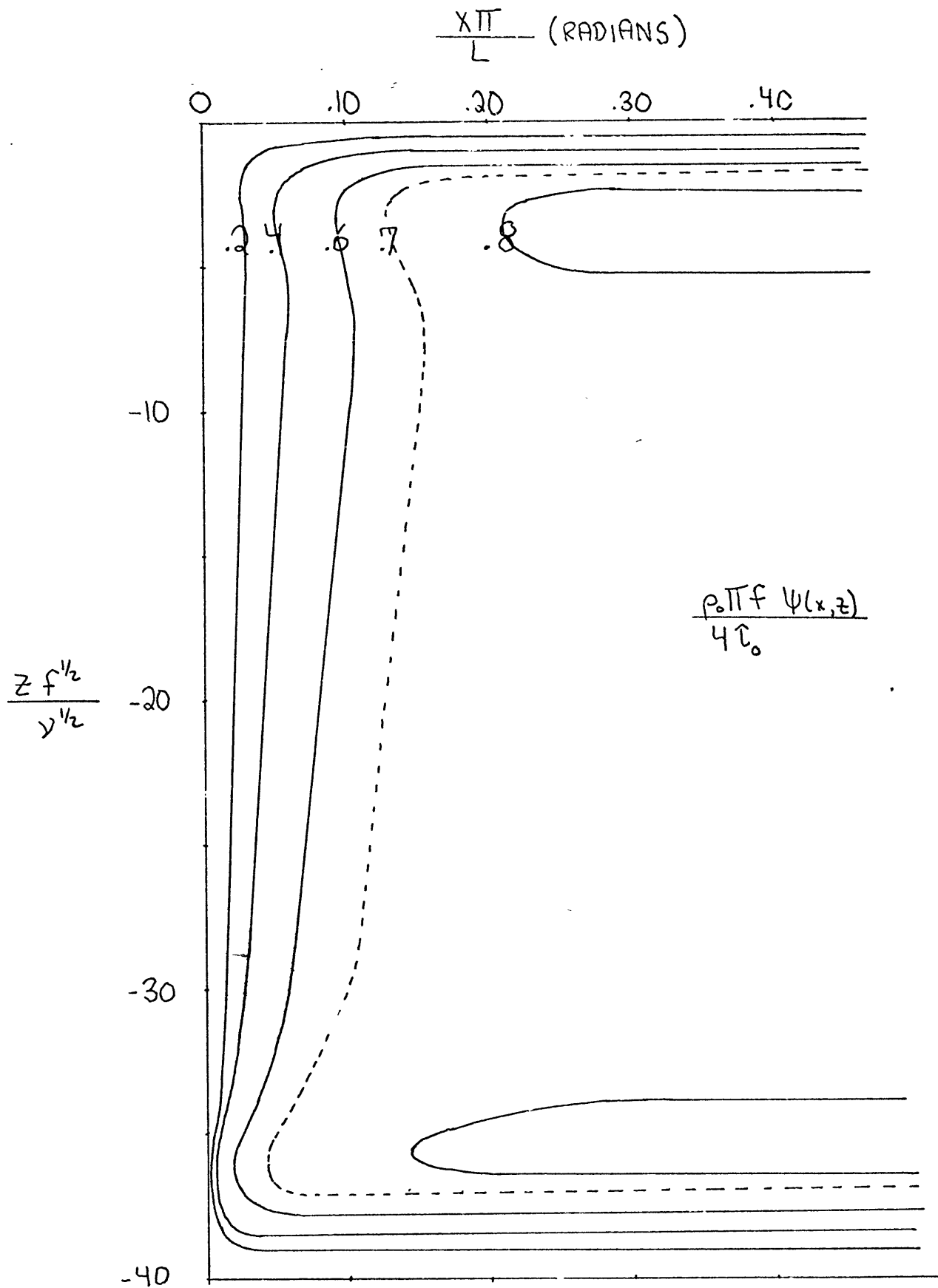


FIGURE 23

The stream function is plotted in figure 23.

From the results it appears that, as expected, there exists a boundary layer near the coast. As the coast is approached, this layer absorbs more and more of the surface stress. Consequently the net transport in the Ekman layer drops to zero as the wall is approached. A more detailed examination of the solution and its dependence on the parameters is postponed until the next section.

7.30 Boundary Layer Approach for the Semi-Infinite Ocean:

In the present circumstances we expect that far from the coast (large negative x) the motion will be independent of x . This x -interior solution will be the same as the solution for the square wave problem away from the regions where the stress changes sign. It consists of non-divergent Ekman layers at top and bottom in which transports in the x -direction exist. These are separated vertically by a region with uniform geostrophic v in the direction of the stress and zero u . W and T vanish everywhere. The formulae for this solution are given below:

$$v = \sqrt{2} \hat{v} + \frac{\hat{v}}{\sqrt{2}} \exp \frac{\sqrt{2}}{2} E_v^{-1/2} z \left[\cos \frac{\sqrt{2}}{2} E_v^{-1/2} z + \sin \frac{\sqrt{2}}{2} E_v^{-1/2} z \right] \\ + \sqrt{2} \hat{v} \exp \frac{\sqrt{2}}{2} E_v^{-1/2} (-z+1) \cos \frac{\sqrt{2}}{2} (-E_v^{-1/2} (z+1))$$

$$u = \frac{\hat{v}}{\sqrt{2}} \exp \frac{\sqrt{2}}{2} E_v^{-1/2} z \left[\cos \frac{\sqrt{2}}{2} E_v^{-1/2} z - \sin \frac{\sqrt{2}}{2} E_v^{-1/2} z \right] - \sqrt{2} \hat{v} \exp \frac{\sqrt{2}}{2} (-E_v^{-1/2} (z+1)) \sin \frac{\sqrt{2}}{2} (-E_v^{-1/2} (z+1))$$

Next to the coast we expect to be able to reduce the u velocity to zero by adding appropriate boundary layer solutions. The possibilities are as follows.

As was shown in section 7.1 the set of governing equations can be combined to give:

$$\begin{array}{ccc} \textcircled{1} & \textcircled{2} & \textcircled{3} \\ E_v^2 P_{zz} + P_{zz} + (\sigma_v \delta) P_{zz} x x = 0 & & (2) \end{array}$$

We recall that now the only restriction on L , the length used to non-dimensionalize x , is that $L \gg L_0$, where L_0 is the width of the boundary layers next to the coast. For $\frac{\partial}{\partial z} = O(1)$, the only balance in (2) which yields a boundary layer solution in x is between terms

② and ③. The boundary layer variable in this case is:

$$\eta = (\sigma_v \delta \delta)^{1/2} \chi$$

Since this is the Couette-Lineykin balance of Part I, it is called the Couette-Lineykin layer.

However, if we don't demand that $\delta_z^2 = O(1)$, there is another x-length scale. This is the scale on which the Ekman layers disappear. Consider equation (2) and let $z = E^{1/2} \xi$; then

$$P_{\delta \xi} + P_{4 \xi} + (\sigma_v \delta \delta) E_v P_{\chi \xi} = 0.$$

All three terms are the same order of magnitude when:

$$\chi = (\sigma_v \delta \delta E_v)^{1/2} \eta$$

From Part I we recall that for scales of this order or less, the boundary layers along horizontal surfaces no longer accept any of the applied stress and serve only to bring the temperature field to its specified boundary value. On these scales the Lineykin part of the Couette-Lineykin solution no longer exists and the interior solution consists only of the Couette flow.

In the boundary layer solution to the problem in which the applied stress is constant, two types of boundary layers occur. These are the Couette-Lineykin and Ekman layers. We are neglecting the boundary layer which occurs for x-scales of $(\sigma_v \delta \delta E_v)^{1/2}$ at horizontal surfaces, and whose function is only to adjust the temperature field to its boundary value.

7.31 Ekman Layers:

At the horizontal boundaries, Ekman layers can occur. Dynamically the top and bottom Ekman layers are similar, so only the top solution is examined. The equations are:

$$\begin{aligned} -\tilde{V} &= \tilde{u}_{\xi\xi} \\ \tilde{u} &= \tilde{V}_{\xi\xi} \\ 0 &= \tilde{u}_x + \tilde{w}_z \end{aligned}$$

$$z = E^{1/2} \xi$$

where

$$\tilde{u} = o(E^{1/2})$$

$$\tilde{V} = o(E^{1/2})$$

$$\tilde{w} = o(E)/o(x)$$

$$\tilde{T} = o(\sigma_s \delta E)/o(x)$$

$$\tilde{P} = o(\sigma_s \delta E^{3/2})/o(x)$$

These yield:

$$\tilde{V} = \exp \frac{\sqrt{z}}{2} \xi \left[A(x) \cos \frac{\sqrt{z}}{2} \xi + B(x) \sin \frac{\sqrt{z}}{2} \xi \right]$$

$$\tilde{u} = \exp \frac{\sqrt{z}}{2} \xi \left[B(x) \cos \frac{\sqrt{z}}{2} \xi - A(x) \sin \frac{\sqrt{z}}{2} \xi \right]$$

$$\tilde{w} = \frac{\sqrt{z}}{2} \exp \frac{\sqrt{z}}{2} \xi \left[-(A(x)_x + B(x)_x) \cos \frac{\sqrt{z}}{2} \xi + (A(x) - B(x))_x \sin \frac{\sqrt{z}}{2} \xi \right]$$

7.32 The Couette-Lineykin Layer:

The equations for the Couette-Lineykin layer are:

$$\begin{aligned}\hat{V} &= \hat{P}_\eta \\ \hat{u} &= \hat{V}_{zz} \\ 0 &= -\hat{p}_z + \hat{T} \\ 0 &= \hat{u}_\eta + \hat{w}_z \\ \hat{w} &= \hat{T}_{zz}\end{aligned}$$

The magnitudes of the variables are:

$$\begin{aligned}\hat{P} &= O((\sigma_v s \delta)^{1/2}) \\ \hat{T} &= O((\sigma_v s \delta)^{1/2}) \\ \hat{V} &= O(1) \\ z &= O(1) \\ \hat{u} &= O(E_v) \\ \hat{w} &= O\left(\frac{E_v}{(\sigma_v s \delta)^{1/2}}\right) \\ \chi &= (\sigma_v s \delta)^{1/2} \eta\end{aligned}$$

These were obtained by assuming that the layer could carry the Ekman transport and that the vertical shear was order one, i.e.

$$O(\hat{w})O(\chi) = E_v \quad ; \quad \frac{\partial(\hat{V})}{\partial(z)} = O(1)$$

Since this layer is much thicker than an Ekman layer, Ekman layer dynamics still hold within the layer. In the Ekman layer when $\chi = O((\sigma_v s \delta)^{1/2})$ we have:

$$\begin{aligned}\tilde{\omega} &= 0 \left(\frac{E_v}{(\sigma_v s \delta)^{1/2}} \right) \\ \tilde{\tau} &= 0 \left((\sigma_v s \delta)^{1/2} E_v \right)\end{aligned}$$

As in Examples I and II of Part I, the \hat{v} , $\hat{\tau}$ have to satisfy the boundary conditions by themselves while at $z=0$,

$$\hat{\omega} = -\tilde{\omega}$$

The general solution to the Couette-Lineykin layer equations is found to be:

$$\hat{P}(\eta, z) = \sum_{\sigma} \exp \sigma \eta \left[C(\sigma) \cos \sigma z + D(\sigma) \sin \sigma z + \frac{A(\sigma) z + B(\sigma)}{\sigma^2} \right] \quad (3)$$

$$\hat{V}(\eta, z) = \sum_{\sigma} \sigma \exp \sigma \eta \left[C(\sigma) \cos \sigma z + D(\sigma) \sin \sigma z + \frac{A(\sigma) z + B(\sigma)}{\sigma^2} \right] \quad (4)$$

$$\hat{\omega}(\eta, z) = - \sum_{\sigma} \sigma^3 \exp \sigma \eta \left[C(\sigma) \cos \sigma z + D(\sigma) \sin \sigma z \right] \quad (5)$$

$$\hat{\tau}(\eta, z) = \sum_{\sigma} \sigma \exp \sigma \eta \left[D(\sigma) \cos \sigma z - C(\sigma) \sin \sigma z + \frac{A(\sigma)}{\sigma^2} \right] \quad (6)$$

$$\hat{\omega}(\eta, z) = - \sum_{\sigma} \sigma^3 \exp \sigma \eta \left[D(\sigma) \cos \sigma z - C(\sigma) \sin \sigma z \right] \quad (7)$$

7.33 The Uniform Stress Model:

Consider the following problem with the boundary conditions:

$$\begin{array}{l}
 @ z=0 \quad V_z = \hat{U} \\
 \quad \quad u_z = \bar{T}_z = \omega_z = 0 \\
 @ z=-1 \quad u = v = \omega = \bar{T} = 0
 \end{array}
 \left. \vphantom{\begin{array}{l} @ z=0 \\ @ z=-1 \end{array}} \right\} x \leq 0$$

where

$$\hat{U} = \frac{1}{2} |$$

At $x=0$, as was discussed in section 6.4, we require that

$$u = 0.$$

From the square-wave solution, we essentially know the dynamics of the solution. Within $(\sigma_v \delta \epsilon_v)^{1/2}$ of the wall, the solution is essentially Couette flow, and there are no Ekman layers. Within a region $(\sigma_v \delta \epsilon_v)^{1/2}$ of the wall, Ekman layers and the Couette-Lineykin solution exist. At distances greater than this from the wall, Ekman layers exist, and an interior v -velocity, independent of z , is required to drive the lower Ekman layer.

The Region of Thickness $(\sigma_v \delta \epsilon_v)^{1/2}$:

Since Ekman layers don't exist, the Couette-Lineykin solution has to satisfy the boundary conditions by itself. These are:

$$\begin{array}{l}
 @ z=0 \quad \hat{V}_z^{(3)} = \hat{U} \exp \eta \quad ; \quad \hat{\omega}^{(3)} = 0 \\
 @ z=-1 \quad \hat{V}^{(3)} = \hat{\omega}^{(3)} = 0
 \end{array}$$

The solution to these is:

$$\hat{V}^{(3)} = \hat{\tau}(z+1)\exp m$$

$$\hat{u}^{(3)} = 0$$

$$\hat{\omega}^{(3)} = 0$$

$$\hat{T}^{(3)} = \hat{\tau}\exp m$$

Note that this solution satisfies the top boundary condition on temperature, but it doesn't satisfy the one at $z=-1$. This can be corrected for by including the boundary layer which is the solution to equation (3). However, since this only brings the temperature to zero and is otherwise passive, it is neglected.

The Region of Width $(G_V S \delta)^{1/2}$:

The stress condition at the surface has essentially been reduced to

$$V_z = V_{z\text{TOTAL}} - \hat{V}_z^{(3)} = \hat{\tau}(1 - \exp m) = \hat{\tau}(1 - \exp \hat{m}\eta)$$

where

$$\hat{m} = E^{-1/2}$$

Let the interior Couette-Lineykin solution consist of two parts:

$$\hat{V}^{(1)} = \text{SOLUTION WHICH BRINGS } V_z \text{ TO ZERO}$$

$$\hat{V}^{(2)} = \text{SOLUTION OF } (G_V S \delta)^{1/2} \text{ SCALE}$$

The stress at the surface is then given by

$$V_z = \hat{V}_z^{(1)} + \hat{V}_z^{(2)} + \tilde{V}_z = \hat{\tau}(1 - \exp \hat{m}\eta)$$

Pick

$$\hat{V}_z^{(u)} = -\tau \exp \hat{m} \eta$$

consequently

$$\tilde{V}_z = \tau - \hat{V}_z^{(u)}$$

Substituting for $\hat{V}_z^{(u)}$ from equation (4) we get that

$$\tilde{V}_z = \tau - \sum_{\sigma} \sigma^2 \exp \sigma \eta \left[D(\sigma) + \frac{A(\sigma)}{\sigma^3} \right]$$

The total Ekman layer solution consists of a solution far from the wall and a boundary layer correction. Let $\tilde{V}^{(u)}$ represent the solution far from the wall and $\tilde{V}^{(u)}$ be the boundary layer correction. The boundary layer correction has a surface stress of the form:

$$\tilde{V}_z^{(u)} = -\sum_{\sigma} \sigma^2 \exp \sigma \eta \left[D(\sigma) + \frac{A(\sigma)}{\sigma^3} \right]$$

Thus we can look for the total solution to the upper Ekman layer to be of the form:

$$\begin{aligned} \tilde{u}(\eta, \xi) &= \frac{1}{\sqrt{2}} \left(\tau - \sum \sigma^2 \exp \sigma \eta \left[D + \frac{A}{\sigma^3} \right] \right) \exp \frac{\sqrt{2}}{2} \xi \left[\cos \frac{\sqrt{2}}{2} \xi - \sin \frac{\sqrt{2}}{2} \xi \right] \\ \tilde{v}(\eta, \xi) &= \frac{1}{\sqrt{2}} \left(\tau - \sum \sigma^2 \exp \sigma \eta \left[D + \frac{A}{\sigma^3} \right] \right) \exp \frac{\sqrt{2}}{2} \xi \left[\cos \frac{\sqrt{2}}{2} \xi + \sin \frac{\sqrt{2}}{2} \xi \right] \\ \tilde{w}(\eta, \xi) &= \sum \sigma^3 \exp \sigma \eta \left[D + \frac{A}{\sigma^3} \right] \exp \frac{\sqrt{2}}{2} \xi \cos \frac{\sqrt{2}}{2} \xi \end{aligned}$$

From the condition

$$\hat{w}^{(u)}(\eta, 0) = -\tilde{w}(\eta, 0)$$

$A(\sigma)$ is found to be zero. At the wall, all the applied stress is transmitted to the Couette-Lineykin flow; consequently the Ekman velocities at the wall vanish. Either one of these conditions

gives:

$$\hat{L} - \sum_{\sigma} \sigma^2 D(\sigma) = 0$$

The application of the boundary conditions

$$\begin{aligned} @ z=0 & \quad \hat{T}_z^{(2)} = 0 \\ @ z=-1 & \quad \hat{T}^{(2)} = \hat{V}^{(2)} = 0 \end{aligned}$$

determines the remaining arbitrary constants in the $\hat{V}^{(2)}$ solution.

The solution is

$$\begin{aligned} \hat{V}^{(2)} &= 2\hat{L} \sum_{n=0}^{\infty} \frac{(-1)^n}{\sigma^2} \exp n \eta [\sin \sigma z + (-1)^n] \\ \hat{U}^{(2)} &= -2\hat{L} \sum_{n=0}^{\infty} (-1)^n \exp n \eta \sin \sigma z \\ \hat{W}^{(2)} &= -2\hat{L} \sum_{n=0}^{\infty} (-1)^n \exp n \eta \cos \sigma z \\ \hat{T}^{(2)} &= 2\hat{L} \sum_{n=0}^{\infty} \frac{(-1)^n}{\sigma^2} \exp n \eta \cos \sigma z \end{aligned}$$

where

$$\sigma = \frac{(2n+1)\pi}{2}$$

The calculation of the $\hat{V}^{(1)}$ solution is also straightforward.

The relevant boundary conditions are:

$$\begin{aligned} @ z=0 & \quad \hat{W}^{(1)} = 0 \\ & \quad \hat{V}^{(1)} = -\hat{L} \exp \hat{m} \eta \\ @ z=-1 & \quad \hat{T}^{(1)} = \hat{V}^{(1)} = 0 \end{aligned}$$

These give the solutions:

$$\begin{aligned} \hat{V}^{(1)} &= \hat{L} \exp \hat{m} \eta \left[\frac{1}{\hat{m} \sin \hat{m}} (\cos \hat{m} z - \cos \hat{m}) - (z+1) \right] \\ \hat{U}^{(1)} &= -\frac{\hat{m} \hat{L}}{\sin \hat{m}} \exp \hat{m} \eta \cos \hat{m} z \end{aligned}$$

$$\hat{w}^{(1)} = \frac{\hat{m} \hat{l}}{\sin \hat{m}} \exp \hat{m} \eta \sin \hat{m} z$$

$$\hat{r}^{(1)} = -\frac{\hat{l}}{\hat{m}} \exp \hat{m} \eta \left[\frac{\sin \hat{m} z}{\sin \hat{m}} + 1 \right]$$

It should be noted that while $\hat{w}^{(2)} = 0$ at $z = -1$, $\hat{w}^{(1)}$ is not. Thus an Ekman layer is required at $z = -1$ to bring the total w to zero there. Physically this Ekman layer is required to transport water away from the wall which was brought toward the wall in the upper Ekman layer. A simple calculation shows that the Ekman layer solution at $z = -1$ is:

$$\tilde{v} = -\sqrt{z} \hat{l} \exp \frac{\sqrt{z}}{2} \xi \cos \frac{\sqrt{z}}{2} \xi (1 - \exp \hat{m} \eta)$$

$$\tilde{u} = +\sqrt{z} \hat{l} \exp \frac{\sqrt{z}}{2} \xi \sin \frac{\sqrt{z}}{2} \xi (1 - \exp \hat{m} \eta)$$

$$\tilde{w} = -\hat{m} \hat{l} \exp \hat{m} \eta \left[\exp \frac{\sqrt{z}}{2} \xi \left(\sin \frac{\sqrt{z}}{2} \xi - \cos \frac{\sqrt{z}}{2} \xi \right) \right]$$

where

$$\xi = -E^{-1/2} (z+1)$$

To drive this Ekman layer an interior flow of the form

$$V = +\sqrt{z} \hat{l} (1 - \exp \hat{m} \eta)$$

is required.

There are several points which should be noted about these solutions. First of all, the infinite series for $\hat{w}^{(2)}$ and $\hat{u}^{(2)}$ converge everywhere except at $x=0$. Similar non-convergences, right at the boundaries, also occur for the boundary layer solutions to the Stewartson $E^{1/3}$ -layer and probably for solutions to the hydrostatic layer. Consequently the boundary solution for these layers should be taken as the limit of the interior solution as the

boundary is approached. The stream functions for all these layers converge.

Secondly, although the condition of no normal flow through the wall is satisfied through $O(E^{1/2})$, there is an $O(E)$ flow in and out of the wall for $\hat{u}^{(1)}$ and $\hat{u}^{(2)}$. However,

$$\int_{-1}^0 (\hat{u}^{(1)} + \hat{u}^{(2)}) dz = 0 \quad @ x=0$$

despite the fact that $\hat{u}^{(2)}$ itself does not converge at $x=0$. A simple integration shows that all the flow which enters into the Couette-Lineykin layer through the upper Ekman layer leaves through the lower one.

If drawn, these solutions would resemble quite closely those of the square wave (figures 19-23). The main difference occurs for the v -velocity. This no longer drops to zero, and in a distance within $(\sigma_s \delta \epsilon_v)^{1/2}$ of the wall is essentially Couette flow. At the wall it is Couette flow, and its surface value at the wall is 40. Because this solution does resemble the square-wave one so closely and because of the practical difficulty in resolving both the η and ν scales where $\eta = \bar{c}^{-1/2} \nu$, the solutions are not displayed.

The dimensional width of the upwelling zone is $(\sigma_s \delta)^{1/2} L$. This is independent of the width of the basin, "L". Initially the non-dimensionalization of some of the fields depended on this "L". Now it would be possible to change the non-dimensionalization such that the horizontal length scale was the width of the upwelling zone. The response in the zone would then be independent of the width of the ocean.

7.4 Discussion of Results:

A spatially uniform stress applied parallel to a wall produces a net transport of water, in the Ekman layer, toward or away from the wall. Suppose it is toward the wall. The initial piling up of water at the wall produces a pressure gradient perpendicular to the wall. This creates an interior flow in the direction of the stress which results in the formation of an Ekman layer at the bottom. The transport in this Ekman layer is away from the wall. The pressure gradient builds up until the sum of the transports in the upper and lower Ekman layers perpendicular to the wall is zero. Close to the wall (on the scale of the Couette-Lineykin layer) vertical advectons of the mean temperature field create horizontal temperature gradients. These produce a thermal "wind" shear which balances the surface stress at the wall. Consequently at the wall the Ekman layer velocities vanish.

Away from the wall, but still on the scale of $(\sigma_s \delta)^{1/2}$, the Couette-Lineykin layer does not transmit the stress directly to the bottom. The surface stress is balanced by a body force which is distributed throughout the depth of the fluid. Close to the wall, on a scale of $(\sigma_s \delta \epsilon_v)^{1/2}$, the stress is directly transmitted to the bottom by the Couette flow and consequently at the wall

$$\int_{-1}^0 (\hat{u}^{(1)} + \hat{u}^{(2)}) dz = 0$$

Oceanic Application:

The restrictive assumptions made in this idealized model of coastal upwelling clearly limit its applicability to actual oceanic conditions. However, there are some features of the model which are in qualitative agreement with what is observed. The width of the upwelling zone, which is of the order of tens of kilometers, is predicted by the model. Furthermore, as the observations indicate, there is a region close to the coast in which the velocity along the coast is higher than it is further offshore. The width of this region is of course the width of the upwelling zone. The question arises as to whether thermal "wind" shears of sufficient magnitude to balance the wind stress occur in oceanic upwelling zones.

Observations in most of the upwelling zones indicate that the thermal "wind" shear at the inshore edge of the upwelling zone is of the order of 50 cm/sec/100 meters. The wind stress on the sea surface for a wind of 15 knots is about 4 dynes/cm (this value is highly uncertain). The vertical eddy coefficient, if the thermal "wind" shear is to balance the surface stress, must be approximately 8×10^2 cm/sec. This is not an unreasonable value. Although this is not proof that this physical mechanism is operative in the upwelling zone, it does point to its possible existence. Even if all of the wind stress is not balanced by the thermal "wind" shear, a portion of it very easily could be.

Observations indicate that upwelling is generally confined

to the top 100-300 meters. However, the steady solution to our model indicates that it extends to the bottom. This shortcoming of the model appears to be a result of our assumption that the flow is steady. The Couette flow develops on the order of the diffusion time scale. This is of the order of

$$T_{\text{diffusion}} = \frac{D^2}{K_v} = \frac{10^3}{10^3} = 10^3 \text{ sec}$$

or about 100 days. Of course in the ocean K_v is some function of depth so this estimate represents a lower bound. Probably in most upwelling zones the Couette flow and consequently the lower Ekman layer would not have a chance to develop. This means that the compensating flow, which previously came through the lower Ekman layer, must come through the interior and is probably balanced by the time accelerations. An additional factor, which might be of importance in limiting the depth of upwelling, is that the upwelling zones are of limited north-south extent and consequently are not independent of this direction. This dependence allows compensatory water to be drawn from the interior.

A conspicuous feature which is missing in the theoretical model, is the deep, poleward counter-current. There is some reason to believe, as was mentioned earlier, that the existence of this counter-current is related to the north-south variations in the oceanic and atmospheric conditions. Since these are not considered it is not surprising that the model does not exhibit a counter-current.

From Part I it is clear that the boundary conditions played

an important role in determining the nature of the solution in the examples which were considered. Suppose the ocean is driven both mechanically and thermally. At the surface specify that (non-dimensionally)

$$\frac{\partial v}{\partial z} = h(x, y)$$

$$T = g(x, y)$$

If in some region these are related such that

$$\frac{\partial v}{\partial z} = T_x \quad ; \quad \text{i.e.} \quad h = g_x$$

then, the stress is transmitted directly to the interior, and Ekman layers are absent. This can obviously cause some very interesting flows. Is the Antarctic Convergence a physical phenomena of this type?

Appendix A: Arabian Upwelling

The data for these sections came from Discovery stations 5006-5015, 5033-5045, and 5047-5054. During the period these stations were taken, June-August 1963, the southwest monsoon blows steadily over the northwestern Indian Ocean. For sections A and B, the wind blew from about 200° - 220° with a speed of 25-30 knots. The average wind speed in section C was somewhat less at about 15 knots. The positions of these sections are shown in figure 24.

The salinities at stations 5040 and 5041 of section B were excluded from that section because of the great difficulty of making sense of the contours if they had been included.

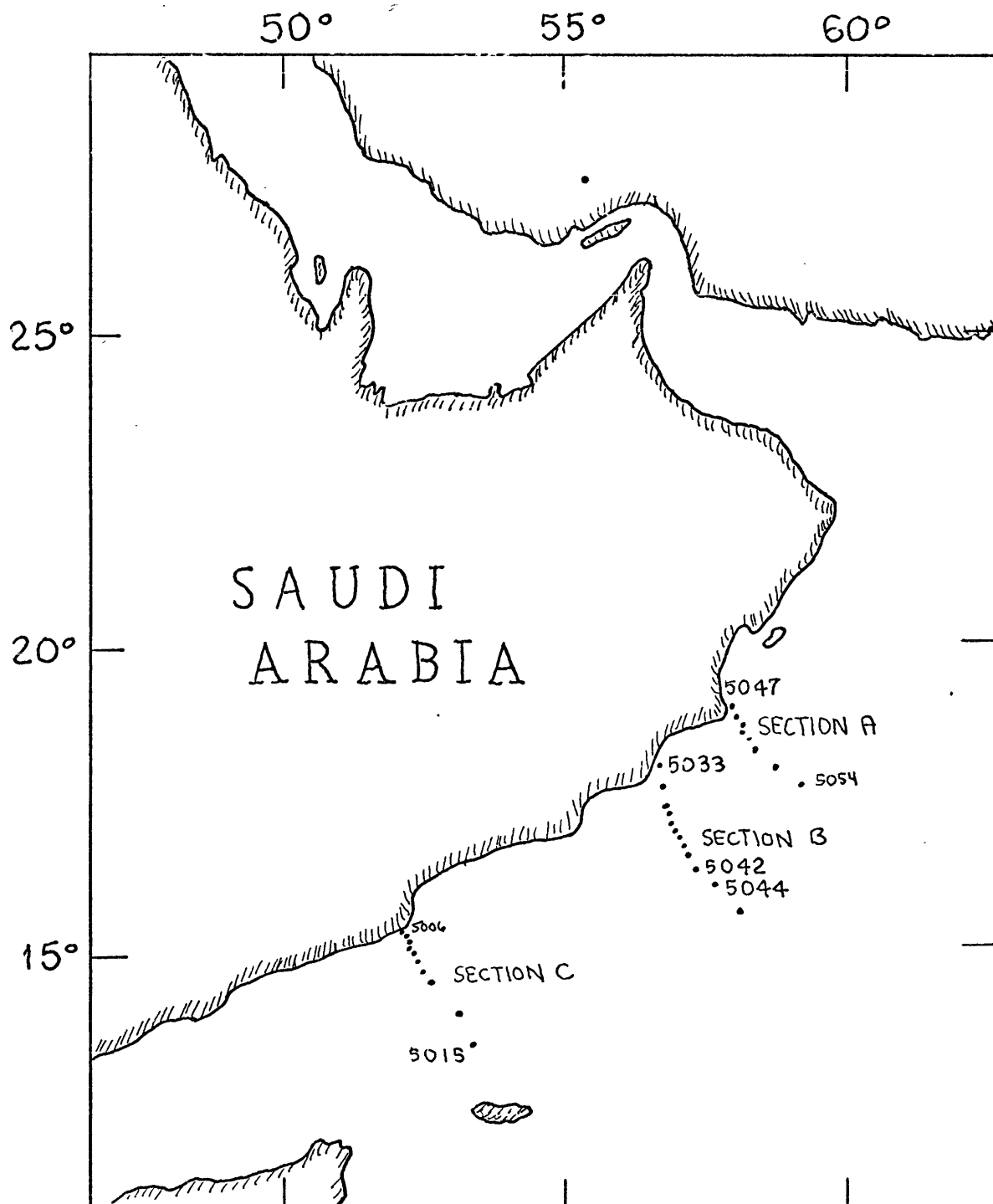


FIGURE 24

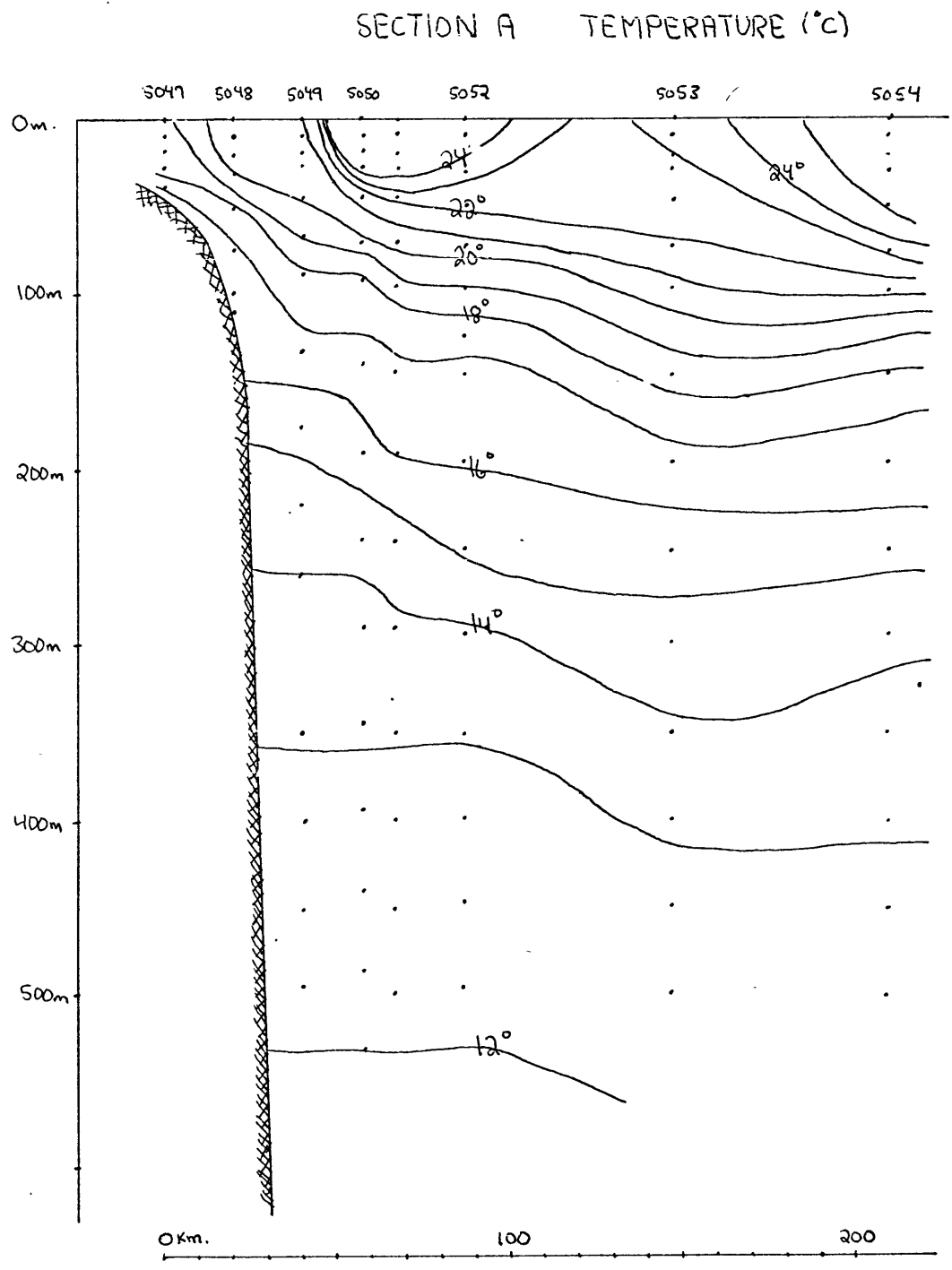


FIGURE 25

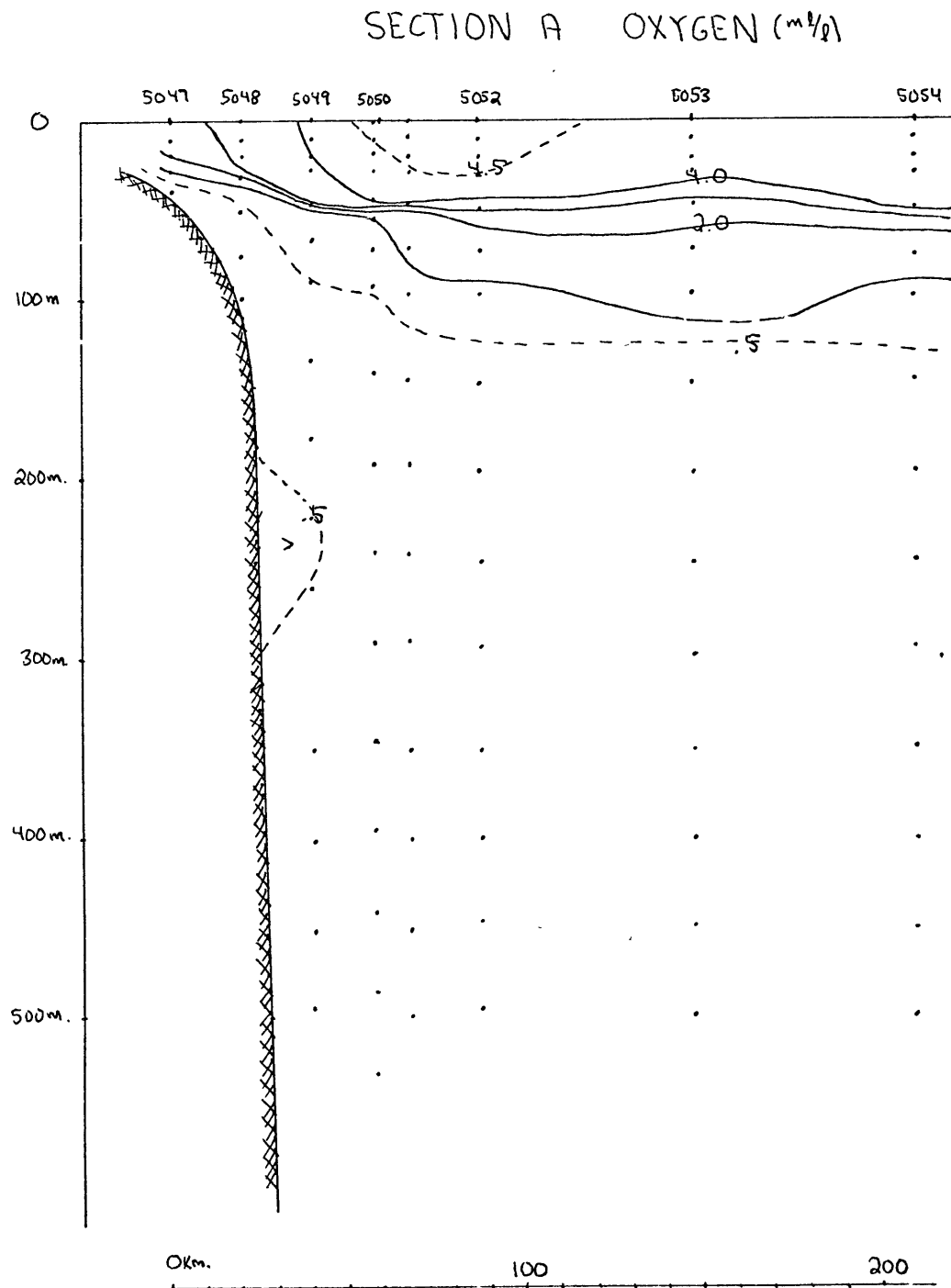


FIGURE 27

SECTION B TEMPERATURE (°C)

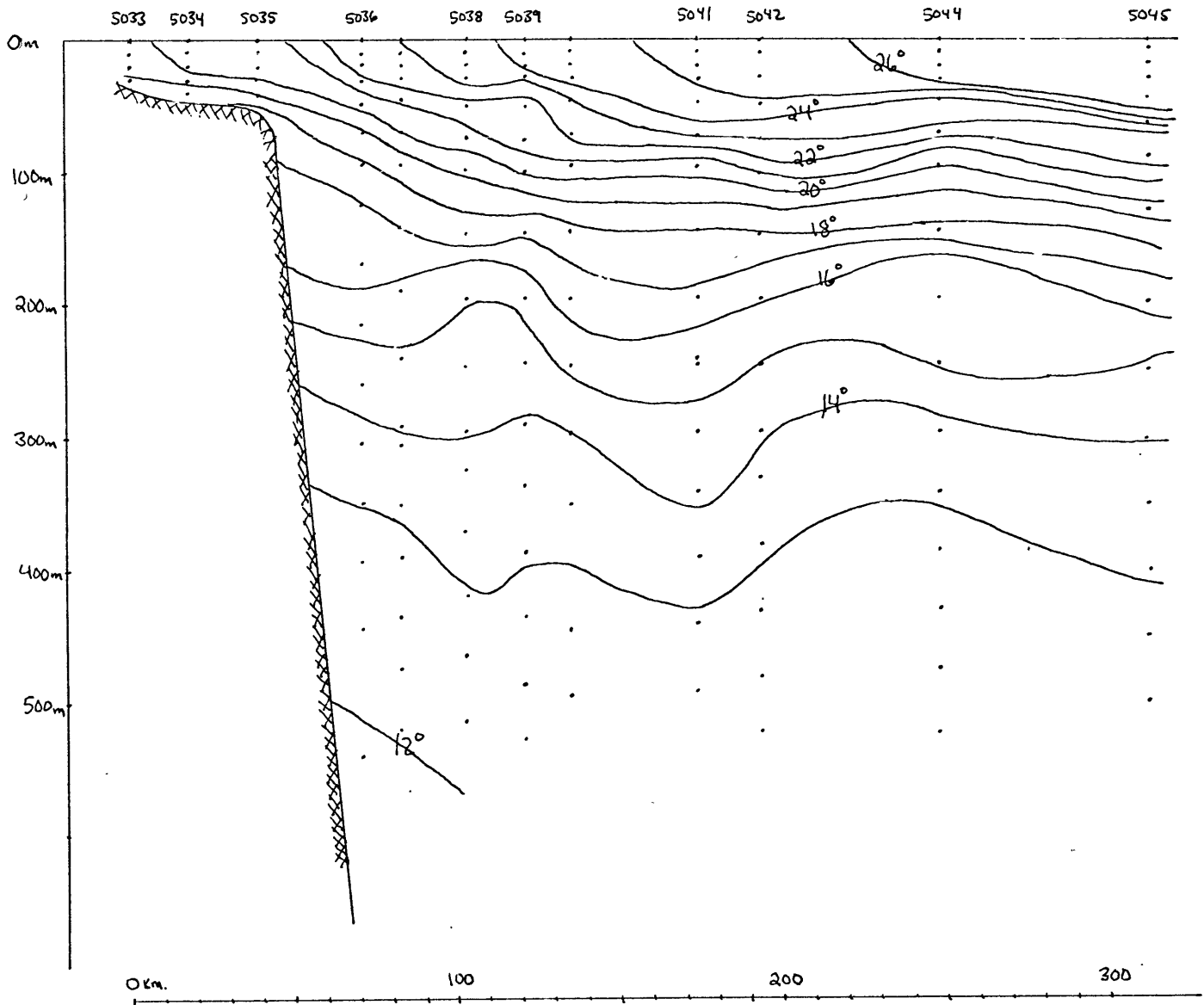


FIGURE 28

SECTION B SALINITY (‰)

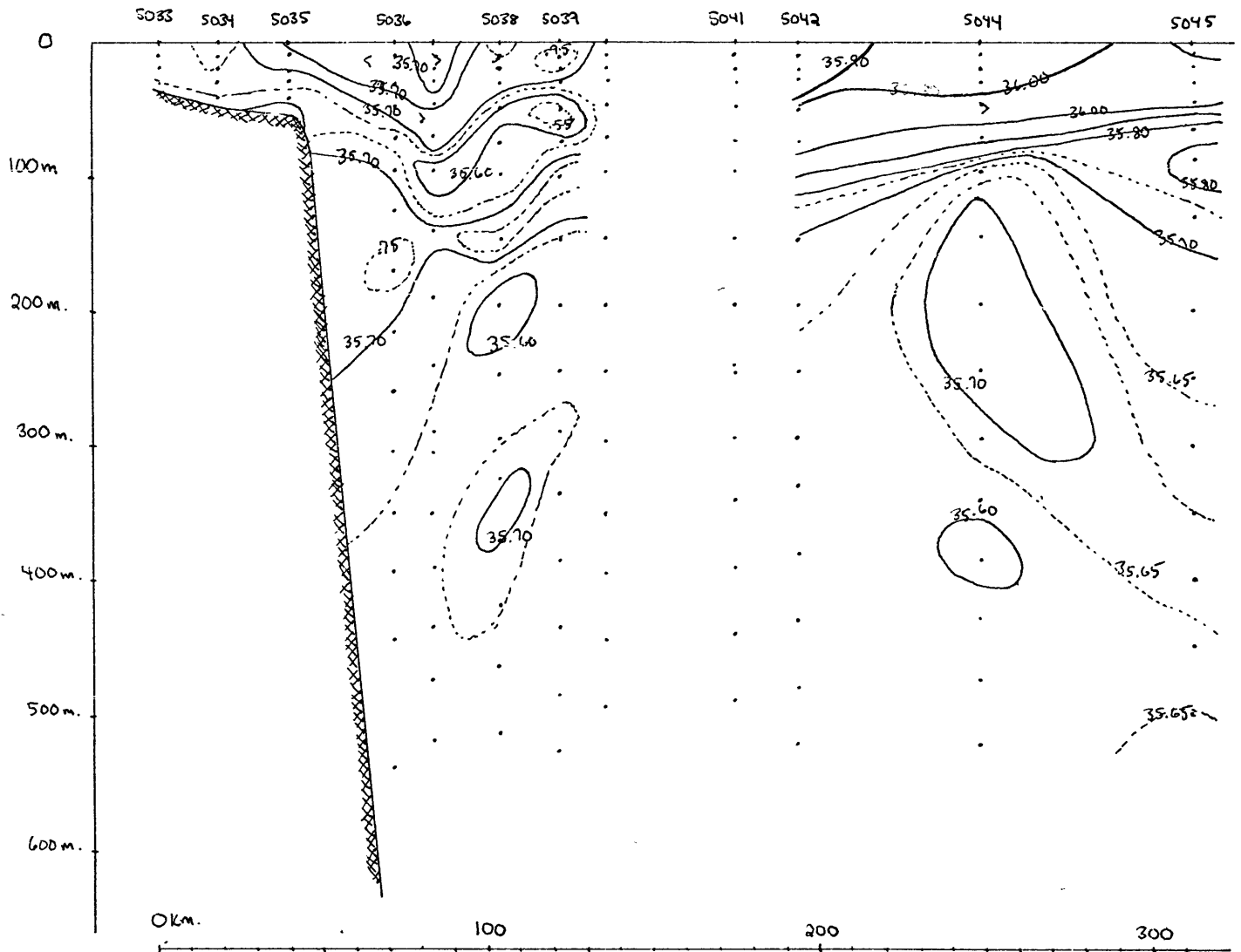


FIGURE 29

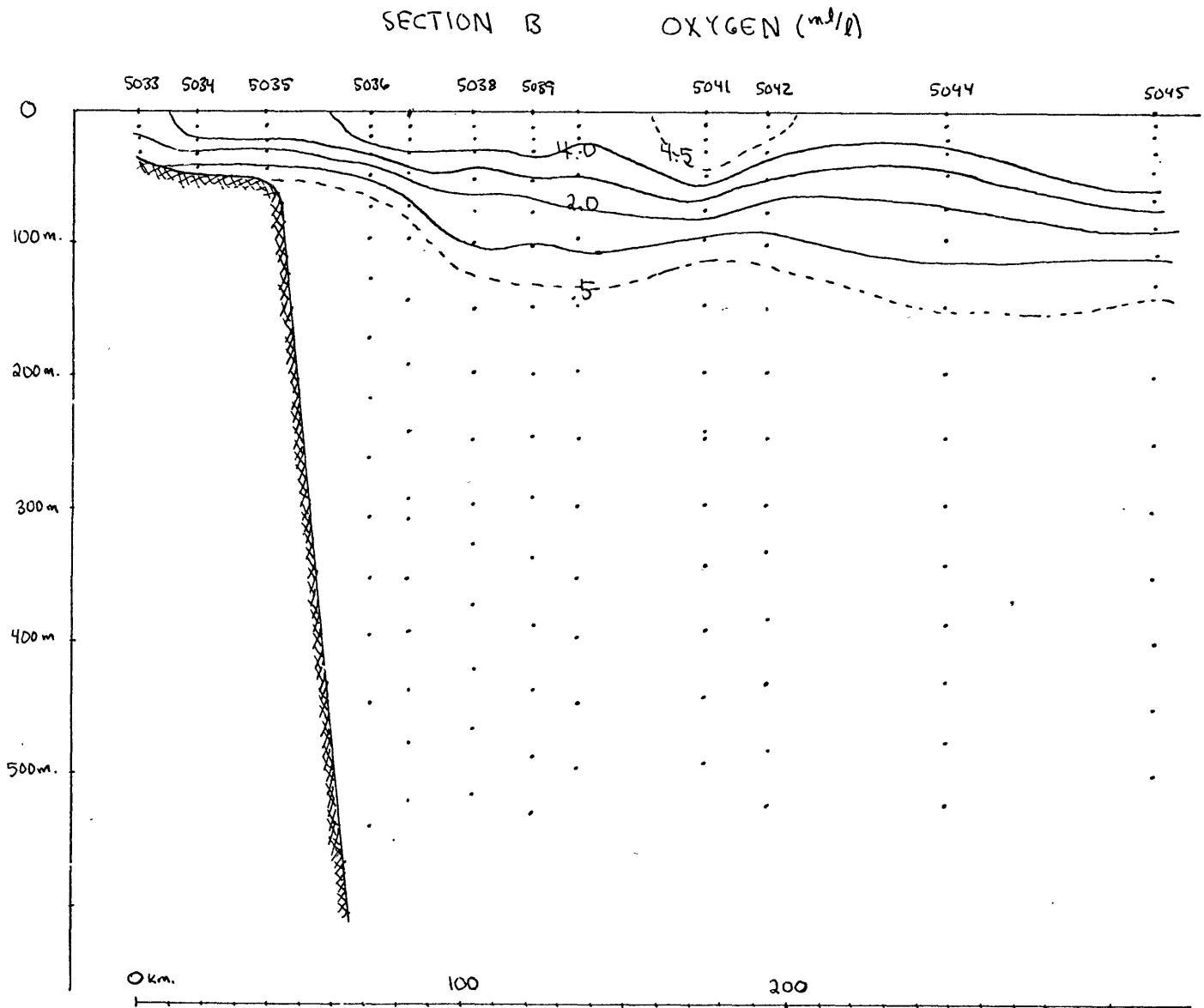


FIGURE 30

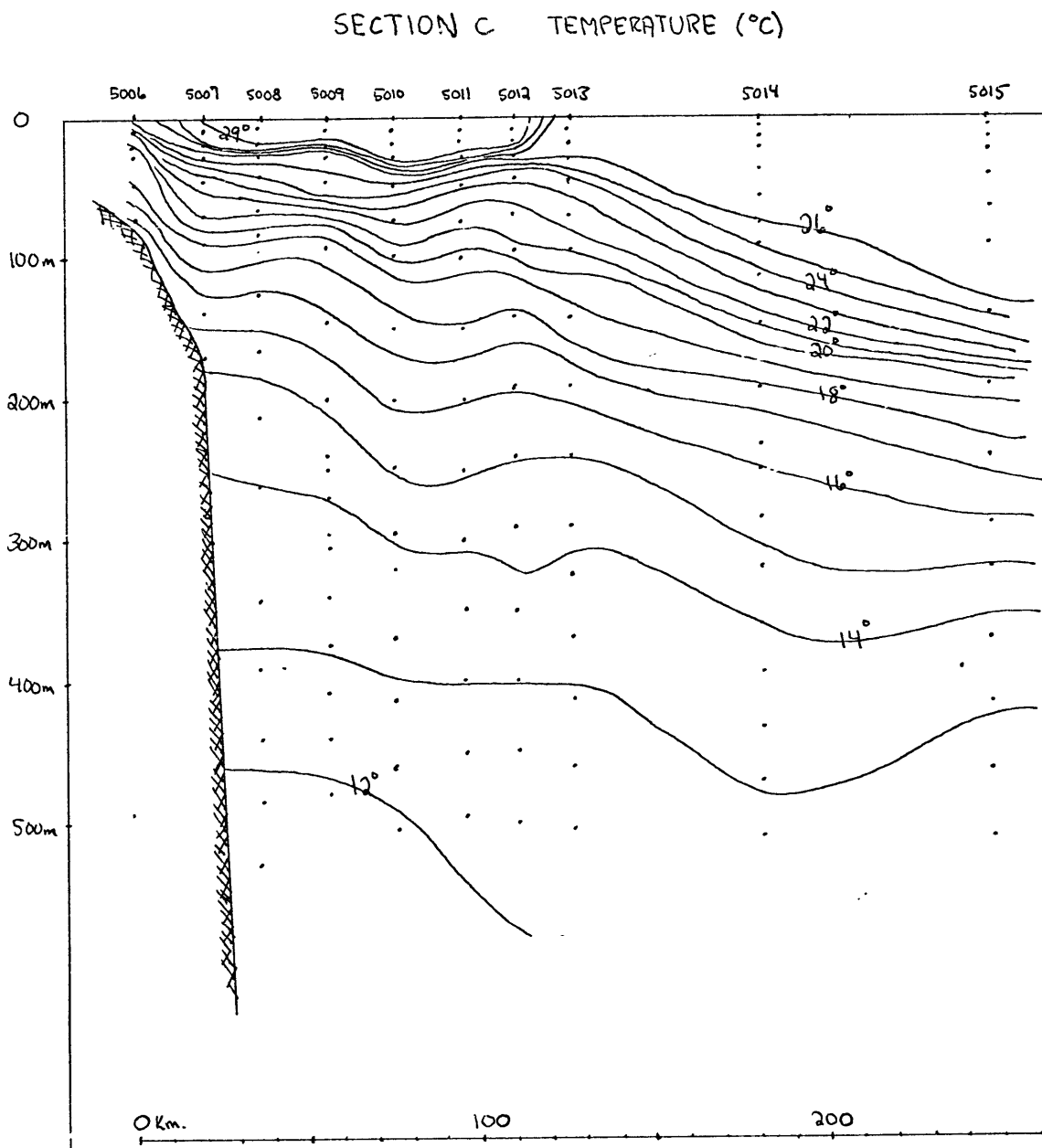


FIGURE 31

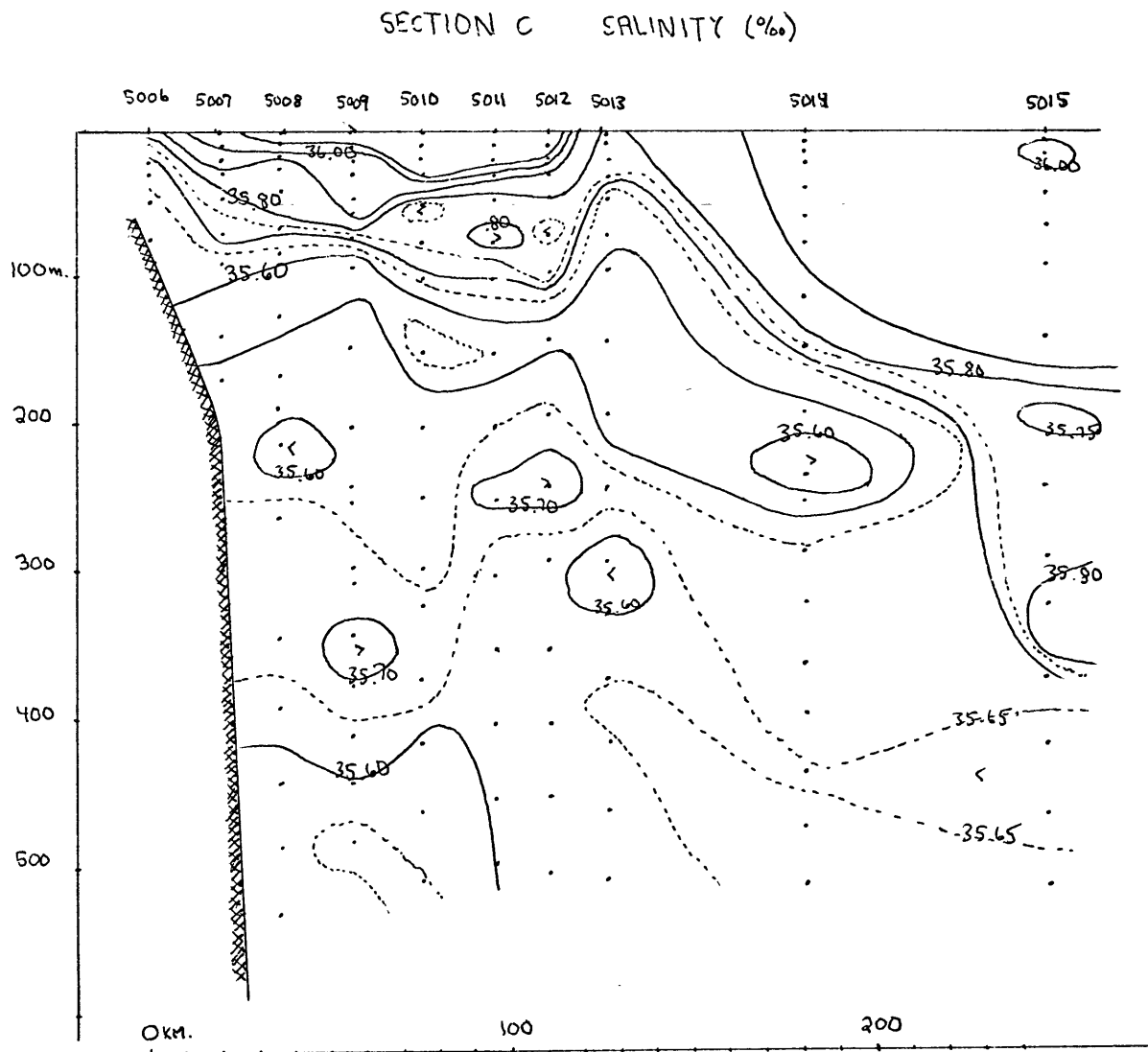


FIGURE 32

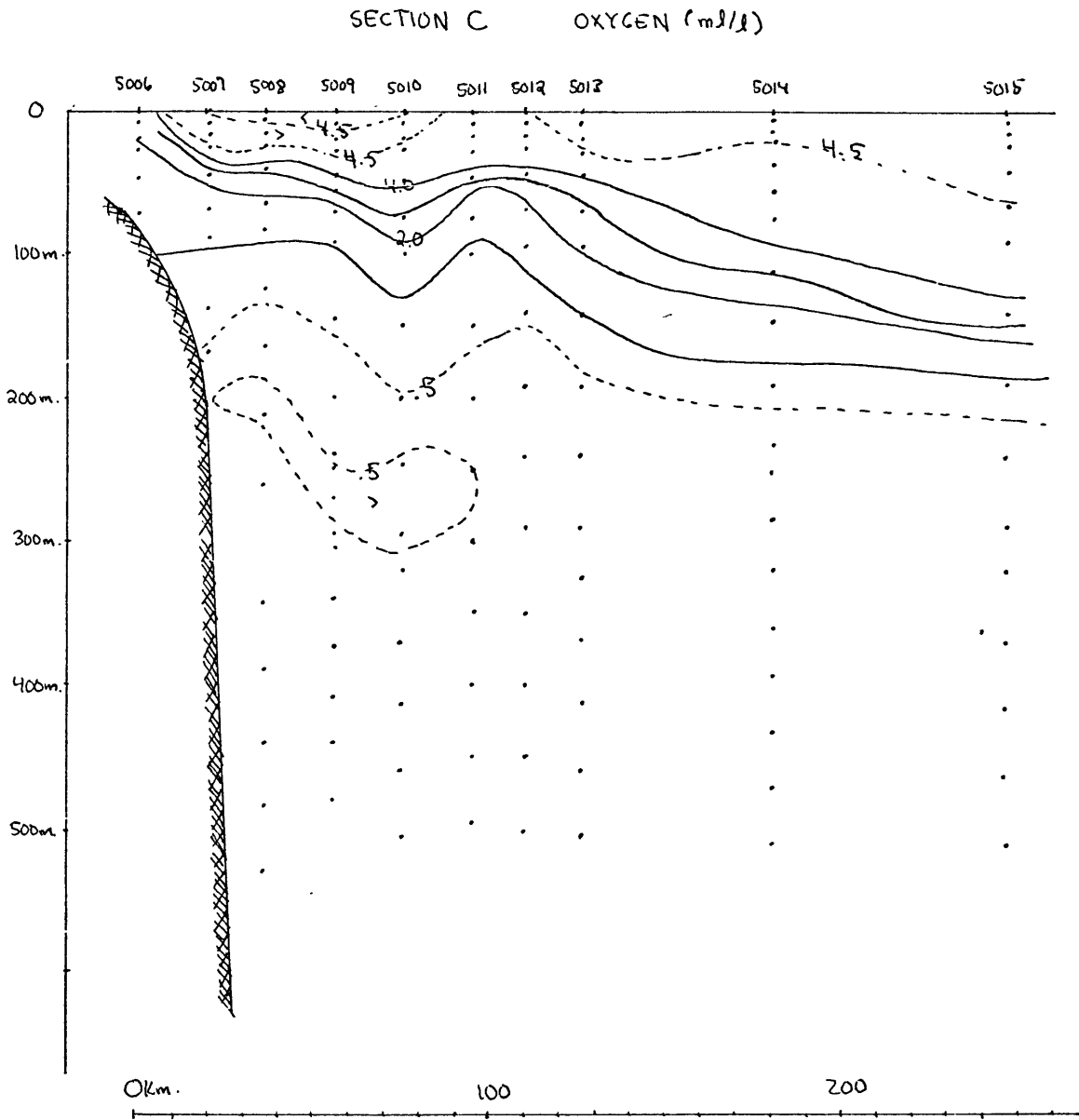


FIGURE 33

Appendix B: The Buoyancy Layer

Because of the important role the buoyancy layer (Barcilon and Pedlosky (1967a,b), Veronis (1967a,b)) plays in rotating, stratified fluids, its effects in this problem are examined.

The solution to the upwelling problem without lateral friction has an $O(1)$ heat flux through the wall at $x = 0$. If this is to be brought to zero, the effects of lateral friction must be considered. This would be done through the introduction of the buoyancy layer. If the $O(1)$ heat flux is brought to zero, we get for the buoyancy layer that

$$O(x) = (E_H \delta)^{1/2} / (\sigma_v \delta)^{1/4}$$

$$O(u) = E_H / (\sigma_v \delta)$$

$$O(\omega) = E_H^{1/2} / (\sigma_v \delta)^{3/4} \delta^{1/2}$$

$$O(T) = (E_H \delta)^{1/2} / (\sigma_v \delta)^{1/4}$$

$$O(v) = (E_H \delta) / (\sigma_v \delta)^{3/2}$$

and

$$u = v_{pp}$$

$$0 = u_p + w_z$$

$$0 = T + w_{pp}$$

$$w = T_{pp}$$

where

$$p = (\sigma_v \delta)^{1/4} (E_H \delta)^{-1/2} x$$

It is easy to show that the buoyancy layer in this case is thinner than the smallest x-scale considered in the upwelling problem, i.e. $(\sigma_v \delta \delta \epsilon_v)^{1/2}$. The ratio of the width of the buoyancy layer to this thickness is given by

$$\frac{(\delta \epsilon_H)^{1/2}}{(\sigma_v \delta \delta)^{1/4}} \cdot \frac{1}{(\sigma_v \delta \delta \epsilon_v)^{1/2}} = \left(\frac{\epsilon_H}{\epsilon_v}\right)^{1/2} \frac{\delta^{1/2}}{(\sigma_v \delta \delta)^{1/4}} \ll \frac{\delta^{1/2}}{(\sigma_v \delta \delta)^{1/4}} \sim O(1)$$

where we have used the fact that $\epsilon_H \ll (\sigma_v \delta \delta) \epsilon_v$ and have substituted for ϵ_H .

In the Couette-Lineykin layer the magnitude of the u-velocity was $O(\epsilon_v)$. Because $\epsilon_H \ll (\sigma_v \delta \delta) \epsilon_v$ the secondary u-circulation caused by the buoyancy layer is much less than the one in the Couette-Lineykin layer. Furthermore, for this particular problem, this secondary circulation is identically zero. From the equations for the buoyancy layer we have

$$\omega_z = \bar{T}_{pp} z .$$

But \bar{T}_{pp} is independent of z because in the Couette flow next to the wall the heat flux is independent of z . Consequently

$$u_p = 0$$

This implies that $u = 0$.

It appears that the addition of the buoyancy layer would not change the nature of the solution to the upwelling problem. Even if the heat flux were brought to zero through the addition of a buoyancy layer, the no slip conditions on \hat{V} and $\hat{\omega}$ still remain to be satisfied. It does not appear that this can be done in the framework of the linear theory of rotating, stratified fluids.

BIBLIOGRAPHY

- Barcilon, V. (1969) Private communication.
- Barcilon, V. and J. Pedlosky. (1967a) "Linear theory of rotating stratified fluid motions". J. Fluid Mech. 29, 1-16.
- Barcilon, V. and J. Pedlosky, (1967b) "A unified linear theory of homogeneous and stratified rotating fluids." J. Fluid Mech. 29, 609-621.
- Gunther, E. R. (1936) "A report on oceanographical investigations in the Peru coastal current." Discovery Repts. 13, 207-276.
- Hamon, B. V. (1967) "Medium-scale temperature and salinity structure in the upper 1500 m in the Indian Ocean." Deep Sea Res. 14, 169-181.
- Hart, I.J. and R. I. Currie. (1960) "The Benguela Current". Discovery Repts. 31, 123-298.
- Hidaka, K. (1954) "A contribution to the theory of upwelling and coastal currents." Trans. Amer. Geophys. Un. 35, 431-444.
- Lanczos, G. (1956) Applied Analysis, Prentice Hall.
- Latun, V. S. (1962) "The upwelling of deep water near the south-coast of Africa". Izv. An. USSR., (Geophys. Ser.) 9, 1229-1239, (770-775 Trans.)
- Reid, J. L., Jr. (1962) "Measurements of the California counter-current at a depth of 250 meters." J. Mar. Res. 20, 134-137.
- Reid, J. L., Jr., G. I. Roden and J. G. Wyllie. (1958) "Studies of the California current system." Prog. Rep., Calif. Coop. Ocean. Fish. Invest., 1 July, 1956 to 1 January, 1958, 27-57.
- Stommel, H. and G. Veronis. (1957) "Steady convective motion in a horizontal layer of fluid heated uniformly from above and cooled non-uniformly from below." Tellus. Vol. 9; 401-407.
- Stommel, H. and W. S. Wooster. (1965) "Reconnaissance of the Somali current during the southwest monsoon." Proc. Nat. Acad. Sci. 54, 8-13.

- Sverdrup, H. U. (1937) "On the process of upwelling". Journal of Marine Research. Vol. 1, No. 2, pp. 155-164.
- Sverdrup, H. U. and R. H. Fleming. (1941) "The waters off the coast of Southern California, March to July 1937." Bull. Scripps Inst. Oceanog. 4, 261-378.
- Sverdrup, H. U., M. W. Johnson and R. H. Fleming. (1942) The Oceans, Their Physics, Chemistry and General Biology. Prentice Hall, New York, 1087 pp.
- Swallow, J. C., and J. G. Bruce. (1966) "Current measurements off the Somali coast during the southwest monsoon of 1964." Deep-Sea Res. 13, 861-888.
- Veronis, G. (1967a) "Analogous behavior of rotating and stratified fluids." Tellus. 19, 620.
- Veronis, G. (1967b) "Analogous behavior of homogeneous, rotating fluids and stratified, non-rotating fluids." Tellus. 19, 326.
- Warren, B., H. Stommel and J. C. Swallow. (1966) "Water masses and patterns of flow in the Somali basin during the southwest monsoon of 1964." Deep-Sea Res. 13, 825-860.
- Wooster, W. S. (1960) "El Nino." Calif. Coop. Ocean. Fish. Invest. Rep. 7
- Wooster, W. S. (1961) "Yearly changes in the Peru current." Limnol. Oceanog. 6, 222-226.
- Wooster, W. S. and T. Cromwell. (1958) "An oceanographic description of the eastern tropical Pacific." Bull. Scripps Inst. Oceanog. 7, 169-282.
- Wooster, W. S. and M. Gilmartin. (1961) "The Peru-Chile undercurrent." J. Mar. Res. 19 (3), 97-112.
- Wooster, W. S. and J. L. Reid, Jr. (1963) "Eastern boundary currents" in The Seas, Vol. 1, (ed. M.N. Hill), Interscience, New York.
- Wyrtki, K. (1962) "The upwelling in the region between Java and Australia during the south-east monsoon." Australian J. Mar. and Fresh Water Res. 13, 217-225.
- Wyrtki, K. (1963) "The horizontal and vertical field of motion in the Peru current." Bull. Scripps Inst. Oceanog. 8, 313-346.
- Yoshida, Kozo (1967) "Circulation in the eastern tropical oceans with special references to upwelling and undercurrents." Japanese Journal of Geophysics. Vol. 4, No. 2, March.

Acknowledgments

I am deeply grateful to Professor Henry Stommel for his tolerance, example, and inspiration.

I would like to thank Prof. N.A. Phillips, Dr. W.F. Simmons, and Dr. B.A. Warren for their assistance.

I would also like to thank Mr. John L. Bowen for his assistance in programming and Mrs. Karen MacQueen for her excellent job of typing the thesis.

This research has been supported by the National Science Foundation under grant GA-1613.

BIOGRAPHICAL NOTE

The author was born in Viljandi, Estonia on 16 November 1942. The Russian invasion of Estonia forced his family to flee to Czechoslovakia. The war years were spent there and in Germany. In 1947 his family came to the United States.

He obtained his primary and secondary education in the public school system of Fremont, Ohio. In the fall of 1961 he enrolled at the University of Chicago. He graduated in June of 1965 with a S.B. in physics. In September of 1965 he began his studies at M.I.T.